Technical Report

EVAPORATION FROM SMALL WIND WAVES

by
Juey-rong Lai
and
Erich J. Plate

Prepared under
National Science Foundation
Grant No. GK

Fluid Dynamics and Diffusion Laboratory
Civil Engineering Department
Colorado State University
Fort Collins, Colorado

June 1969

CER68-69JRL35
Also CED68-69RL27

Technical Report

EVAPORATION FROM SMALL WIND WAVES

by

Juey-rong Lai

and

Erich J. Plate

Prepared under

National Science Foundation

Grant No. GK

Fluid Dynamics and Diffusion Laboratory
Civil Engineering Department
Colorado State University
Fort Collins, Colorado
June 1969

CER68-69JRL35

ABSTRACT

The evaporation rates from small wind-waves by forced convection in a range where the spray of water by strong wind action is not important has been studied in the laboratory. The effects of free stream velocity, wave conditions, and temperature difference between air and water (either inversion conditions or lapse conditions) on evaporation were investigated, and the results were compared with previous work. The experimental data were correlated in terms of dimensionless groups, which were based on well-known theories for exchange processes in forced convection over solid surface. The transitional phenomenon was analyzed for evaporation as the wind blew over the solid surface onto the water surface.

For the lapse condition, the temperature difference was found to cause larger growth rates of the waves as well as increased evaporation rates. The stratification of air velocity above the water surface was calculated, based on the Richardson criterion. No significant change was detected based on this criterion in this study.

ACKNOWLEDGMENTS

The author wishes to express his deep gratitude to his major professor, Dr. Erich J. Plate and to Dr. George M. Hidy for their advice and encouragement at all stages of the work.

The author is also indebted to other members of his committee, Dr. R. N. Meroney and Dr. R. D. Haberstroh, who reviewed the rough draft and gave many valuable comments.

Finally, the author would like to thank Mr. K. S. Su and Mr. Aziz F. Eloubaidy for helping in the data collection.

The work was sponsored by the National Science Foundation through its contract with the National Center for Atmospheric Research, and through the grant to Colorado State University, No. GK .

TABLE OF CONTENTS

LIST OF TABLES

LIST OF FIGURES

NOMENCLATURE

Symbol	Definition	Dimension
A	Constant	
a	Wave height	[cm]
B	Constant or mass transfer parameter	
c	Phase speed of significant waves	[cm/sec]
C_p	Specific heat	[Joules/gm°C]
D	Molecular diffusivity of water vapor	[cm^2/sec]
e	Vapor pressure	[gm/cm^2]
E	Evaporation flux	[gm/cm^2-sec]
f	Wave frequency	[Hz]
f_m	Frequency of spectral peak	[Hz]
g	Acceleration of gravity	[cm/sec^2]
H	Heat flux at wall	[cal/cm^2-sec]
Hℓ	Heat flux due to evaporation [$\equiv \frac{\Delta h x E}{C_p}$]	
Hc	Heat flux due to temperature gradient [$\equiv \alpha (\frac{\partial T}{\partial Z})_s$]	
k	von Karman's constant [= 0.4]	
K_m	Eddy diffusivity for momentum	[cm^2/sec]
K_h	Eddy diffusivity for heat	[cm^2/sec]
K_e	Eddy diffusivity for mass	[cm^2/sec]
$\overline{K}$	Evaporation parameter [= K/Z]	[cm/sec]
ℓ	Length scale of turbulence eddy	[cm]
ℓe	Concentration thickness	[cm]
L	Latent heat of evaporation	[cal/gm]
m	Net amplification rate	

Symbol	Definition	Dimension
m_w	Damping factor	
m_a	Growth factor	
P	Pressure	[gm/cm^2]
p	Wave period	[cps]
q	Specific humidity	[$\frac{\text{gm of water vapor}}{\text{gm of dry air}}$]
q_*	Friction specific humidity	[$\frac{\text{gm of water vapor}}{\text{gm of dry air}}$]
s	Source strength	[gm/cm^2-sec]
T	Temperature	[°C]
u	Velocity along x-axis	[cm/sec]
u_*	Friction velocity [$\equiv \sqrt{\frac{\tau}{\rho}}$]	[cm/sec]
v	Velocity along z-axis	[cm/sec]
x	Horizontal axis (fetch)	[cm]
x^+	Dimensionless x-axis	
Z	Vertical axis	[cm]
z_o	Roughness coefficient	[cm]
z_{om}	Saturation length	[cm]
α	Thermal diffusivity	[cm^2/sec]
δ	Boundary layer thickness	[cm]
δ_e^*	Boundary layer thickness for mass transfer	[cm]
λ	Wave length	[cm]
ν	Kinematic viscosity	[cm^2/sec]
ρ	Density	[gm/cm^3]
σ	Standard deviation of water waves	[cm]
τ	Shearing stress	[gm/cm^2]

Symbol	Definition	Dimension
ϕ	Amplitude spectra	$[cm^2/sec]$
Γ_D	Evaporation coefficient	
Γu	Velocity coefficient	
w	Stability function of Miles	

Subscripts

1	Water vapor
2	Dry air
a	Inner layer
b	Outer layer
m	Momentum
rgn	Roughness surface
s	Water surface
t	Turbulence
∞	Free stream
w	Water

Dimensionless numbers

B	Bowen ratio [$\equiv$ Hc/He]
B*	Driving force [$\equiv (q_\infty - q_w)/(1 - q_w)$]
C_f	Drag coefficient [$\equiv \tau/\frac{1}{2}\rho u_\infty^2$]
Gu	Gukhman number [$(T_a - T_b)/T_a$]
Pr	Prandtl number [$\equiv \nu/\alpha$]
Re	Reynolds number [$\equiv \frac{u_\infty x}{\nu}$]
R_f	Richardson number in flux form [$\equiv - gH/c_p T_o \tau (\frac{\partial \bar{u}}{\partial z})$]

Symbol	Definition

Dimensionless numbers continued

Ri	Richardson number in gradient form [$\equiv g(\frac{\partial \bar{\theta}}{\partial z})/T_o(\frac{\partial \bar{u}}{\partial z})^{-2}$]
Rgn	Modified roughness coefficient [$\equiv \frac{\lambda}{h}(1 - \frac{c}{u_*})^{-1}$]
Sc	Schmidt number [$\equiv \nu/D$]
Sh	Sherwood number [$\equiv Ex/\rho D(q_s - q_\infty)$]
St_d	Stanton number [$\equiv Sh/Sc \cdot Re$]

Chapter I

INTRODUCTION

The problem of evaporation by forced convection from a free surface has interested many scientists because of its numerous applications to technology and water conservation. For example, many industrial processes depend on simultaneous heat and mass transfer with evaporation or condensation. Evaporation from the ocean plays an important role in controlling the humidity and temperature distribution near the sea surface. Meteorologists consider the microscale convective transport across the air-sea interface an essential process in affecting the general circulation of the atmosphere (Roll, 1965). The prediction of evaporation rates is also critical to the design and development of water resources systems to reduce water losses from lakes and reservoirs.

The phenomenon of evaporation takes place when the vapor pressure above a free surface is less than the saturated vapor pressure at that surface. When a vapor pressure difference exists, the kinetic theory of gases shows that a net flux of molecules must be directed away from the water surface. When the liquid is in contact with its saturated vapor, the rate of evaporation of molecules is equal to the rate of condensation (i.e., the evaporation and condensation are in dynamic equilibrium). There is no mass loss due to

the evaporation at this condition. The higher the water temperature, the higher the observed saturated vapor pressure; thus, the total amount of evaporation will be increased by raising the water temperature.

When wind blows over a free water surface, the evaporation mechanism becomes more complex. The water vapor near the water surface is carried away by the wind. Thus, a gradient of vapor concentration is established, which combined with the wind field provides the driving force to decrease the vapor pressure at the interface and eventually increase the evaporation rate. The complexity arises from the interrelationship among the velocity, water surface, surface films, say of organic hydrophobic materials, and temperature differences between water and air. The wind velocity distribution is affected by the surface waves (Miles, 1962; Kinsman, 1965; Plate and Hidy, 1967; and Chang, 1968). The water surface waves are affected by the temperature difference (Fleagle, 1956; and Hidy and Plate, 1968) and the surface film (Le Mer and Schaefer, 1965; and Hidy and Plate, 1968). These four factors are interrelated to some extent and do not independently contribute to the evaporation. It is, therefore, very difficult to describe the whole evaporation mechanism by a simple relationship.

Clean water has been assumed in most laboratory studies or field observations, so the effect of surface film is

presumed small. Yet, the three other major factors which strongly affect the evaporation rates have not been studied simultaneously. In previous analytical or experimental work, as will be described briefly in Chapter II, one or two factors were emphasized, but the temperature difference between air and water was left out. Furthermore, some experimental results contradicted each other. (See Okuda and Hayami, 1959; and Easterbrook, 1968)

The purpose of this study was to provide experimental data which can be used for developing a practical method to predict the evaporation rates from small wind waves. The situation of this study is indicated in Figure 2, (see Chapter III, p. 26). A turbulent boundary layer develops first over a solid boundary and continues onto the water surface. When waves are generated, the approaching boundary layer flow becomes the outer layer while a new inner layer develops over the waves. The boundary layer for mass transfer (inner layer for mass transfer) develops from the leading edge ($x = 0$), while the inner layer for momentum transfer develops somewhere at a position downstream of the region where the water surface changes from smooth to rough. The inner layer for momentum transfer is associated with a change in shear stress at the surface. For the flow far enough downstream, the inner layer has grown to encompass the whole shear layer, and this layer is in essential

equilibrium with the rough surface underneath. The portion of flow in this zone is defined as a fully developed turbulent flow. The experiments were conducted in a laboratory channel in a range where a spray of water from breaking waves as would be caused by a strong wind was unimportant.

The specific objectives of the study were:

(1) to bring together the previous results of other investigations on predicting evaporation rates by using the analysis of the author's experiment;

(2) to investigate the effect of free stream velocity, fetch, and temperature difference on evaporation rates;

(3) to analyze the transitional phenomenon of evaporation when the wind blew over the solid plate onto the water surface; and

(4) to correlate the aerodynamic and thermodynamic factors in the form of dimensionless equations.

Chapter II

REVIEW OF LITERATURE

As wind blows over a water surface, the evaporation rate is affected by velocity, wave shapes, and temperature differences. This chapter will review the available literature concerning the velocity profile over the small water waves and concentrate on the evaporation problem on the basis of analytical methods and experimental data.

2.1 Wind Over Small Water Waves

2.1.1 Wind Profiles

The mean velocity profile of air above the mean water surface is needed to understand the exchange of energy between air and water during wave generation by wind. Examination of Miles' (1957) inviscid shear flow model showed that a logarithmic velocity profile of air had been assumed to calculate the total energy growth of water waves. In marine physics, the logarithmic profile has been used to describe the air flow in the atmospheric boundary over water. In laboratory studies, Hidy and Plate (1966), Plate and Hidy (1967), Shemdin and Hsu (1966), Hess (1968), and Chang (1968) all used the logarithmic law to correlate the mean velocity data of their experiments. Therefore, the "law of wall" has also been used throughout the author's experiment to describe the velocity profiles, as follows:

$$u = \frac{u_*}{k} \ln \frac{z}{z_o} \qquad (2\text{-}1)$$

where u is velocity, u_* is friction velocity, ($u_*^2 = \frac{\tau}{\rho}$, τ is shear stress at wall), z_o is the roughness length, and k is von Karman's constant and assumed to be 0.4.

To illustrate the wind action over the solid surface onto the liquid surface with different roughness, a two-layer model of shear flow was proposed by Plate and Hidy (1967). The upstream flow and outer layer was referred to as conditions over the smooth solid surface. The inner layer was referred to as conditions over the wavy liquid surface. Both layers were assumed to follow the logarithmic law of the wall with different friction velocity and roughness length. The inner layer will grow in depth downstream and eventually coincide with the outer layer. Plate and Hidy investigated the values of friction velocity in transition with the given velocity profile in the outer layer upstream by applying the momentum balance, mass conservation, and the conditions of velocity continuity. The agreement between the two-layer model and the experiments was quite satisfactory except very close to the leading edge.

Although Equation (2-1) has been verified by many laboratory studies and field observations, the relation between z_o and u_* are not unique (see for example, Karaki and Hsu, 1967). This leads to further studies in measuring the wind profile over the wavy surface. Shemdin (1967)

pointed out that the velocity profile, which was given by a fixed probe, needed correction for the effects of shifting the streamline and of wave-induced perturbation. Chang (1968), using the technique of moving probe, suggested the possible existence of separation near the peak of wave which affected the wind profile near the water surface. Thus, the wind profile above a wave height from mean water surface deviated from the logarithmic law.

Dynamical relations between z_o and u_* have been reported in some laboratory studies. Kunishi (1963) suggested that the aerodynamic roughness of wavy surfaces is related to a characteristic wave height for a small wave, and for the condition that the wave speed is much less than the mean air speed. Hidy and Plate (1966) found that a Reynolds number which is based on u_* and σ, (σ is the standard deviation of water waves), correlated quite well with z_o on log-log paper.

2.1.2 Moving and Flexible Boundary

The concept of turbulent flow and boundary layer theory over the rigid wall has been studied quite extensively both theoretically and experimentally. For the first approximation, the theoretical approach of turbulent flow over rigid wall could be used to describe the wind over wavy surface, which was moving and flexible, and the experimental results could also be compared. Gupta and Mollo-Christenson (1966) measured pressures and constant speed lines in the

air flow over a boundary of solid waves to compare with Benjamin's (1959) theoretical prediction of phase-shift in wind-wave theory. The resulting shifts were only one-tenth of Benjamin's values. The reason for this is at present not understood. Zagustin et al. (1966) carried out experiments in a laboratory flume with a moving belt in sine wave motion. Their results were compared to Miles' (1959) theoretical estimation of pressure component in shear flow model of wind-wave theory. It only agreed qualitatively, because the coupling of the flow in the two fluids cannot be neglected. The flexible and moving boundary can induce fluctuation and turbulence, which are not considered in studying the turbulent flow over solid boundary. Thus, applications of the results of turbulent flow over solid boundaries are limited in the study of air-sea interactions.

2.2 Analytical Method to Evaluate Evaporation Rates

The purpose of this section is to present and compare various formulas to estimate the evaporation rates from liquid surface. In reviewing the mechanism for the water vapor transport from interface to the gas stream, the relatively straightforward theories for direct mass balance and turbulent transport are considered first as opposed to more sophisticated methods attempting to account for a changing surface structure. The dimensionless correlations, which are based on analytical equation, are also included in this

section. The effect of roughness changes and other transitional phenomenon on evaporation are discussed later.

2.2.1 Direct Mass Balance

By using the concept of direct mass balance in control volume, an integral boundary-layer equation of mass transfer can be expressed as (see Eckert and Drake, 1959):

$$E = \frac{d}{dx} \int_{o}^{\delta_e^*} \rho [q(z) - q_\infty] \, u(z) \, dz \qquad (2\text{-}2)$$

where q is the concentration of water vapor. In deriving Equation (2-2), one basic assumption was made; that is, neglecting the vertical velocity at the interface. For a given velocity profile and concentration displacement, the evaporation rate is calculated from Equation (2-2). This procedure was adopted in this thesis for obtaining the "measured evaporation rate E."

2.2.2 Turbulence Diffusion

A general eddy diffusion equation for evaluating the evaporation rate in turbulent flow is derived from aerodynamic theory, and may be written as (see for example, Bird, Stewart, and Lightfoot, 1960):

$$E = - \rho K_e \frac{\partial \bar{q}}{\partial z} \qquad (2\text{-}3)$$

where E is the evaporation rate, which is assumed constant everywhere, K_e the eddy diffusivity for mass, and $\bar{q}$ the specific humidity. Knowledge of K_e is still a challenge to the investigators of this field. In fact, K_e is affected by velocity, temperature, concentration, surface condition, and

position. Different expressions for K_e have been derived analytically in terms of many factors at different boundary conditions (Brutsaert, 1965). Yet, only under very limited conditions has even the most simple equation for K_e been verified.

By using the Equation (2-3), evaporation rates can be determined by averaging across the boundary layer. One integral technique approach has been described by Sheppard (1958). He considered the existence of diffusion sublayer near the water surface and applied Equation (2-3) in the form:

$$E = - \rho (D + K_e) \frac{\partial \bar{q}}{\partial z} \qquad (2\text{-}4)$$

where D is the molecular diffusivity of water vapor in air. The molecular and turbulent exchanges were supposed to occur simultaneously. He further assumed that K_e increased linearly with height, z, or,

$$K_e = k\, u_* z \ . \qquad (2\text{-}5)$$

By inserting the relationship (2-5) into (2-4), Equation (2-4) was integrated, yielding the following relationship:

$$E = \rho k (\bar{q}_s - \bar{q}_a)\, u_* / \ell n[(D + k u_* a)/D], \qquad (2\text{-}6)$$

where the subscripts s and a refer to heights, $z = 0$, and $z = a$. Since there are few field or experimental data

available to confirm this equation, the extent of applicability for this equation remains to be verified (Roll, 1965).

2.2.3 Profile Method

To derive a logarithmic law of mass transfer, the following classical assumptions may be made: (1) the change in scale of the eddy motion is a function of distance from the surface; and (2) the air is saturated at the free surface at the surface temperature. Based on assumption 1, the coefficient of turbulent diffusion has the relationship (Levich, 1965):

$$K_e \sim \ell^2 \frac{\partial \bar{u}}{\partial z} \sim z^2 \frac{\partial \bar{u}}{\partial z} \qquad (2\text{-}7)$$

where ℓ is the length scale of important eddies. With Equations (2-3) and (2-7), the evaporation rate, E, can be expressed as:

$$E = \rho \beta z^2 \frac{\partial \bar{u}}{\partial z} \frac{\partial \bar{q}}{\partial z} \qquad (2\text{-}8)$$

where β is a constant. Using Equations (2-1) and (2-8), the logarithmic law of mass transfer is obtained as:

$$\bar{q} - \bar{q}_s = q_* \ln \frac{z}{z_{om}} \qquad (2\text{-}9a)$$

$$E = - \rho k' u_* q_* \ , \qquad (2\text{-}9b)$$

where the value of k' is normally set equal to Karman's

constant as a first approximation, and in analogy to u_*, q_* can be defined as a friction humidity. The length scale, z_{om}, may be considered a hypothetical length or distance across a "layer" of saturated air near the surface. Equation (2-9) also can be derived from the concept of Reynolds analogy which is demonstrated in Schlichting's book (1962), or by other methods described by Roll (1965). The concept of Reynolds analogy is based on the assumption, i.e.:

$$\frac{\tau}{\tau_w} = \frac{m}{m_w} = \frac{H}{H_w} \quad ,$$

to express the analogy between momentum, heat and mass as:

$$\frac{\tau}{\tau_w} = (1 + \frac{K_m}{\nu}) \frac{du^+}{dy^+} \qquad (2\text{-}9c)$$

$$\frac{H}{H_w} = (\frac{1}{P_r} + \frac{K_h}{\nu}) \frac{dt^+}{dy^+}$$

and

$$\frac{\dot{m}}{E} = (\frac{1}{S_c} + \frac{K_e}{\nu}) \frac{dq^+}{dy^+}$$

where τ is shear stress; $\dot{m}$ is mass flux; H is heat flux; $u^+ = u/u_*$, $t^+ = (t_w - t)\ \rho C_p u_*/H_w$, $q^+ = (q_w - q)\ \rho k u_*/E$ and $y^+ = y/y_o$.

The evaporation rates determined by this method depend on knowledge of suitable values of q_* and z_{om}, which vary with $\bar{u}$, $\bar{T}$, $\bar{q}$ surface conditions and height z. Unfortunately, our knowledge is still rather limited on this aspect of the problem. At present, the only way to determine

these values is empirically from the profiles taken by experiments for different boundary conditions.

2.2.4 Dimensionless Correlation

Correlations in terms of dimensionless number were derived based on different approaches, such as dimensional arguments, Reynolds analogy, numerical solution, and boundary layer theory. For the heat transfer problem, these correlations have been studied extensively. Based on the analogy between heat and mass transfer, dimensionless mass transfer rates can be obtained from heat transfer problems by replacing the Nusselt number with the Sherwood number and the Prandtl number with the Schmidt number. Based on Reynolds analogy, Chilton and Colburn (1934) derived the following dimensionless correlation for a smooth flat plate:

for laminar flow:

$$Sh = \text{const.} \ (Sc)^{1/3} \ (Re)^{1/2} \qquad (2\text{-}10)$$

for turbulent flow:

$$Sh = \text{const.} \ (Sc)^{1/3} \ (Re)^{0.8} \qquad (2\text{-}11)$$

where

$Sh = \rho Ex \ D \ (q_s - q_\infty)$, (= Sherwood number)

$Sc = \nu/D$, (= Schmidt number)

The above relation, Equation 2-10, was derived numerically by Lighthill (1950). Equations were also shown in Schlichting's book (1962), which were derived from the boundary layer theory. Reynolds et al. (1958) carried out a series of experiments to arrive at a similar result. They

considered the effect of drag force and found the following relation for turbulent flow:

$$Sh = \text{const.} \left(\frac{C_f}{2}\right)^{1/2} (Sc)^{1/3} (Re)^{0.8} \qquad (2\text{-}12)$$

where

$$C_f = \tau / \frac{1}{2} u_\infty^2 \text{ , (= drag coefficient).}$$

If the drag coefficient is independent of the Reynolds number, then Equations (2-11) and (2-12) are seen to be identical. Either of the equations is commonly used to express the Sherwood number.

When wind blows over the water waves, the air flow near the interface is affected by the wavy surface. For the first approximation, this effect can be considered as the roughness effect on a flow system over solid boundary.

Papers citing the effect of surface roughness on heat (or mass) transfer are limited and contradict each other. For example, Smith and Epstein (1957), after examining commercial pipes of different roughness, indicated that the roughness increased the pressure drop, and thus substantially increased the heat (or mass) transfer rate. According to Kolar's results (1965), the rough pipe has low efficiency in heat (or mass) transfer. The efficiency is defined as the ratio of the amount of energy transferred as heat per unit temperature difference with the amount of energy needed to passing the fluid through the tube. The efficiency of the rough tube decreases with increasing velocity more

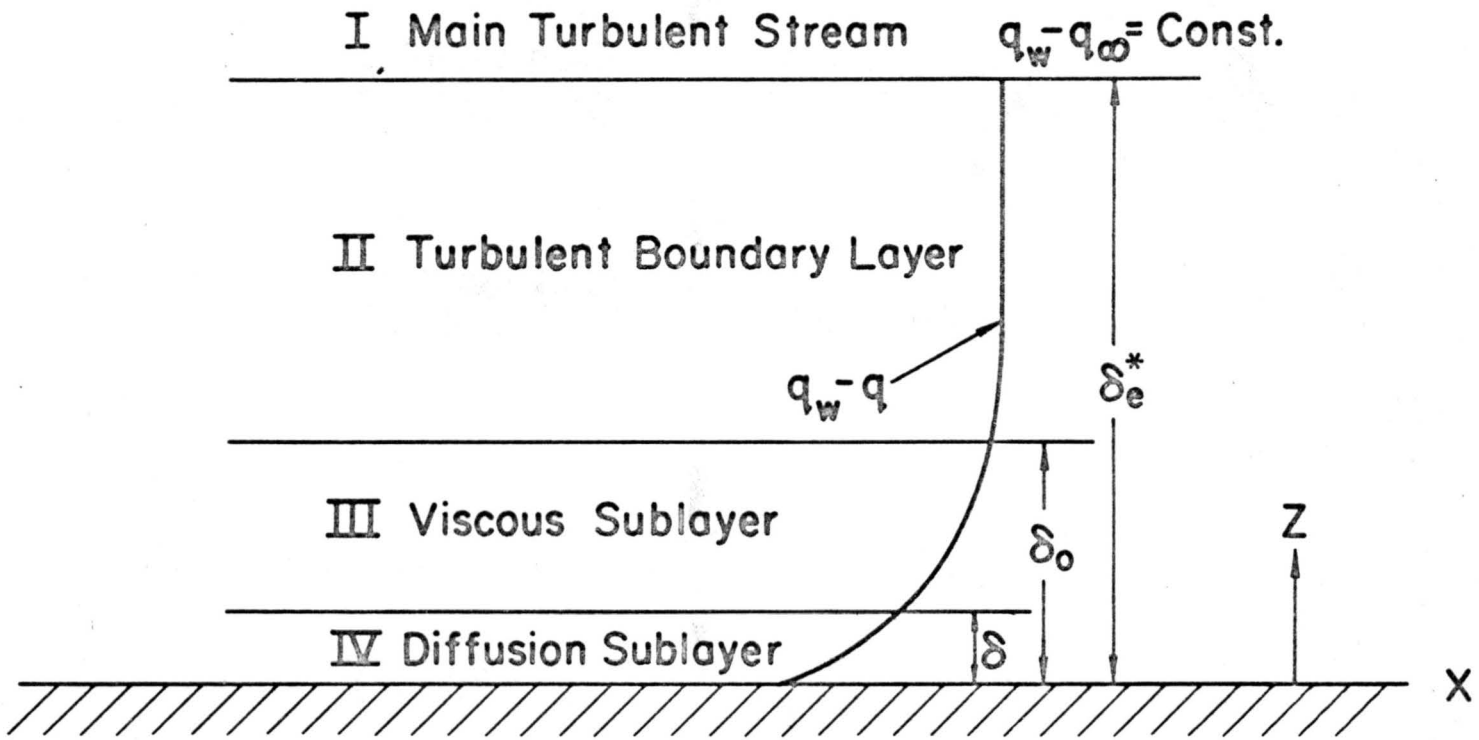

Fig. 1. Distribution of the diffused substance in turbulent stream (from Levich, 1962).

rapidly than that for smooth tube. Thus, beyond some limit, for any combination of Reynolds number and Prandtl number, an increase of roughness will no longer increase the heat transfer coefficient.

Levich (1965) proposed an explanation of the effect of surface roughness on mass transfer in turbulent flow. His model is shown in Figure 1. For a fully developed turbulent flow over the plate, the concentration remained constant some distance away from the wall. At $\delta_o < z < \delta_e^*$, there is a turbulent boundary layer in which both mean velocity and average concentration decrease according to logarithmic law. In this zone, both momentum and matter are transferred by turbulent eddies. In the zone of the viscous sublayer ($\delta < z < \delta_o$), turbulent eddies became so weak that the momentum transferred by the molecular process exceeds that transferred by turbulent eddies. In the diffusion sublayer ($z < \delta$), the molecular mechanism dominates over the turbulent mechanism.

The thickness of the diffusion sublayer, which forms the main resistance to mass transfer, is related to the thickness of the viscous sublayer. A viscous sublayer usually will develop around the roughness peak. However, a separation in the flow over individual protrusions will also occur in the case of solid roughness where the roughness height h is greater than δ_o but smaller than the boundary layer

thickness of momentum transfer δ_m, and where the Reynolds number based on h and u_* ($Re_{rgn} = \frac{hu_*}{\nu}$) is much larger than unity. The motion in the region, $z = h$, therefore must be turbulent, or at least highly agitated. The nature of the motion in this zone, then, is likely not to be a function of viscosity; it should be the function principally of height of roughness, h. So the scale of characteristic turbulent eddies must be proportional to h, or:

$$l \simeq h \ . \tag{2-13}$$

Due to the above hypothesis, the velocity distribution of a turbulent flow in the zone $z = h$ is obtained as

$$u = \frac{u_* z}{h} \ . \tag{2-14}$$

Levich suggested that this velocity distribution is valid only when the corresponding Reynolds number $u\delta_o/\nu$ is greater than or equal to unity. Thus, the viscous sublayer develops near the roughness peak. The thickness δ_o of the viscous sublayer is determined by the condition

$$\frac{u\delta_o}{\nu} = \frac{u_* \delta_o^2}{h\nu} \simeq 1 \ ,$$

or

$$\delta_o \simeq \frac{\nu h}{u_*}^{1/2} = h/(Re_{rgn})^{1/2} \ . \tag{2-15}$$

The evaporation rate can also be determined by expressing the thickness of the diffusion sublayer as

$$E \simeq \rho D(q_x - q_\infty)\delta \ . \qquad (2\text{-}16)$$

In the case of $Sc \simeq 1$, where $\delta = \delta_o$, from Equations (2-15) and (2-16), the evaporation rate is given by:

$$E \simeq \rho D u_*^{1/2} (q_s - q_\infty)/(\nu h)^{1/2} \qquad (2\text{-}17a)$$

and using the relation

$$u_* = \frac{C_f}{2} \cdot u_\infty \ ,$$

$$E \simeq \rho D (\frac{C_f}{2})^{1/4} (\frac{u_\infty}{\nu h})^{1/2} (q_s - q_\infty) \qquad (2\text{-}17b)$$

In dimensionless form, the above equation can be written as:

$$Sh_{rgn} \simeq Ex/\rho D(q_s - q_\infty) \ ,$$

or

$$Sh_{rgn} = \text{const.} \ (\frac{C_f}{2})^{1/4} (Re)^{1/2} (\frac{\lambda}{h})^{1/2} \qquad (2\text{-}18)$$

where $(\frac{\lambda}{h})$ is the roughness coefficient, λ is width of protrusion and rgn refers to roughness surface.

For the case $Sc >> 1$, such as for salt in water, Levich derived the following correlation of dimensionless groups:

$$Sh_{rgn} = \text{const.} \ (\frac{C_f}{2})^{1/4} (Re)^{1/2} (Sc)^{1/4} (\frac{\lambda}{h})^{1/2} \qquad (2\text{-}19)$$

This has been partially verified in the case of the pipe flow for dissolved oxygen in water by Mahato and Shemitt (1967) in the range where $5 \times 10^3 < Re < 3 \times 10^5$.

2.2.5 Solution of Transitional Boundary Layer

A transitional boundary layer starts to grow with fetch, from $x = 0$, as wind blows over the plate onto the

free surface. As the wind passes over the flat plate, a boundary layer forms near the plate which is referred to as the outer layer further downstream. Air proceeds onto the water surface, and the inner layer of mass transfer will immediately develop with fetch, but the inner layer of momentum transfer will grow later as waves develop. After the fetch reaches some values in downstream position, these three layers will coincide if $Sc \simeq 1$. Outer and inner layers no longer can be defined in the fully developed flow. The problem of heat transfer in transitional boundary layers, of the type involving a sharp change in surface condition, has been solved by Spalding (1963). He used a numerical method in solving the two-dimensional heat transfer problem for the case of $Pr = 1$. He predicted the heat transfer rate across a turbulent boundary for a stepwise change in wall temperature. By analogy between heat and mass transfer, his result can be used to estimate the mass transfer rate as:

$$St_o \left(\frac{C_f}{2}\right)^{1/2} \simeq (x^+)^{-1/3} (Sc)^{-2/3} \quad \text{for } x^+ < 10^3 \tag{2-20a}$$

$$St_D \left(\frac{C_f}{2}\right)^{1/2} \simeq (x^+)^{-1/9} (Sc)^{-2/3} \quad \text{for } 10^3 < x^+ < 10^6, \tag{2-20b}$$

where $St_D = E/\rho\ (q_s - q_\infty)\ U_\infty$ (= Stanton number) and

$x^+ = \int_1^x \frac{\tau}{\rho}/\nu\ d\xi$ (dimensionless distance). Spalding's results were derived from a smooth surface and were identical to Lighthill's (1950) laminar flow solution (2-9) for small

values of x^+. For large values of x^+, his results were compared with the empirical results of Reynolds et al. (1959) (Equation 2-11)). The scatter between experimental points and the theoretical prediction were less than $\pm$ 5%.

2.3 Evaporation from Field and Experimental Data

A number of semi-empirical solutions have been introduced based on field observations. Some experiments have been carried out in the laboratory to study the phenomenon of evaporation. This section will discuss briefly some of the results.

2.3.1 Semi-Empirical Method

For a large amount of experimental data, an empirical formula to estimate the evaporation rate is given by:

$$E = (e_o - e) \quad (A + B\bar{u}), \tag{2-21}$$

where e_o and e are the vapor pressure at the surface and air, A and B are constants, and $\bar{u}$ is the mean wind speed at some specific elevation. Equation (2-21) was derived from theoretical considerations by Brutsaert (1965). For different boundary conditions, different constants, A and B, have been suggested.

A logarithmic humidity profile has often been observed. Montgomery (1940) introduced an evaporation coefficient Γ_D as:

$$\Gamma_D = \left(\frac{1}{q_\infty - q_s}\right) \quad \frac{\partial \bar{q}}{\partial (\ell n\ z)} \quad . \tag{2-22}$$

The evaporation rate was obtained from the above equation as

$$E = \rho k u_* \Gamma_D (q_s - q_\infty) \quad . \tag{2-23}$$

A similar expression for wind distribution with height has been used (Deacon and Webb, 1962). It is

$$\Gamma_u = 1/u_a \; \partial\bar{u}/\partial(\ell n(z + z_o)) = u_*/ku_a \quad . \tag{2-24}$$

Combining Equations (2-23) and (2-24), the evaporation rate is given by

$$E = \rho k^2 \Gamma_u \Gamma_D a (q_s - q_a) \; \bar{u}_a \quad . \tag{2-25}$$

The reference height, z = a, is valid when the measured quantities $\bar{u}$ and $\bar{q}$ at this level follow logarithmic curves. A large number of ship observations at the single height on the ship bridge and the sea surface have been interpreted in terms of air-sea heat transfer, evaporation, and other relevant problems. Good agreement between experiment and theory was found as long as the field conditions were close to adiabatic.

2.3.2 Evaporation by Forced Convection

Due to the analogy between heat and mass transfer, many workers have used the heat transfer problem. For example, Cermak (1956) used the von Karman equation of heat transfer to solve the problem of vapor transfer. The results of von Karman's analysis is given below for flow over a plate:

$$St_x = Nu_x/Re_x \; Pr = \frac{1}{1 + 5(\frac{c_f}{2})^{1/2} \; [(Pr-1) + \ell n \frac{5Pr+1}{6}]} \tag{2-26}$$

This equation was transferred to the mass transfer problem by using the same procedure discussed in Section 2.2.4. His

hypothesis was compared with the results of a wind tunnel study. For a smooth, plane boundary, the agreement between theory and experiments was quite satisfactory.

Smolsky and Sergeyev (1962) have investigated the heat and mass transfer during liquid evaporation. They found that an increased evaporation rate from a free surface over that expected from boundary layer calculations could be due to the effect of driving force of free stream. To account for such an effect, they introduced the Gukhman number, $Gu = (T_a - T_w)/T_a$, which characterized the mass loss of evaporation attributed to the volumetric evaporation (LyKov, 1966). The temperatures T_a and T_w are the dry and wet bulb temperatures of free stream. Volumetric evaporation is a hypothetical mechanism for mass transfer in which sub-microscopic liquid particles are released from microscopic ripples at the free surface and carried into the outer air stream, where they evaporate. From Smolsky and Sergeyev's experimental data, the final form for the Sherwood number over a smooth free surface was given by:

$$Sh_x = 0.094\ Re^{0.8}\ Sc^{0.33}\ Gu^{0.2} \qquad (2\text{-}27)$$

This is similar to the previous results (Equation 2-12) but includes the temperature ratio, Gu. They investigated the mass transfer ratio from different liquid surfaces, including water, acetone, benzol and butanol. Using Equation (2-27), the experimental points were grouped close to a straight line on log-log paper, the scattering not exceeding $\pm$ 7%. For a high free stream temperature, the Gukhman number may

be significant on empirical grounds, but the concept of volumetric evaporation is hard to imagine physically as a part of the transport mechanism.

Okuda and Hayami (1959) carried out a series of experiments in a wind tunnel on evaporation of water from a wavy surface. They found that the values of the evaporation coefficient, Γ_D, were independent of free stream velocity when the spray of water was not important at fixed fetch. Their results were not generalized to estimate the evaporation rate. They used filter paper above the water surface to measure spray of water. They found that the splashing of sprays from breaking waves in strong wind increased the evaporation rate (observed in a tank) far beyond evaporation rates produced by non-breaking waves.

Easterbrook (1968) has also studied the effects of waves on evaporation from a free surface by using a wave tank-wind tunnel combination. He used a simplified equation, which was derived from Equation (2-3), to evaluate the evaporation rate:

$$E = \underline{\overline{K}} \ (q_s - q_z) \qquad (2\text{-}28)$$

where $\underline{\overline{K}} = K_e/z$ is a measure of eddy diffusivity for the layer from $z = 0$ to $z = z$, and $\underline{\overline{K}}$ is assumed to be independent of the height, z, and of the characteristics of the boundary layer turbulence. From his experimental results in the laboratory, Easterbrook determined a quantitative relationship between $\underline{\overline{K}}$ and wave characteristics, including

H (wave height) and P (wave period), and air flow characteristics, u_∞, at the same time. He found a decrease of evaporation rate in a certain wave range, while the wave properties, P and H, were increasing. This is in contrast to Okuda and Hayami's results which showed a general increase in evaporation rates with wind speed practicality. Easterbrook's laboratory results were used to fit the field data from Lake Hefner in Oklahoma. Only some of the field data points agreed with laboratory results.

The information on evaporation from wind generated waves by forced convection is still limited. Some measurements have been made, such as those of Brutsaert, Okuda and Hayami, and Easterbrook. However, the results are not satisfactory and some are contradictory to each other. Actually, the phenomenon of evaporation depends strongly on the wind generated waves and on the flow near the wave surface. Therefore, the author investigated the vapor transport from wind generated waves in the Colorado State University wind-wave channel facility by considering the effect of fetch, velocity, and temperature difference between air and water.

Chapter III

THEORETICAL CONSIDERATION

All of the previous works did not consider explicitly the effect of raising the water temperature on evaporation by forced convection. When the water temperature is raised higher than the air temperature, the evaporation rate will increase rapidly, so that the net vertical velocity at the surface is not necessarily negligible. In this chapter, the integral method of solving the evaporation problem is discussed by considering the evaporation on the surface as a plane source of variable strength.

The modified analytical model proposed by Plate and Hidy (1967) has been adopted for the analysis. They suggested an idealized model in which the air boundary layer over the water downstream from a solid plate can be separated into two-layered shearing flow. The schematic diagram of this model is shown in Figure 2. In the case of evaporation, the molecular diffusion near the wall dominates the transfer mechanism. Also the physical phenomenon of phase conversion yields a source strength which contributes a vertical velocity, v_s, of the vapor at the surface. The rectangle ℓmno is taken as a control volume in Figure 2. The mass balance for the control volume is obtained by

$$x\rho_a v_a = \int_o^{\delta_e^*} \rho_a u_a \, dz - \int_o^{\delta_e^*} \rho_b u_b \, dz - x \cdot \rho_s v_s \qquad (3\text{-}1)$$

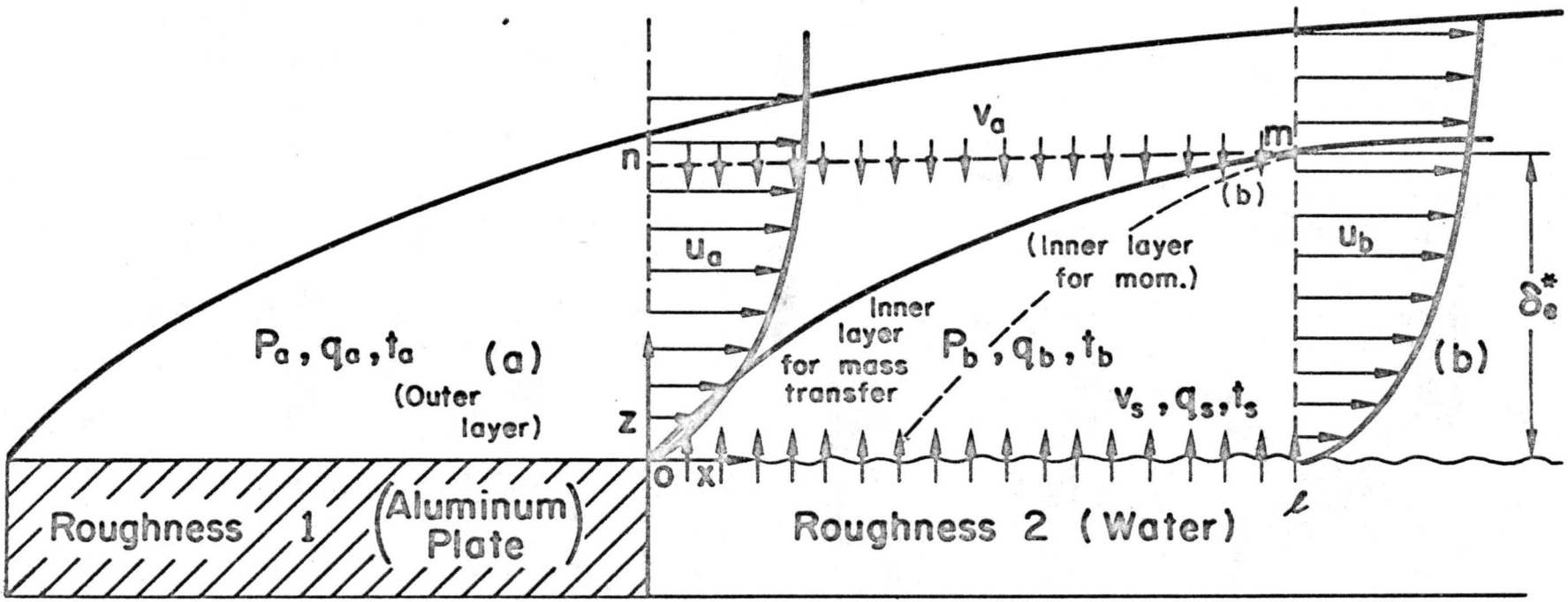

Fig. 2. Sketch of air and water motion associated with evaporation and growing waves.

where the source strength due to the phase conversion is set equal to $\rho_s v_s$ (Eckert and Drake, 1959). The value of $\rho_s v_s$ is usually very small; however, at high positive temperature difference between water and free stream, the term $\rho_s v_s$ may become important. An additional equation is obtained when only the conservation of water vapor in the control volume is considered:

$$x \cdot E = \int_o^{\delta_e^* - \delta} \rho_{1a} u_a dz + \int_o^{\delta_e^*} \rho_{1b} u_b dz - x \cdot \rho_{1a} v_a \qquad (3\text{-}2)$$

where the indices 1 and 2 referred to water vapor and dry air separately, while the subscripts a and b denote the outer and inner layers, respectively. Eliminating v_a from Equations (3-1) and (3-2), E becomes:

$$x \cdot E = \int_o^{\delta_e^*} (q_a - q_b)\, \rho_b u_b\, dz + x \cdot \rho_s v_s q_a \qquad (3\text{-}3)$$

where

$$q_a = \frac{\rho_{1a}}{\rho_{1a} + \rho_{2a}} \quad \text{and} \quad q_b = \frac{\rho_{1b}}{\rho_{1b} + \rho_{2b}} .$$

For an air-water mixture, E and v_s can also be expressed, following Eckert and Drake (1959):

$$E = - \rho_{1s} D_s \left(\frac{\partial \bar{q}}{\partial z}\right)_{z=o} + \rho_{1s} v_s \qquad (3\text{-}4a)$$

$$E = - \frac{D_s}{1 - q_s} \left(\frac{\partial \bar{q}}{\partial z}\right)_{z=o} \qquad (3\text{-}4b)$$

Combining Equations (3-3), (3-4a), and (3-4b), the final expression for E is given by:

$$-(1+B)\int_{o}^{x'} E\,dx = \int_{o}^{\delta_e^*} \rho(q-q_s)u_b\,dz - \rho(q_b-q_s)\int_{o}^{\delta_e^*} u_b\,dz \qquad (3\text{-}5)$$

where $B = (q_a-q_s)/(q_s-1)$ (= mass transfer parameter). In deriving Equation (3-5), the vapor concentration in outer layer was assumed small and constant. So the effect of outer layer on evaporation is only shown in u_b and δ_e^* in Equation (3-5). The values of B have been used to express the mass transfer rate in similar solution by Donovan, Hanna, and Yeragunis (1967). They obtained a closed form similar solution of the problem of turbulent boundary layer mass transfer with a finite interfacial velocity. Their results showed that the Stanton number is a function of Schmidt number, drag coefficient, mass transfer parameter B and Spalding function (see Spalding, 1963) with zero interfacial velocity.

For the velocity of Equation (2-1) and the humidity profile of Equation (2-5a) and assuming that the value of $(q_b - q_s)$ is constant in downstream direction (which is true in the laboratory when the wind-water channel reaches steady state, see also next chapter), the evaporation rate is obtained from Equation (3-5) as:

$$E= - \frac{1}{(1+B)} \frac{d}{dx}\{(\frac{\rho q_* u_* \delta^*_e}{k})[(\ell n \frac{\delta^*_e}{z_{om}})(\ell n \frac{\delta^*_e}{z_o}) - (\ell n \frac{\ell^*_e}{z_{om}} + \ell n \frac{\delta^*_e}{z_o}) - 1$$

$$- \frac{z_{om}}{\delta^*_e}(1 - \ell n \frac{z_{om}}{z_o})] - \rho(q_\infty - q_s) \frac{u_* \delta^*_e}{k} [(\ell n \frac{\delta^*_e}{z_o})$$

$$+ \frac{z_{om}}{\delta^*_e}(1 - \ell n \frac{z_{om}}{z_o}) - 1]\} \qquad (3\text{-}6)$$

This equation was checked for consistency through the experimental data of this study, and the results are discussed in Chapter VI. Equation (3-6) applies both to transitional boundary and to a fully developed turbulent boundary.

Chapter IV

EXPERIMENTAL EQUIPMENT AND PROCEDURE

Most of the laboratory instruments and facilities used in this experiment have been described in previous reports by Plate and Hidy (1967), Hess (1968), and Chang (1968), except for the temperature and humidity measurements. The latter equipment will be discussed in detail in the following section, but the facilities and instruments for wind measurements will be summarized only briefly.

4.1 Wind-Water Channel

The wind-water channel in the Fluid Mechanics and Diffusion Laboratory at Colorado State University has been used for this experiment. The channel (Figure 3) consists of a water channel 0.92 m wide and 11.2 cm deep. At the upstream end of the tunnel, a smooth aluminum plate 3.7 m long was installed at approximately the same height as the water surface. Over the aluminum plate and water surface is a wind tunnel 1.09 m high. The channel has a plexiglass test section 13.7 m long. For a reference coordinate, the downstream edge of the plate was considered to be at $x = 0$, and along the water tunnel was a positive direction of x-coordinate (Figure 2).

The air velocity was controlled by an axial fan at the outlet of the tunnel. The air flow was made uniform at the inlet and outlet sections through mesh screen and honeycomb

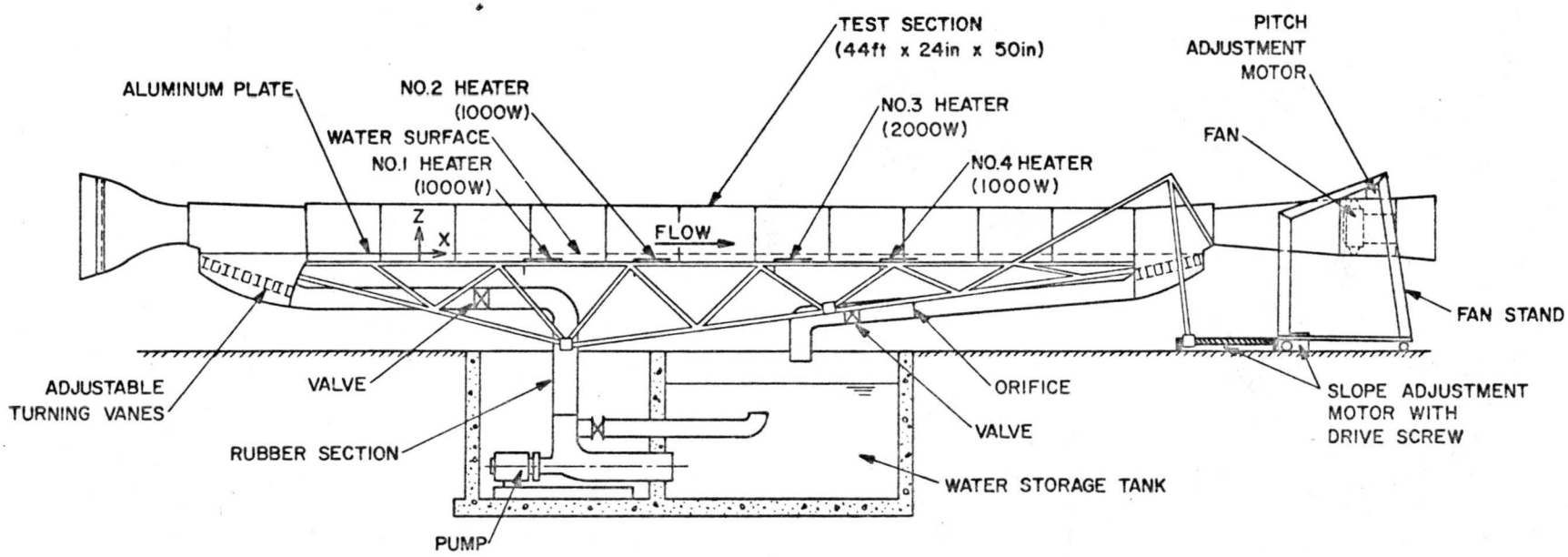

SCHEMATIC VIEW OF WIND-WATER CHANNEL

Figure 3.

grids, as described in previous works. To heat the water, immersion heaters of a total capacity of 5,000 volts were installed at four different positions in the test section at the bottom of the channel (Figure 3). These heaters were controlled by powerstats located outside the channel.

An instrument carriage capable of manual horizontal positioning and automatic vertical positioning was used to hold the sampling tube, thermocouple and the Pitot-static tube during measurements. The movement of the carriage was remotely controlled by a counter in the control panel, located beside the channel. Because previous work has demonstrated that the properties of fluid flow in the channel are approximately uniform in a cross-stream direction horizontally, measurements in the study were made only at different distances, x, along the centerline.

4.2 Instrumentation

4.2.1 Wave Records

A capacitance probe whose sensor was a 34-gauge magnet wire, was installed to continuously measure the water surface displacement at a given distance, x, as a function of time. The gauge was constructed so that the vertically stretched wire and the water surface formed two "plates" of a condenser, and the wire insulation (Nyclad) provided the dielectric medium. The difference in capacitance, due to the water depth, was measured by a capacitance bridge developed in the Engineering Research Laboratory at

CSU. The circuit diagram of the bridge is shown in Figure 4 in Chang's thesis (1968). The output signal of the CSU capacitance bridge was fed to an oscillograph recorder.

The capacitance gauge-oscillograph combination was calibrated against water depth after each series of experiments. The calibrations proceeded as follows: the water in the channel was discharged to the sump very slowly, and the water depth and the output of the recorder was simultaneously read for each period of 0.5 cm of water depth. Typical calibration curves, which indicated a linear proportionality between water depth and recorded elevation of the water surface, are shown in Figures 4 and 5.

For further statistical analysis, the wave records were digitized at equal time intervals of $\Delta t = 0.02$ seconds. Calculations were made to obtain for each run the values of standard deviation, σ, amplitude spectra, $\phi(f)$, and frequency of maximum spectral density, f_m. The statistical computing method used for these properties was that of Blackman and Tukey (1958), as discussed by Hidy and Plate (1966). (See also Chang, 1968).

4.2.2 Air Flow

The mean air velocity was measured by a Pitot-static tube, using a 0.325 cm OD probe manufactured by the United Sensor Co. The probe was placed on the instrument carrier which rose or descended step-by-step to give the mean air velocity profiles. In addition to the traveling

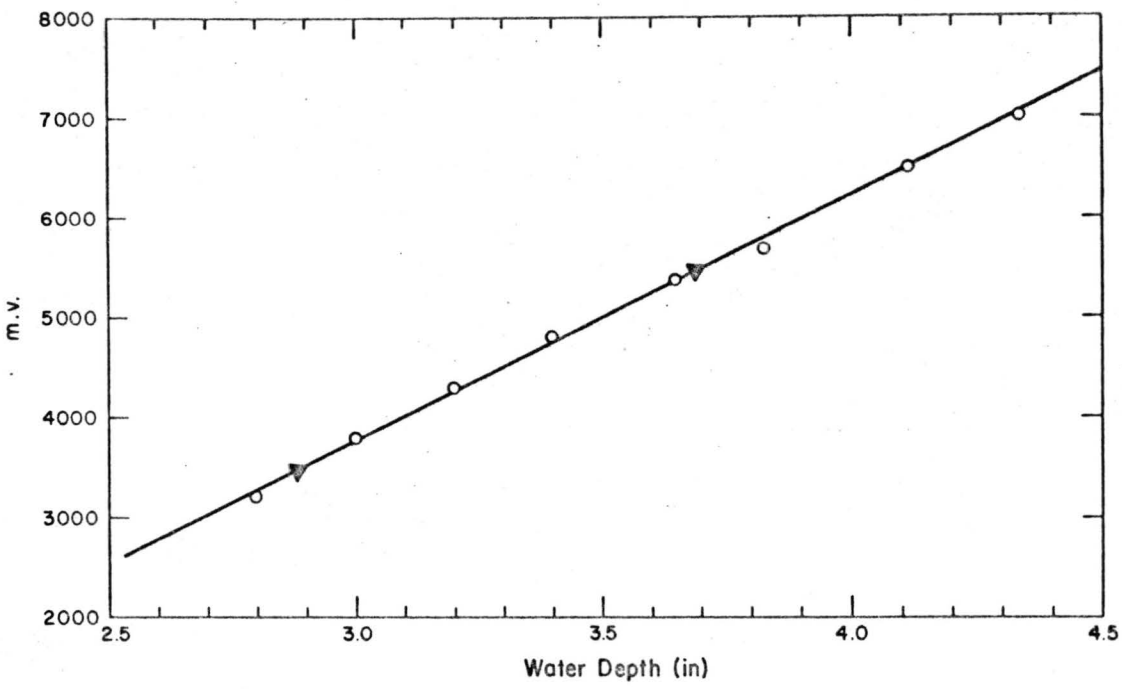

Fig. 4. Calibration curves of waves - gauge for cold and warm water cases.

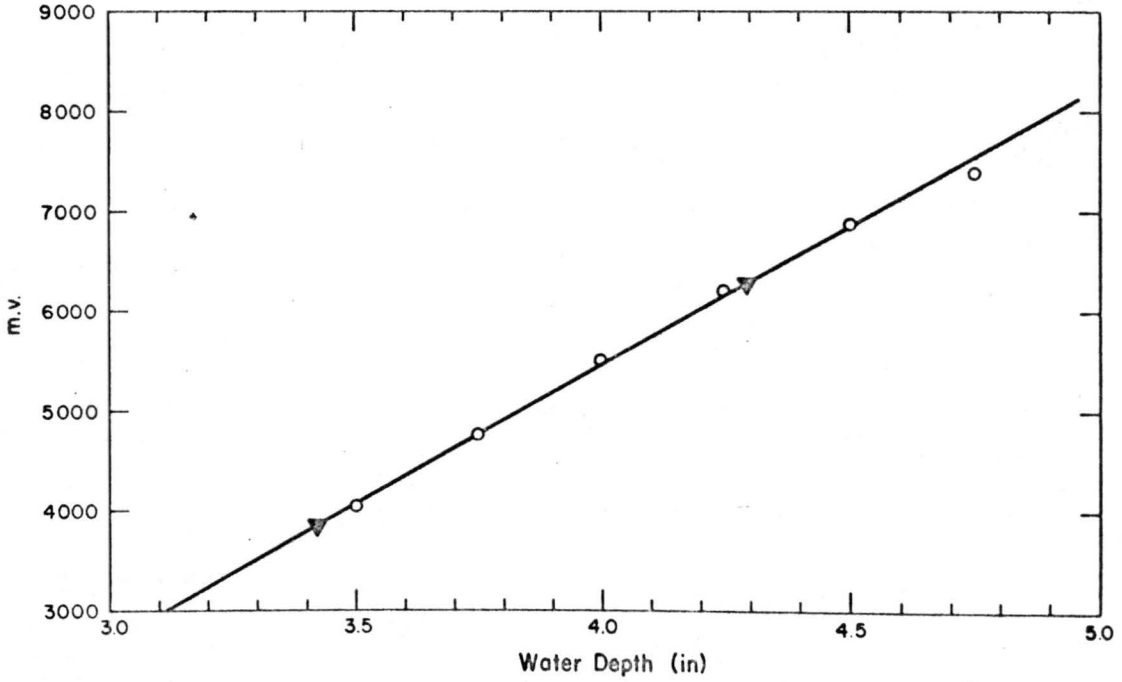

Fig. 5. Calibration curves of waves - gauge for cold and warm water cases.

probe, a fixed Pitot-static tube of 0.65 cm OD, which yielded the reference velocity for every run, was located above the aluminum plate and outside of the boundary layer.

To calculate the air flow, the Pitot tubes were connected to an electronic micromanometer (Transonic Equibar Type 120). The manometer measured the difference between total pressure and the static pressure, from which the mean air speed is calculated by means of the following relationship:

$$u(x,z) = \sqrt{\Delta p} \times 16.5 \text{ (m/sec)} \quad . \qquad (4\text{-}1)$$

The pressure difference read off the micromanometer instrument was calibrated against a water manometer (Flow Corporation, Type MM2).

4.2.3 Mean Temperature

The free stream temperature, T_∞, was measured by a mercury-in-glass thermometer placed on the upper frame of carriage which was located 10 cm below the top of the channel at each run. The local air temperature, T, in the boundary layer was measured with a 40-gauge Copper-Constantan thermocouple (Thermo-Electric Co.) using the free stream temperature as a reference. The output of the thermocouple was read with a potentiometer (Leeds & Northrup Co., Model 8686). Voltage differences were converted to temperature differences ($T-T_\infty$ using standard calibrations, as given in the National Bureau of Standards Circular 561).

The surface temperature of the water, T_s, was measured with an infrared radiometer (Branes Engineering Co., Model IT-3). The radiometer was calibrated against a known, stable black body source (Marlatt and Grassman, 1968). To obtain T_s, the water temperature T_w, which was measured by a thermometer immersed 2.5 cm beneath the mean water surface, was also determined. With the same free stream velocity and temperature, the water surface temperature was found to be a function of water temperature. This relationship is plotted in Figure 6, covering the range 10°C to 32°C. This curve is used as a calibration for obtaining the local surface temperature throughout the wind-water tunnel.

4.2.4 Specific Humidity

The specific humidity of the air-vapor mixture was measured by sampling the gas stream through a static pressure tube connected to a Consolidated Electrodynamic Co. moisture monitor (Model 26-303) at a constant flow rate maintained by a vacuum pump. The sketch of the arrangement is shown in Figure 7. The sampling tube was made of a 0.163 cm OD brass tube. The Pitot-tube, thermocouple and the sampling tube were set 2 cm apart on the instrument carriage. The only inlet for sampling the gas was a side hole in the tube to avoid the pressure drop in the tube. The brass tube was connected to the moisture monitor by a 5 mm OD Teflon Tube. The brass and Teflon tubes were recommended by Consolidated Electro-dynamic Co. because they absorbed only very little

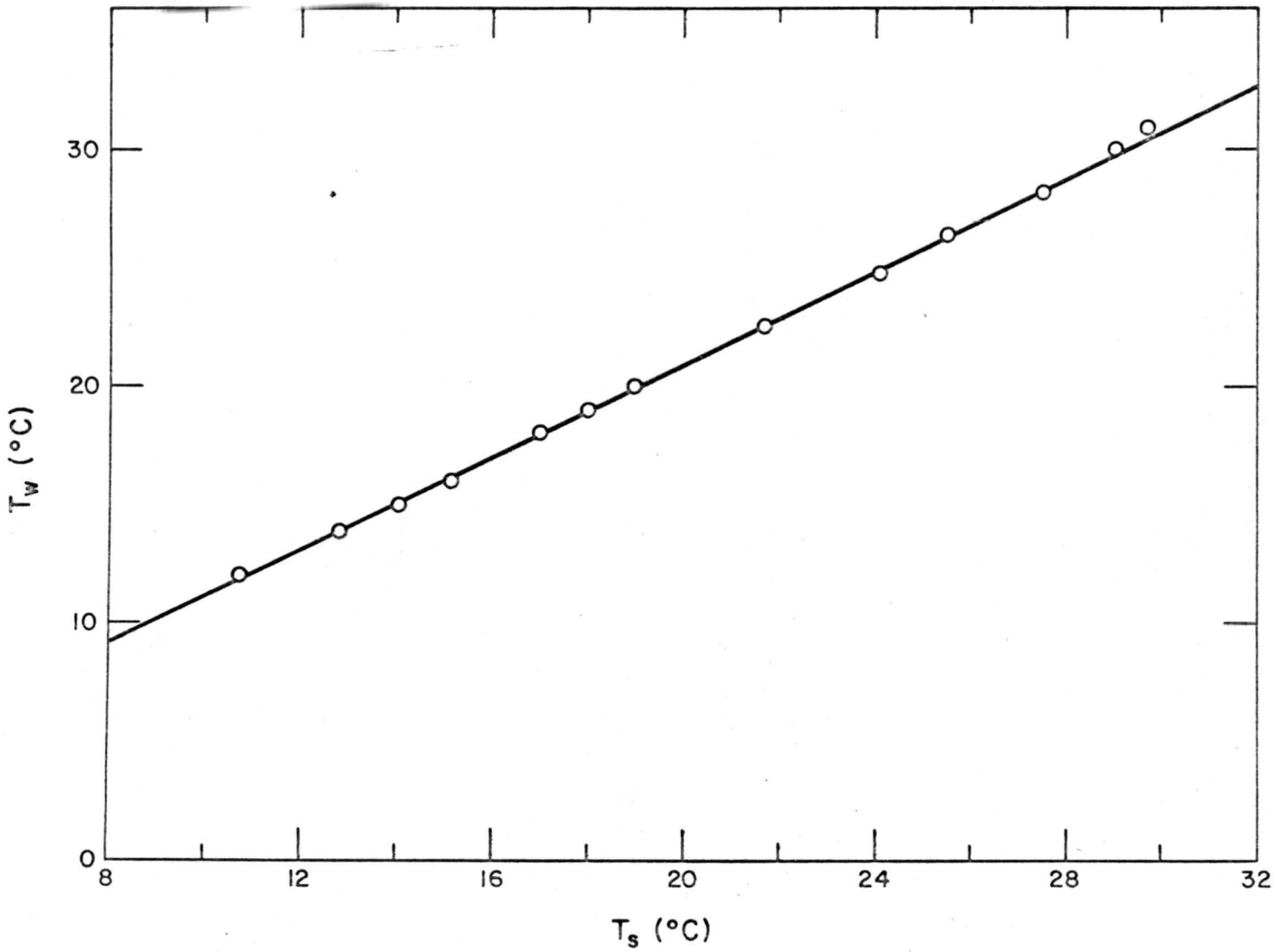

Fig. 6. Calibration curves of water surface temperature.

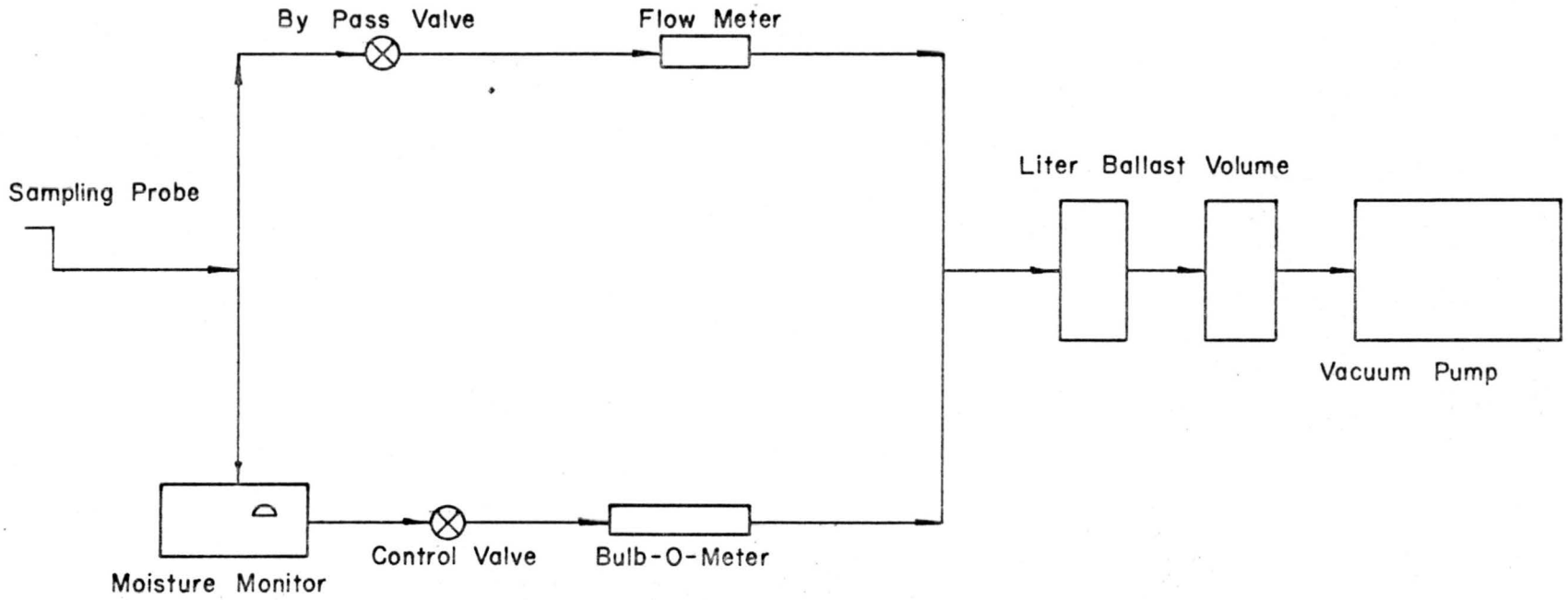

Fig. 7. Schematics of arrangement for measuring humidity.

moisture. The bypass value was used to maintain a large flow rate to insure stable operation, while only small samples of gas were passed into the moisture monitor. A soap film type flowmeter (a "bubble-o-meter") and a valve were used to maintain a constant flow rate through the moisture monitor. Two one-liter ballast volumes in the outlet line smoothed the pulsating motion caused by the vacuum pump.

The moisture monitor offered a practical measure of trace water in the gaseous mixture, since the instrument's electrolytic cell is used specifically to measure water moisture. The electrolytic cell contained two platinum wires, the space between was coated with phosphorous pentoxide (P_2O_5) which is a strong desiccant. When water vapor wetted the P_2O_5, a potential applied to the wires changed, producing a measurable electrolysis current. This current is directly proportional to the mass flow rate of water vapor into the cell. Electrolysis of the water absorbed in the P_2O_5 continuously regenerated the cell, thus permitting it to continuously measure all the moisture in the sample stream.

The CEC moisture monitor used to detect low moisture contents was designed to operate at a constant flow rate (i.e. V=100 cm^3/min.). The instrument's range of application was extended to higher moisture contents by reducing the flow rate. This was done by by-passing the pressure

regulator of the monitor and replacing it by the bubble-o-meter flowmeter circuit described above. The instrument was calibrated for use at different flow rates by the following procedure. A flow of constant humidity was conducted through the moisture monitor and the flow rate was decreased in steps. The relationship between flow rate and apparent moisture content obtained in this manner is shown in Fig. 8. It is seen that the relation $V_1/V_2 = (ppm)_1 / (ppm)_2$ holds for whole testing range. The true moisture contents $(ppm)_2$ can be expressed as:

$$(ppm)_2 = (ppm)_1 \times 100/V_1$$

where $(ppm)_1$ is the meter reading at flow rate V_1 = 100 cm^3/min. Through most of experiments of this study, the flow rates were reduced to 10-15 cm^3/min. Only in two cases, in which the water temperature and wave height were largest, the flow rates were reduced to 3 cm^3/min. The humidity data used were differences between local humidity in the boundary layer and that of the free stream gas. In this manner some of the systematic error due to the errors in the low-flow-rate measurements are cancelled. The response time of the moisture monitor was found to be less than 30 seconds (approximately 63% in 30 seconds to a step change in either direction). A stable reading was obtained by taking the reading at each point at least two minutes after the probe had been positioned and the flow through the meter adjusted.

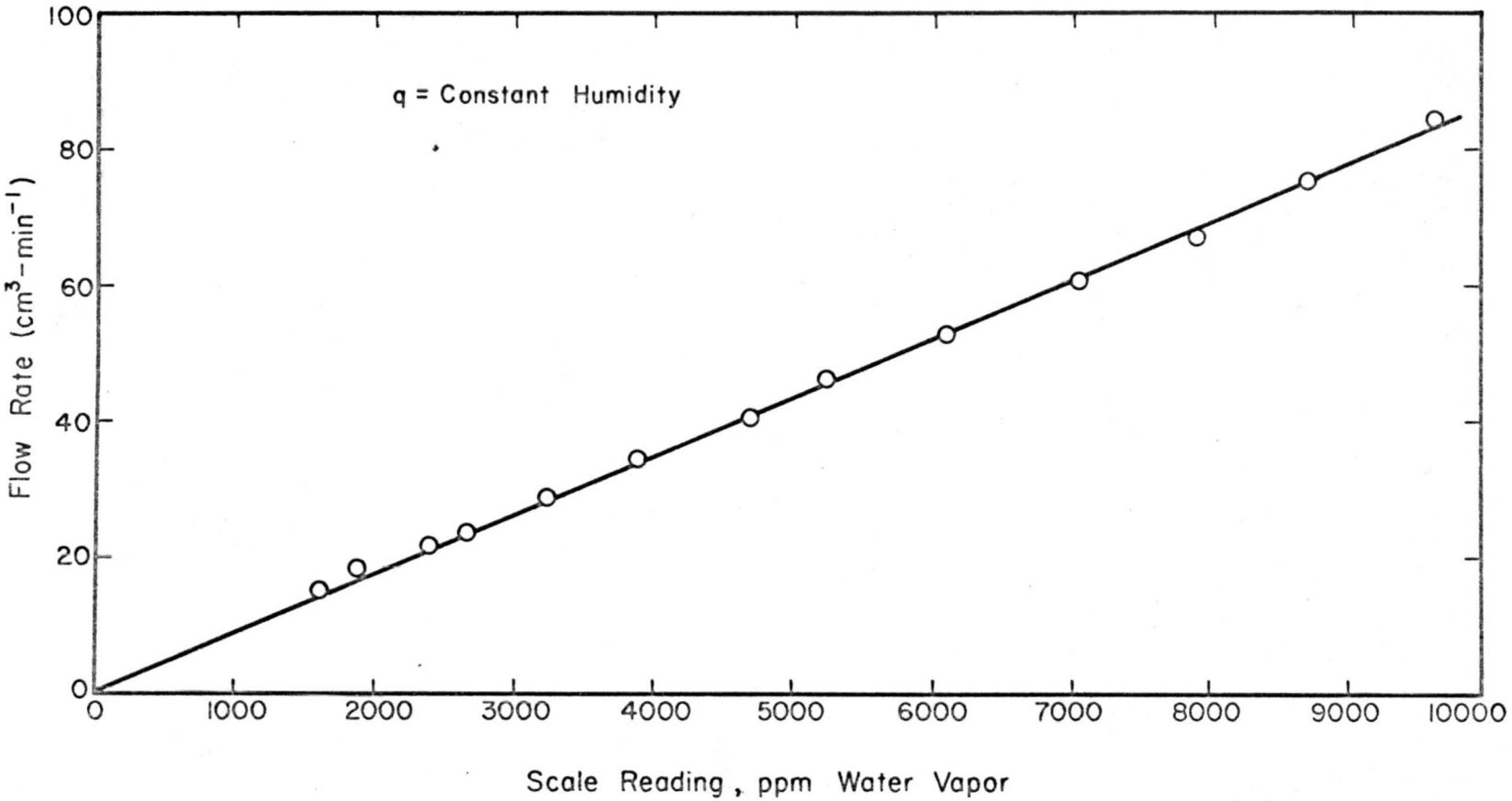

Fig. 8. Reading of ppm water vapor on moisture monitor.

The output reading of the moisture monitor was in part per million (ppm) of water particles by volume. For convenience, ppm was transformed to specific humidity by the relation:

$$q = (\text{ppm}) \times \frac{18}{29} \times 10^{-6} \left[\frac{\text{gm of water}}{\text{gm of dry air}}\right] \quad . \qquad (4\text{-}2)$$

The above equation came from the definition of q and ppm.

4.3 Experimental Procedure

Local measurements of mean velocity, temperature, and specific humidity of air were simultaneously taken by a Pitot-tube, thermocouple, and sampling tube for conditions of steady flow. To achieve such conditions for a case where the water was cooler than air, the following procedure was used.

The tunnel was allowed to operate at a normal air flow for two or three hours. During this period, the water temperature would stop decreasing as a result of evaporative cooling and stay at a nearly constant value, deviating between $\pm$ 0.1°C from an average value. The deviation was caused by room temperature fluctuation. This case was defined as the "cold-water condition," where T_w = 12° ~ 15°C and T_∞ = 20° ~ 25°C. Under such a condition, $\partial T/\partial z$ is positive, and stratification in air flow is stable. When the air temperature was lower than the water temperature, it was difficult to achieve stable temperatures, because of the limited heating capacity of the water channel.

The following procedure was used to slow the temperature drop during the experimental time period. First, the water was heated to about 38°C, and the fan was started to blow air over the water surface for five to ten minutes. The fan was stopped, and the water was heated again. After repeating this process several times, the temperature of the water throughout the channel was very uniform. During one run of the experiment, it would drop 1° ~ 2°C. This case was defined as the warm-water condition, where $\partial T/\partial z$ was negative, and the air flow unstably stratified. The warm-water cases were chosen as $T_w = 27° \sim 34°C$ and $T_\infty = 20° \sim 25°C$.

During all operations, the water level decreased gradually due to the evaporation, and a gap between the aluminum plate and the water surface developed. To maintain a condition of steady flow, it was then necessary to add water (cold or warm) continuously into the channel to keep the water surface depth at $x = 0$, within 0.2 mm of the same depth. This would assure the same boundary condition at a discontinuity line between the solid and the liquid, as well as a satisfactory smooth transition from the plate onto the water surface.

The velocity, humidity, and temperature distribution profiles were obtained for three different series of experiments. First, the data were collected simultaneously for T, $\bar{u}$ and $\bar{q}$ at different downstream positions (x = 56 cm,

112 cm, 214 cm, 460 cm, 778 cm) with different reference velocities (v_f = 4.17 m/sec. 5.64 m/sec, 6.89 m/sec) for the cold-water case. For the warm-water case, the data were collected simultaneously for T, $\bar{u}$ and q at different downstream positions (x = 116 cm, 214 cm, 460 cm, 610 cm) with a moderate temperature difference of $T_s - T_\infty$ = 5° ~ 8°C and then with a small temperature difference of $T_s \sim T_\infty$ = 1° ~ 3°C. For the cold-water case, a third series of experiments was carried out at a fixed fetch of x = 610 cm with a variation of air velocity corresponding to v_∞ = 8 m/sec, 8.8 m/sec, 9.9 m/sec, 12.1 m/sec, and 13.3 m/sec.

The three measuring instruments were set parallel on the carriage 2 cm apart. The carriage was lowered close to the mean water surface, yet far enough away to avoid the instrument being hit by splash of the highest waves. The measured vertical distance from the mean water surface was set equal to z for all calculations. The carriage was raised step-by-step, and measurements were taken after each step until all instruments indicated an output which was independent of height. Then, it was lowered again, step-by-step to reach the initial vertical position. The lowest values of z were measured before and after each run to the vertical displacement. The step-by-step method with a sampling period of two minutes would give enough time for the moisture monitor and the thermocouple to respond. The measurements close to the water surface were taken with 0.5

cm period at different heights. The distance was increased away from the water surface. Eight points per run were taken when the carriage neared the leading edge and increased to fifteen points in downstream position. Finally, after each series of experiments, a recording of the waves was taken on a strip chart recorder.

Chapter V

RESULTS

5.1 Properties of the Water Surface

The properties of the water surface are important factors affecting the evaporation by increasing the apparent surface area, and by changing the air flow near the surface. The characteristics of the surface waves can be determined experimentally from the wave records. The results of typical statistical computation for the water surface displacement were the standard deviation, σ, wave energy spectrum, $\phi(f)$, and frequency, f_m, of the spectral peak. The values of σ and f_m represent the geometric properties of significant waves. The wave energy spectrum $\phi(f)$ is the Fourier transform of the autocorrelation function of the water surface displacement. The values of σ and f_m are given in Table I.

To compare cold- and warm-water cases, the variations of σ, f_m, and u_∞ with fetch are shown in Figure 9, and the effect of u_* on f_m and σ at a fixed position, x, is shown in Figure 10. For the cold-water case, the standard deviation σ was found to increase linearly at a fixed downstream position with friction velocity u_*, and also with fetch x. The peak frequency f_m did change rapidly at small values of x and u_*, but its variation was smaller for the larger values of x and u_*.

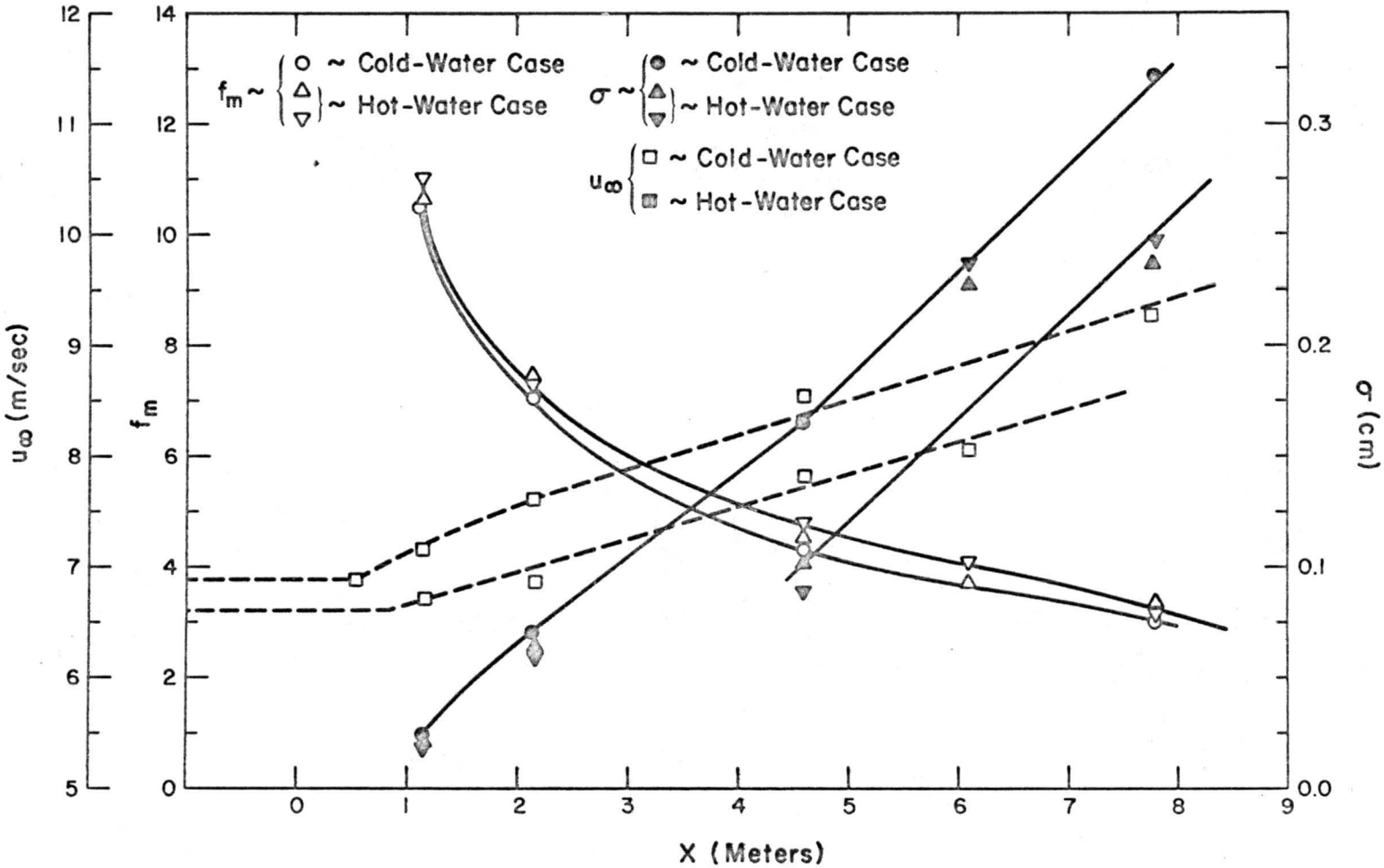

Fig. 9. Variation of σ, f_m and u_∞ against fetches.

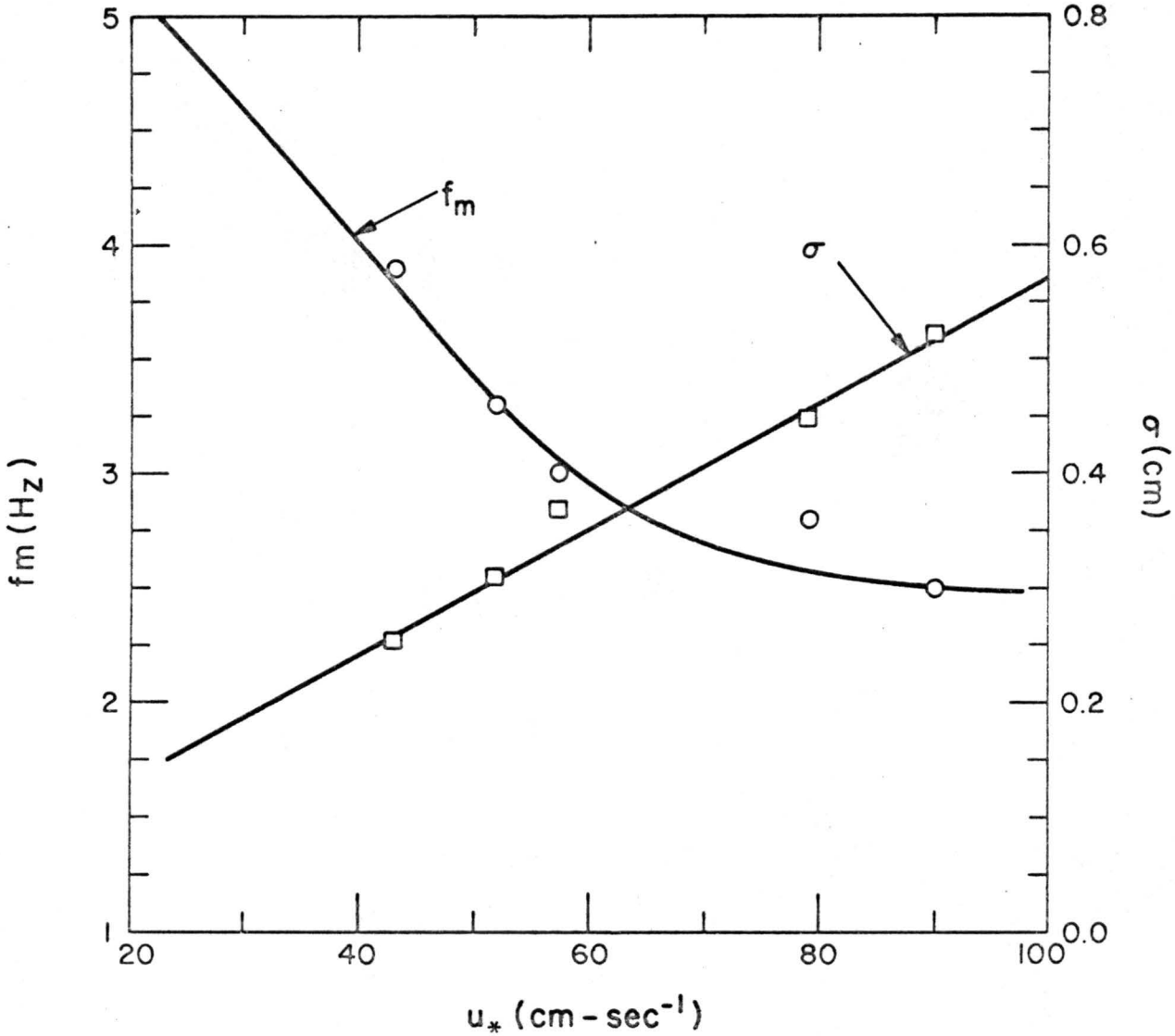

Fig. 10. Variation of σ and f_m with u_* at constant free stream velocity.

The effect of x and u_* on σ and f_m has been shown in Figures 9 and 10. The effect of temperature difference between air and water on wave geometry is shown in Figure 11. However, due to the limited capacity of the heating facility of the wind-water channel, the equilibrium for the warm-water cases was hard to reach. So the data of cold-water cases were adjusted to compare with warm-water cases. In Figure 11, the values of u_* of both cases are identical. This was accomplished by using the relation of Figure 10 to reduce the values of σ and f_m of cold-water cases until both cases had the same value of u_*. The data in Figure 11 showed that in warmer water, a lower frequency f_m is found at $x > 3$ m. Also, the standard deviation, σ, is larger with the exception of two stations, $x = 460$ cm and $x = 778$ cm.

The wave energy spectra of wind waves, as described in Chapter IV, are shown in Figures 12, 13, 14, and 15 for different conditions. In the spectral diagram the difference between cold- and warm-water cases is difficult to distinguish. The peak spectra f_m, of course, decreases with increasing friction velocity u_*, as determined from other work (for example, Hidy and Plate, 1966). An f^{-5} law for $\phi(f)$, which was suggested by Phillips (1966) to show the equilibrium range of the gravity waves, can be applied to the data to describe the slope of the envelope to all the spectral curves. However, beyond the peak, the value of

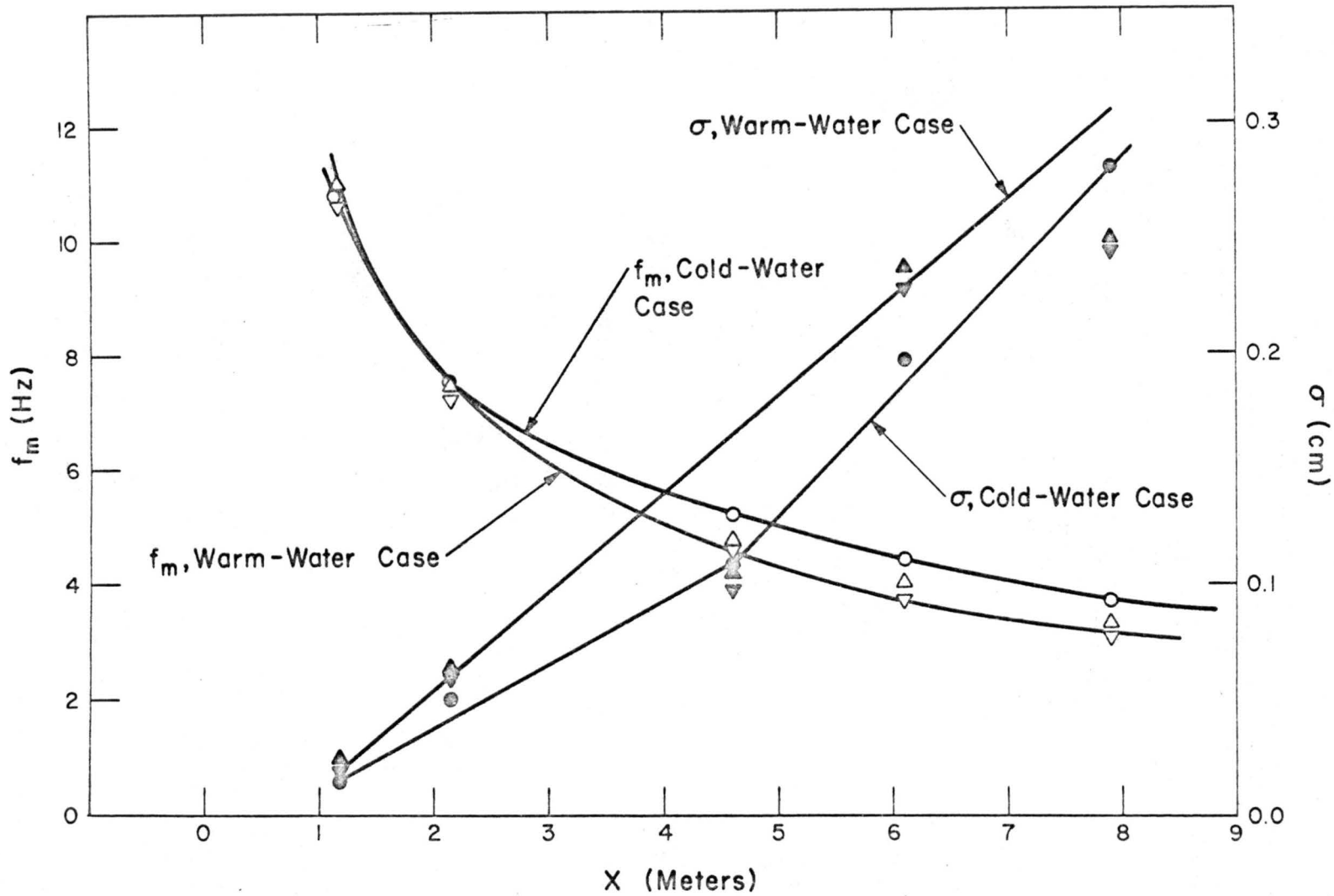

Fig. 11. Thermal effect on σ and f_m.

$\phi(f)$ decreased following a f^{-7} law up to $f = 2 f_m$. For large values of $f (f > 2 f_m)$, $\phi(f)$ tends to follow a slope more like f^{-4} than f^{-5}. At the extreme range of f, an $f^{-7/3}$ law seems to fit the results. This latter slope was suggested for ripples of $f \geq 13$ Hz by Hicks (as quoted by Phillips, 1966) as an equilibrium range for pure capillary waves. All the results of the amplitude spectra of wind waves indicate the consistent agreement of results of this experiment with those of previous works such as Plate et al. (1968), and Chang (1968). The data further suggest that there is no detectable thermal effect on frequency spectra. In wave energy spectra of cold- and warm-water cases for $f > 13$ Hz, the effect of capillary becomes a primary influence on wave behavior. The temperature showed no effect on the break frequency from gravity wave behavior to capillary wave behavior.

5.2 Air Flow

The measured velocity distributions above aluminum plate and water surface are shown in Figures 16, 17, and 18 for cold- and warm-water cases. At the same reference velocity, the free stream velocity u_∞ increased in the downstream direction. This was due to a favorable pressure gradient along the positive x-direction. This was due to a favorable pressure gradient along the positive x-direction in the channel. The boundary conditions at the water surface are given in Table I. The dimensionless velocity

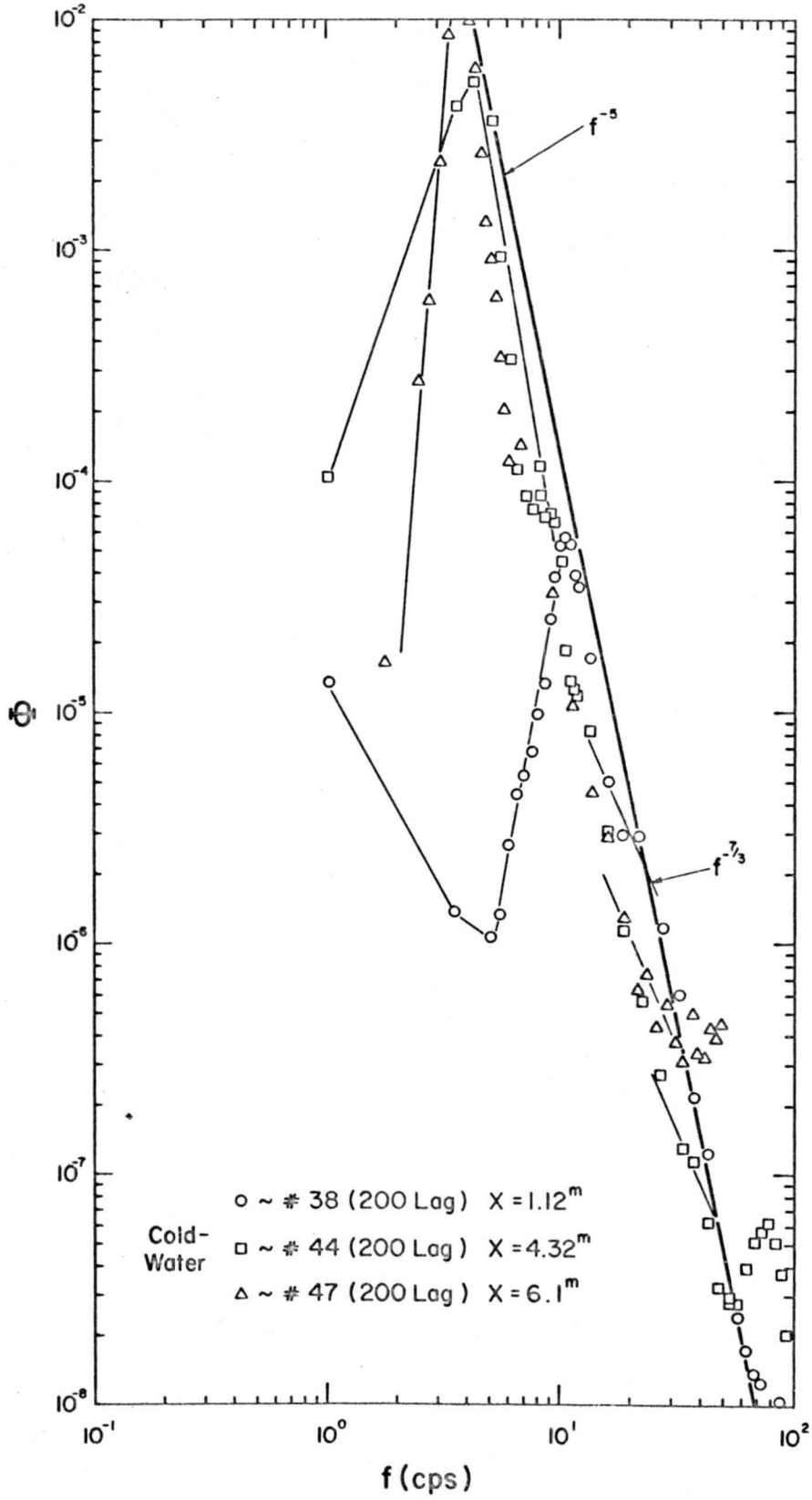

Fig. 12. Spectra diagram of water waves at different fetch, different air velocities and air-water temperature difference.

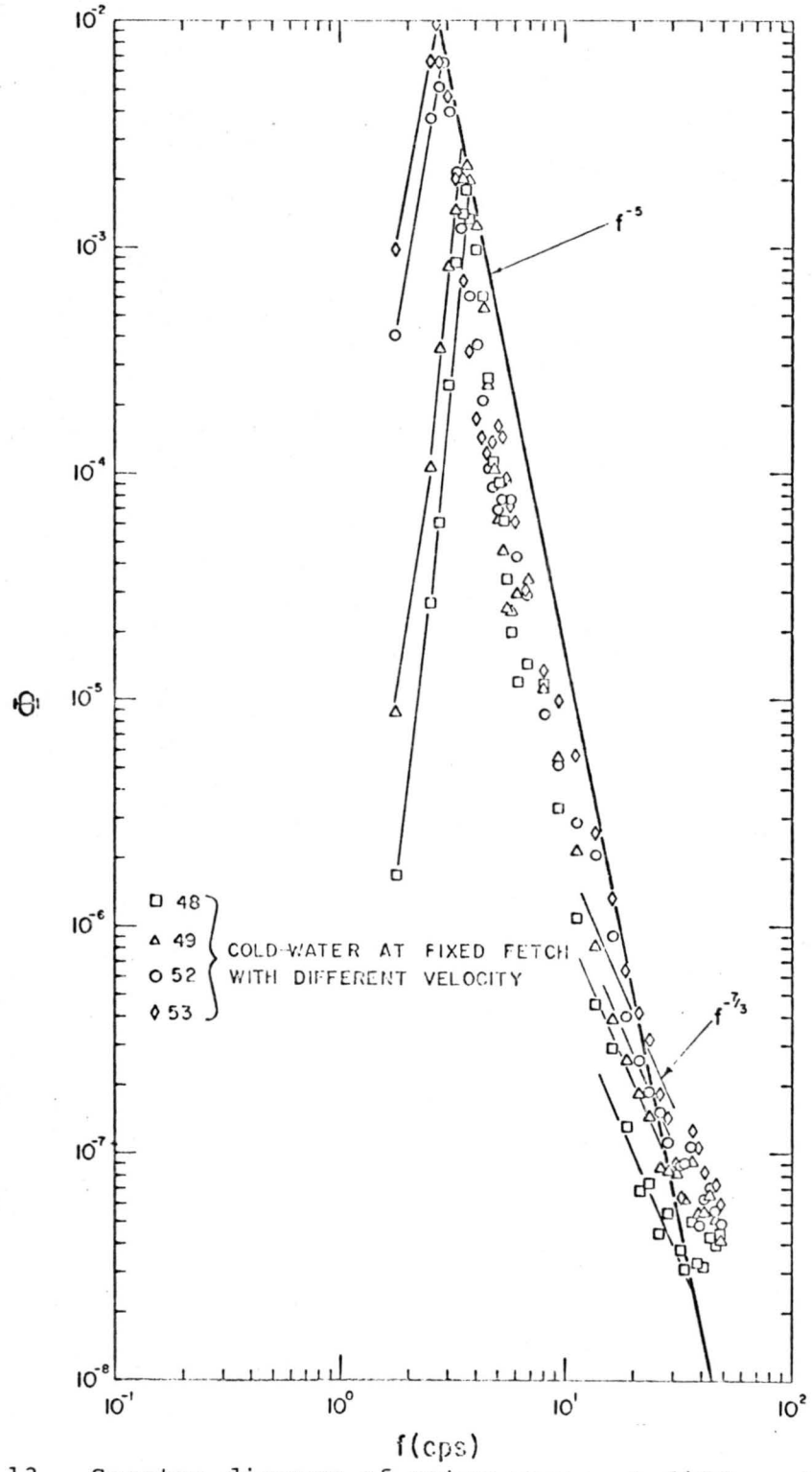

Fig. 13. Spectra diagram of water waves at different fetch, different air velocities and air-water temperature difference.

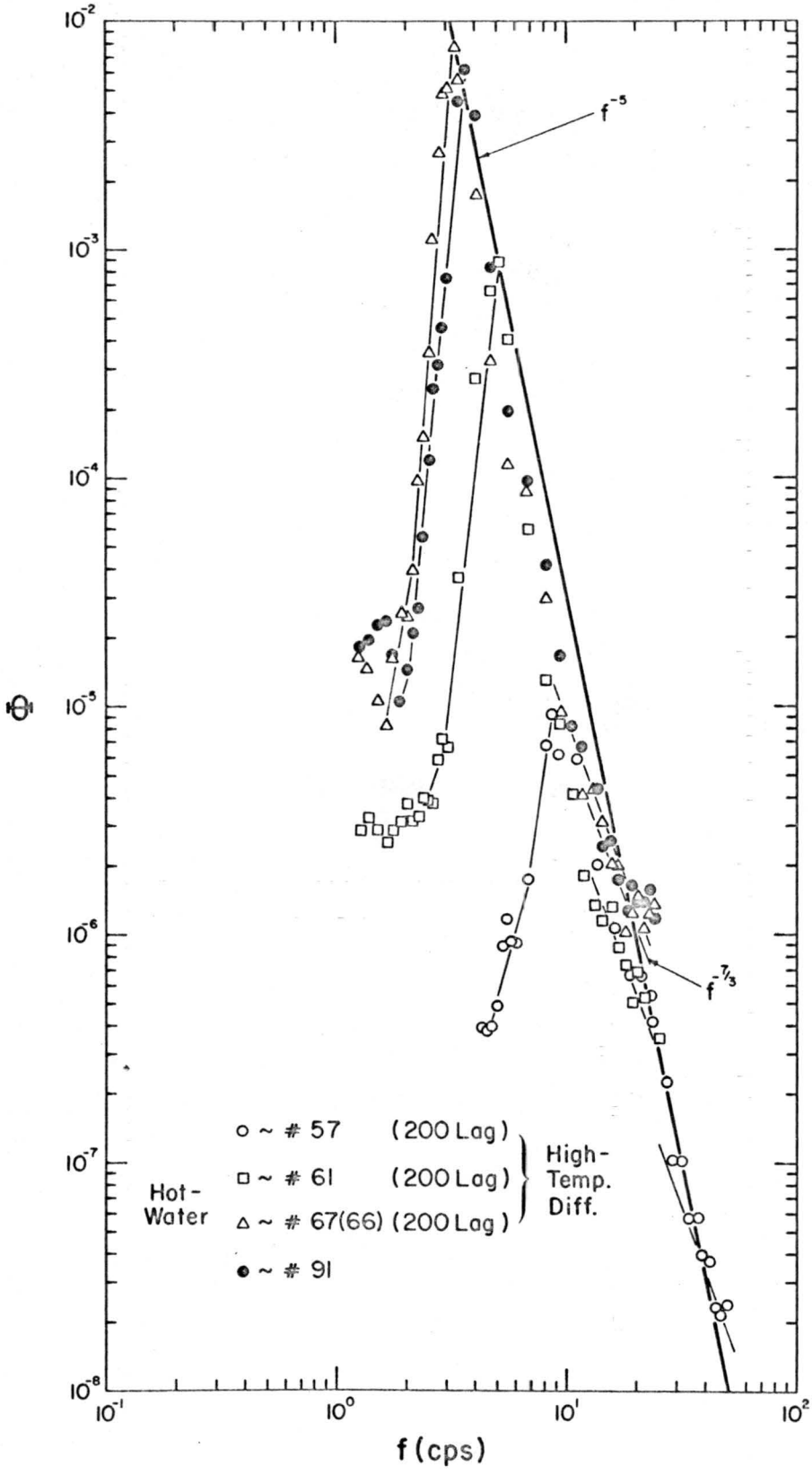

Fig. 14. Spectra diagram of water waves at different fetch, different air velocities and air-water temperature difference.

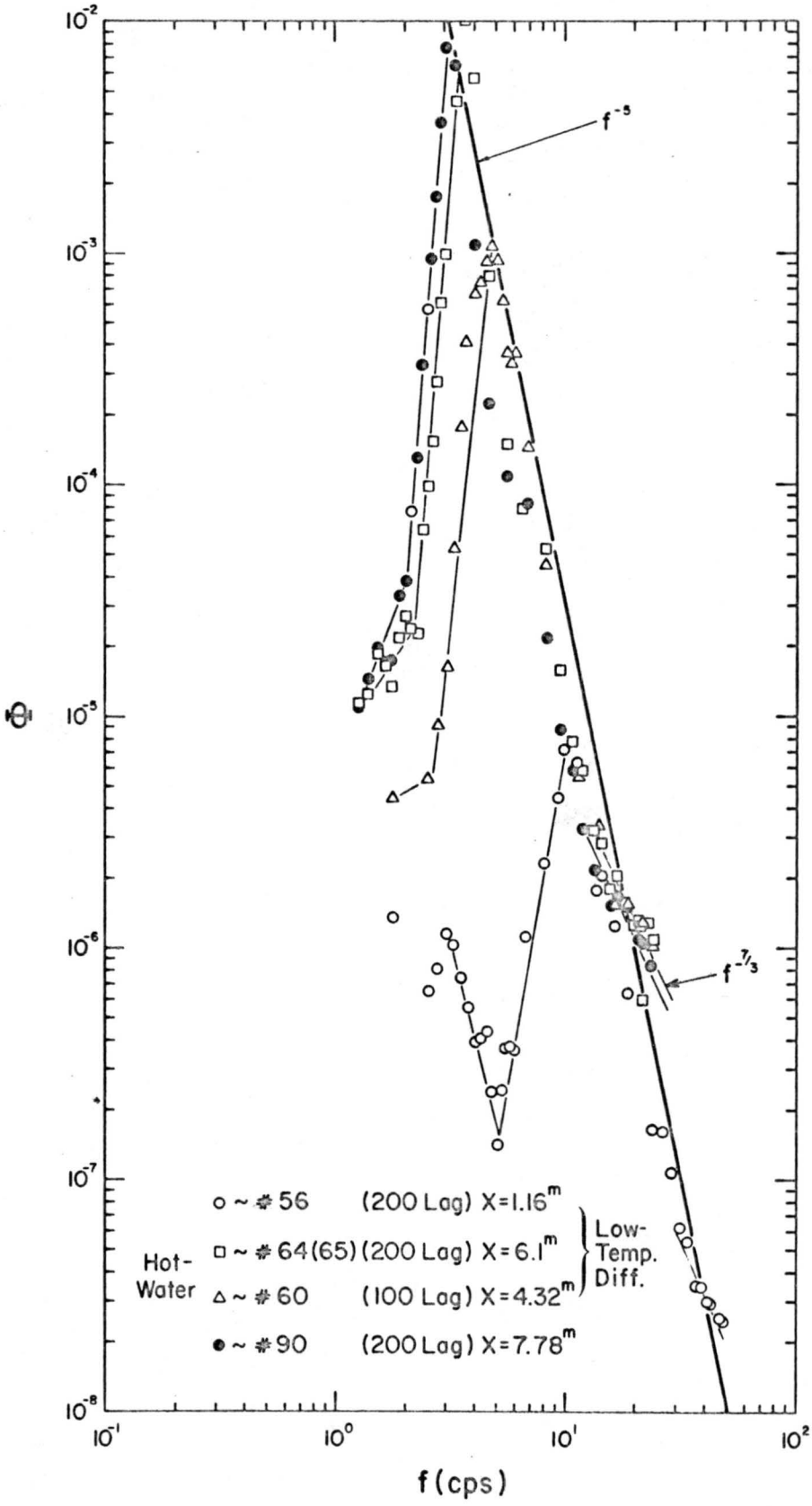

Fig. 15. Spectra diagram of water waves at different fetch, different air velocities and air-water temperature difference.

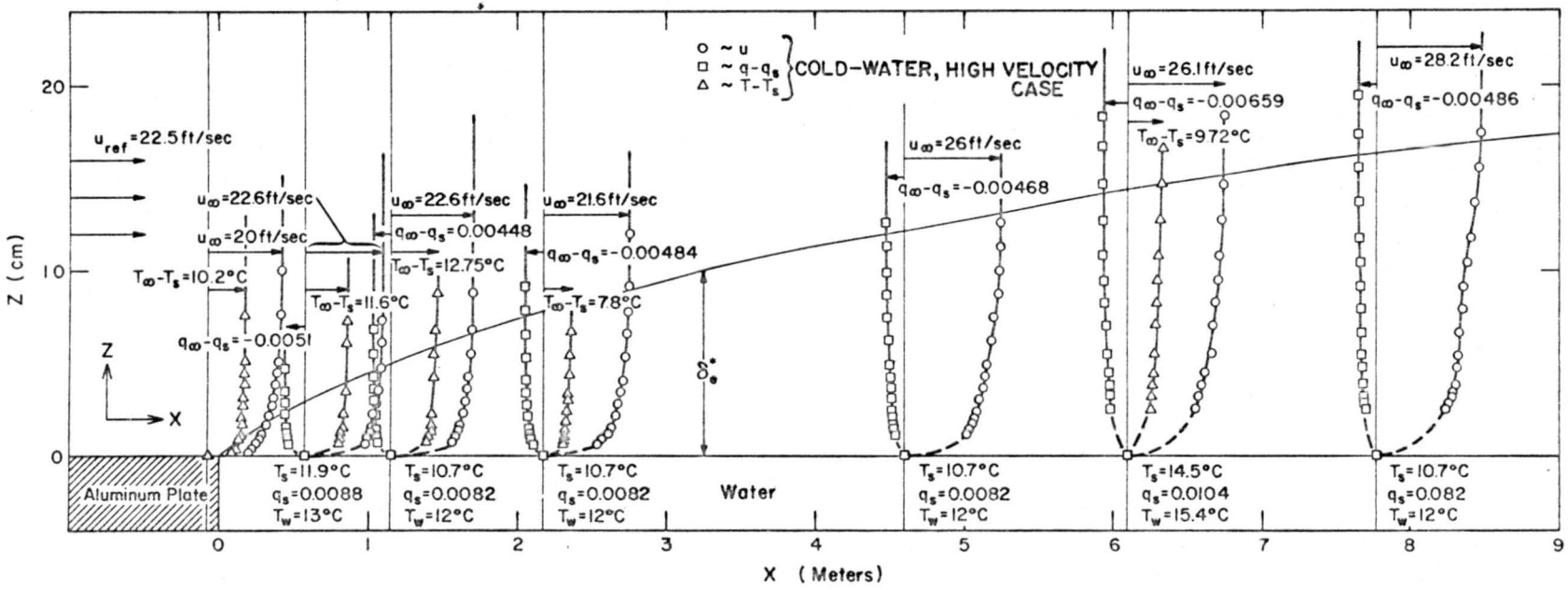

Fig. 16. Measured velocity, temperature and humidity profiles against fetch for cold and warm water cases.

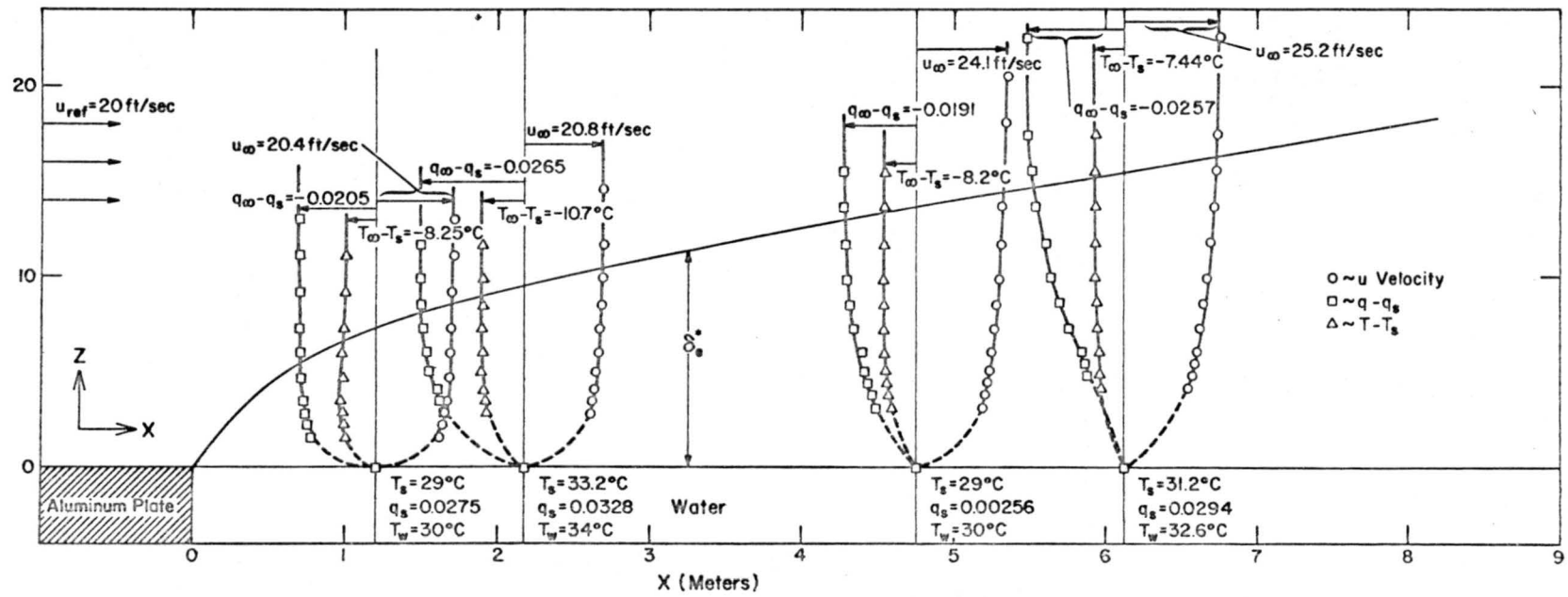

Fig. 17. Measured velocity, temperature, and humidity profiles against fetch for cold and warm water cases.

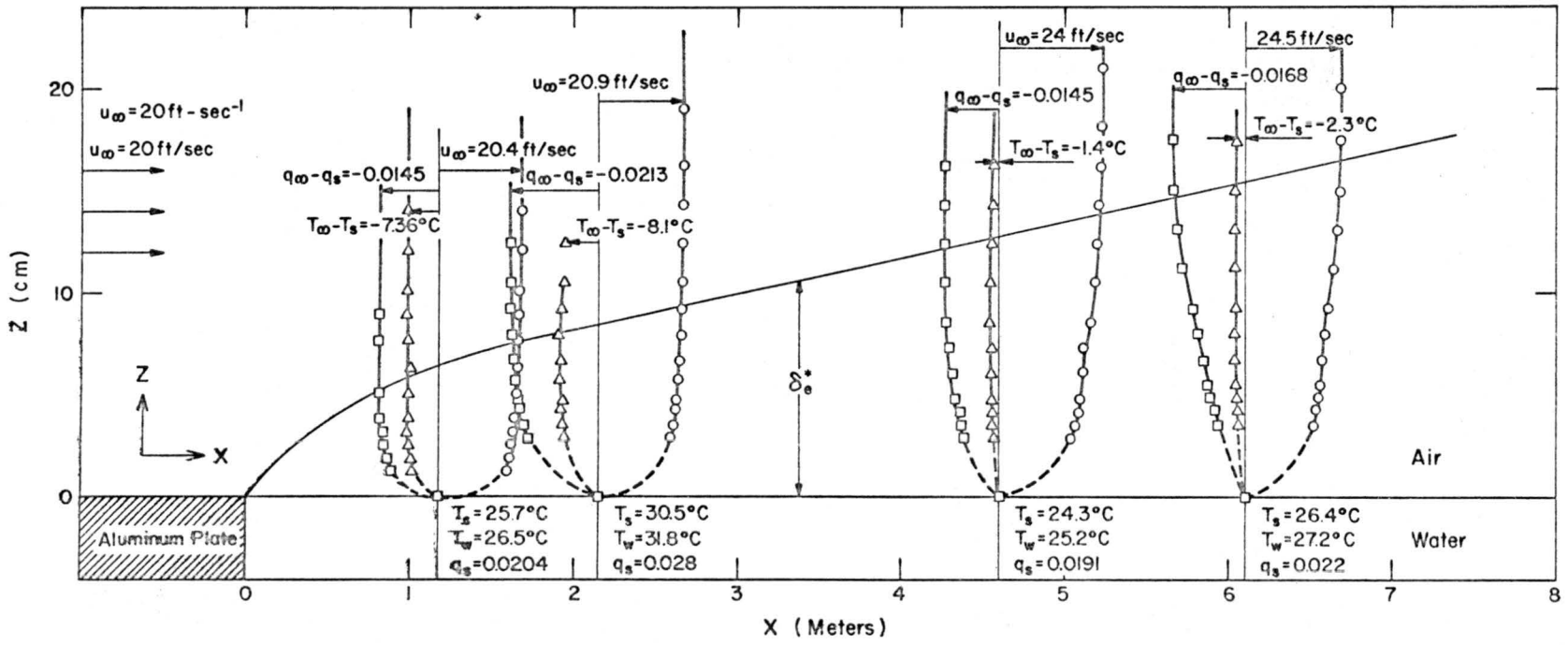

Fig. 18. Measured velocity, temperature, and humidity profiles against fetch for cold and warm water cases.

profiles $(\frac{u}{u_\infty})$ for different fetches are shown in Figures 19 and 20. Like other data taken in the CSU tunnel, all of these profiles also can be correlated satisfactorily by the law of the wall (Eq. 2-1).

In this study, the values of u_* were obtained from the velocity profiles by the following method using two levels of an assumed logarithmic distribution:

$$\frac{u_1}{u_2} = \frac{u_*}{k} \ln \frac{z_1}{z_2} , \qquad (5\text{-}1)$$

where u_1 and u_2 are velocities at z_1 and z_2 which lie in the logarithmic part of the distribution curve. The values of u_* found in this manner are given in Table II. For the fully developed rough flow defined by the regime beyond $\sigma > 0.15$ cm, the values of u_* are also given by an empirical formula given by Hidy and Plate (1967) who combined their findings with earlier results of other workers:

$$u_* = 0.0185\ u_\infty^{1.5} \text{ (cm/sec)}. \qquad (5\text{-}2)$$

Values of u_* determined by use of Equations (5-1) and (5-2) agreed within $\pm$ 5%.

The variation of friction velocity with fetch is plotted in Figures 21 and 22, the curves showing that the friction velocity changes mainly with the free stream velocity and only to a small degree with the temperature difference $(T_s - T_\infty)$. Compared with the previous work of Plate and Hidy

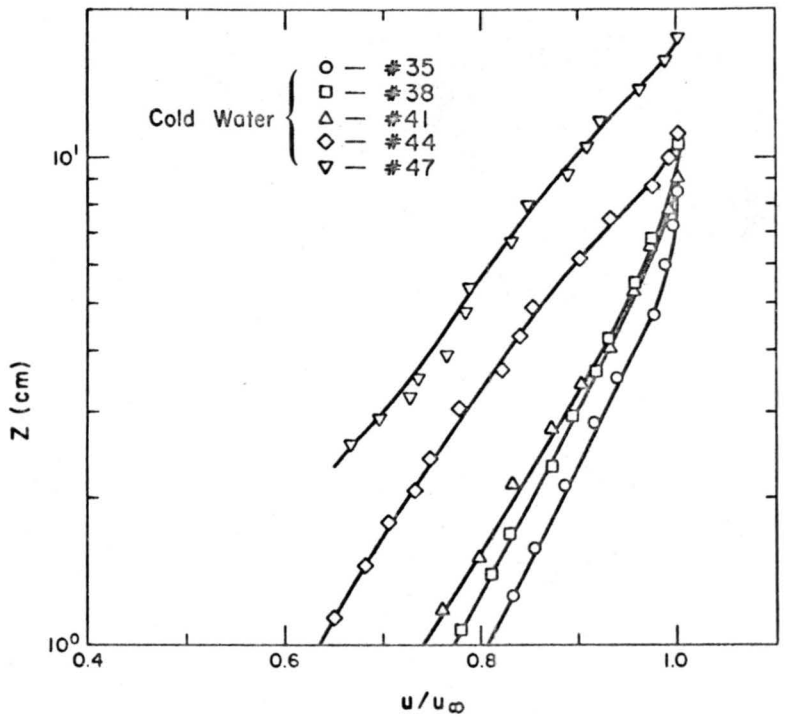

Fig. 19. Vertical velocity profiles of air at different downstream positions of cold and warm water cases.

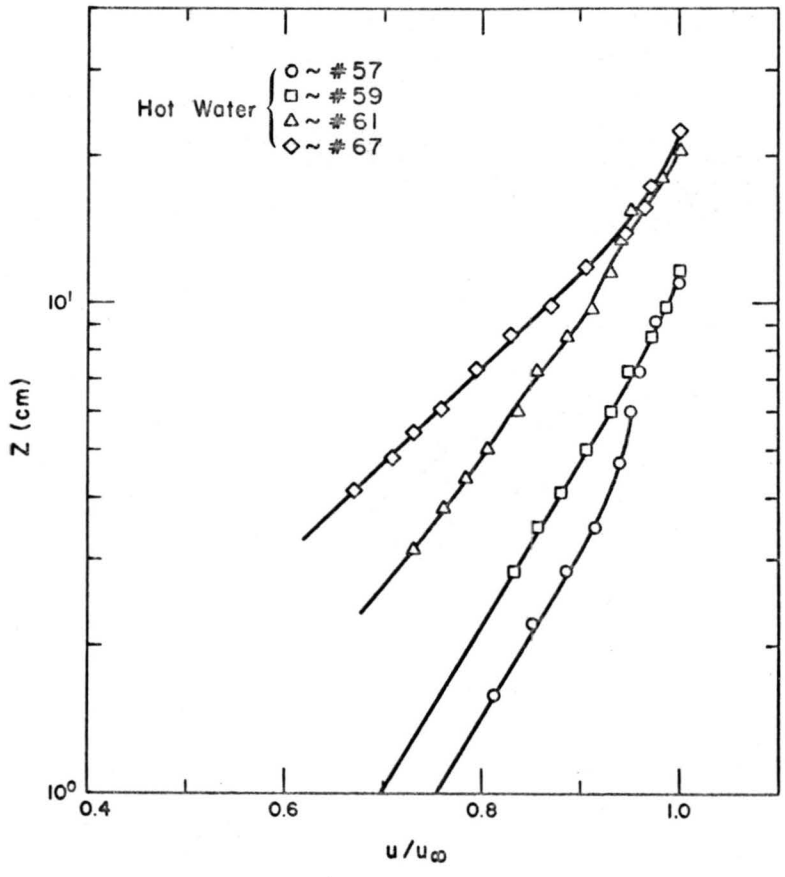

Fig. 20. Vertical velocity profiles of air at different downstream positions of cold and warm water cases.

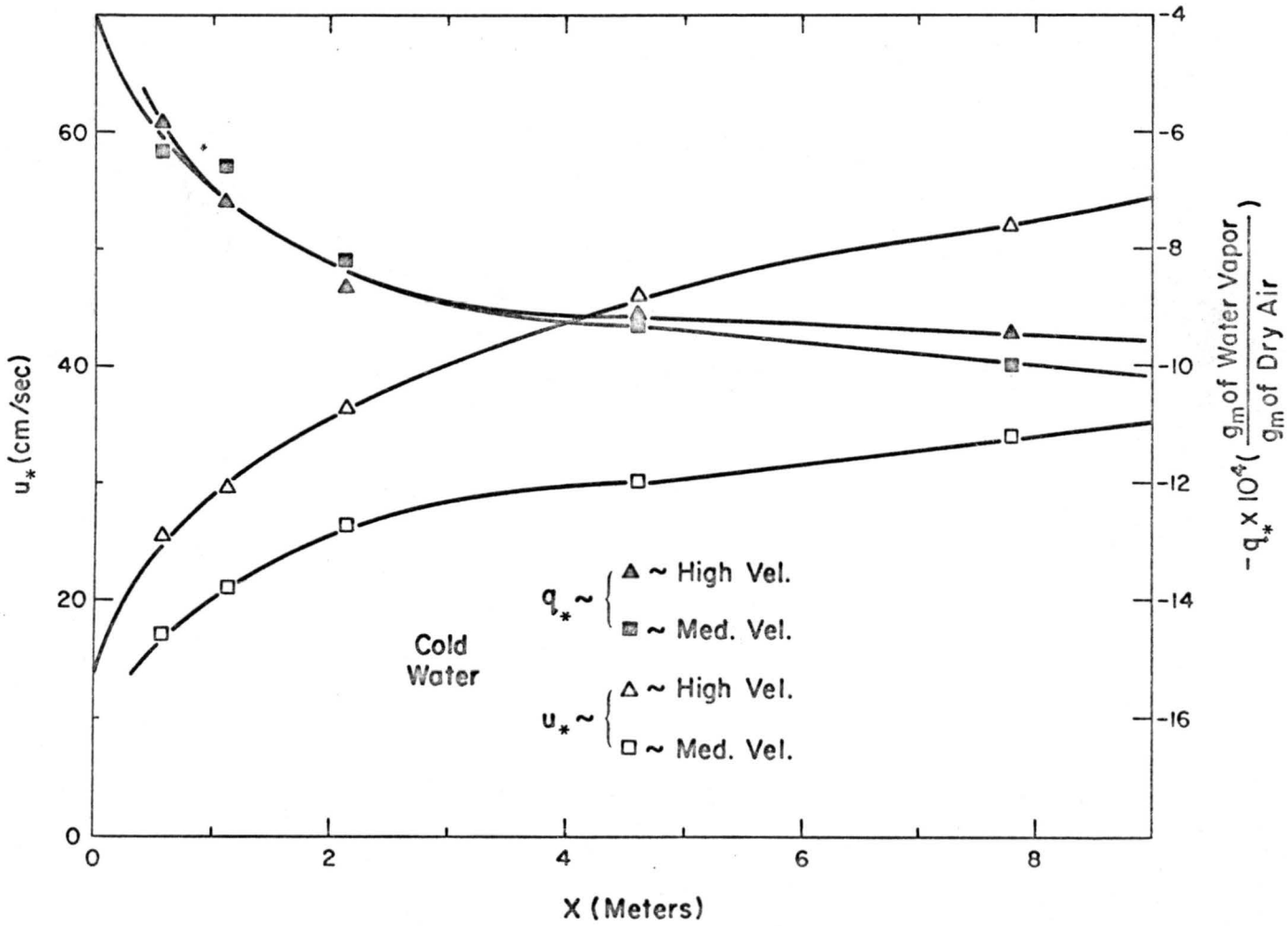

Fig. 21. Variation of u_* and q_* at different downstream position of cold and warm water cases.

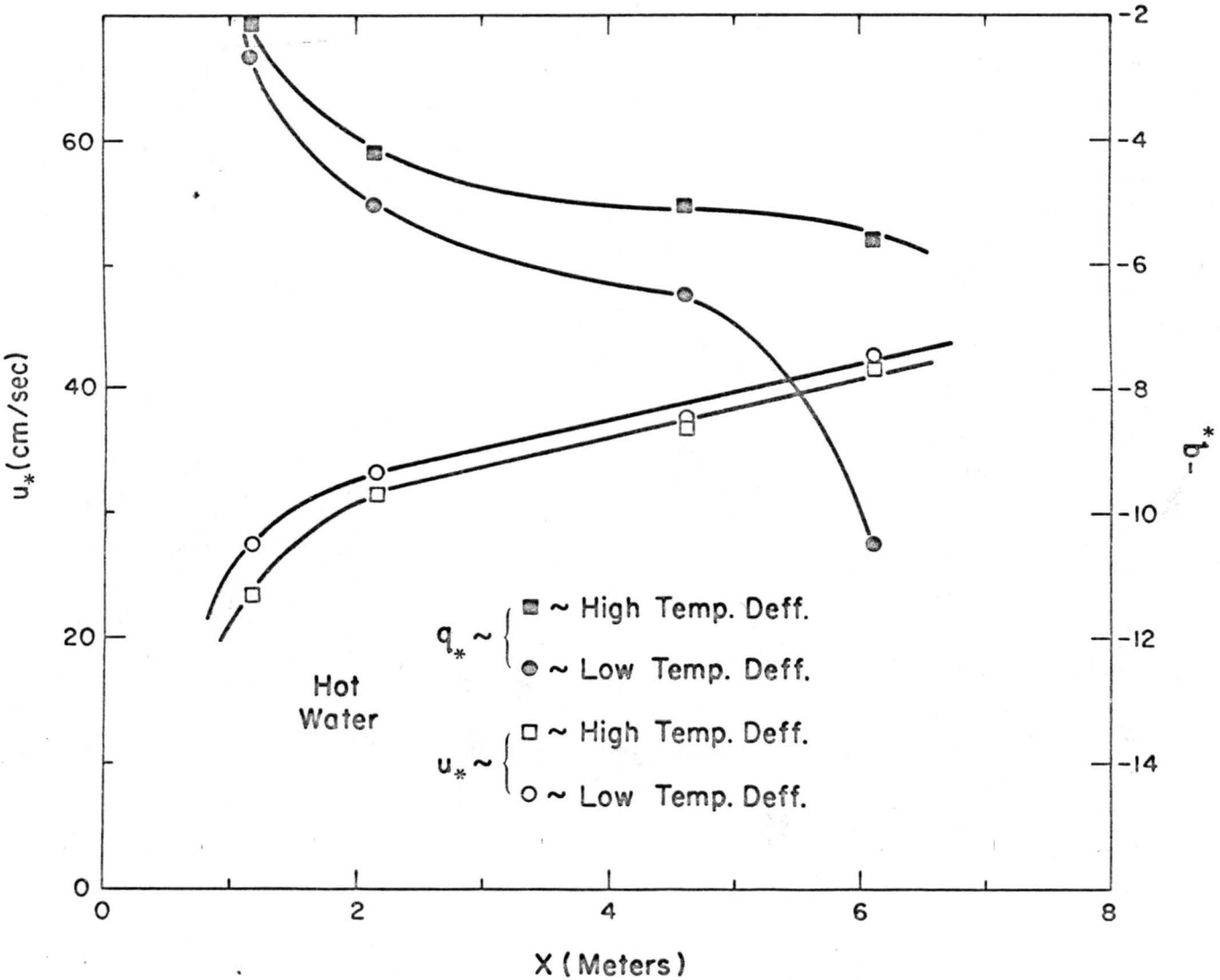

Fig. 22. Variation of u_* and q_* at different downstream position of cold and warm water cases.

(1967), u_* showed a more gradual change from aluminum plate to the wavy surface, probably because the free stream velocity in this experiment was smaller than in the previous one. An increased free stream velocity tended to increase the sharp change of u_* at the transitional zone near $x = 0$.

The values of z_o were obtained from Equation (2-1) after the values of u_* had been obtained from Equation (5-1). Numerical values of z_o for each run are given in Table II. According to Hidy and Plate (1966), the values of roughness length over small water waves, z_{o2}, can be correlated empirically with a Reynolds number $Re_\sigma = u_*\sigma/\nu$ based on friction velocity and the standard deviation of the waves. Hidy and Plate reported an empirical formula for z_{o2} at short fetch e_s in a wind-water channel as:

$$z_{o2} = 1.4 \times 10^{-4} \left(\frac{u_*\sigma}{\nu}\right) . \qquad (5\text{-}3)$$

Such a correlation for this experiment is shown in Figure 23. It indicated satisfactory consistency between the experimental data at high and low free stream velocities of air, and earlier data of Plate and Hidy (1967). The correlation also held reasonably well for both warm- and cold-water cases. However, there may be a small difference related to a thermal effect on momentum transfer, which will be discussed in the next section.

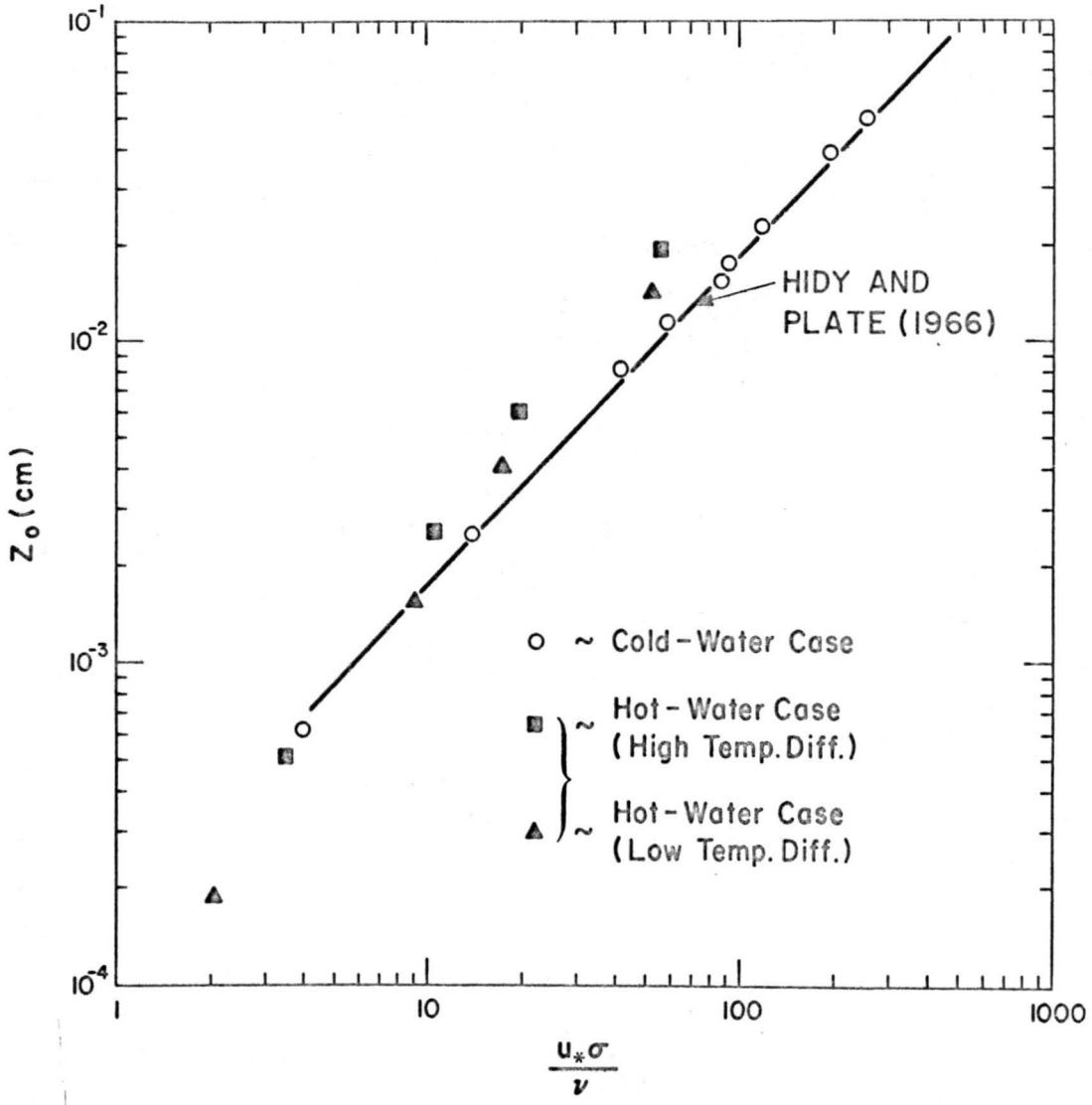

Fig. 23. Variation in aerodynamic roughness length with dimensionless ratio $u_* \sigma / \nu$.

5.3 Mean Temperature

The vertical temperature distributions are also shown in Figures 16, 17, and 18 over the different fetches. The temperature profiles have been modified by assuming that the thermal boundary layer had the same thickness as the concentration boundary layer, thus avoiding the temperature gradient caused by elevation in the building. During summer time, the temperature in the building increased about 1°C per meter in elevation. There was no constant temperature zone. In other words, the temperature, T_∞, was selected as the temperature at $z \geq \delta_e^*$, where δ_e^* indicated the thickness of concentration boundary layer. In the cold-water case, the tendency of increasing the gradient of temperature along the downstream direction was similar to the gradient of velocity. Thus, the tendency of increasing shear stress in downstream position was similar to the heat transfer. In the warm-water case, the temperature profiles near the $x = 0$ showed a small bump, the shape of which enlarged, then disappeared along the downstream direction. This may have been due to the effect on an outer boundary layer formed along the cold aluminum plate. The thermal conditions at the boundary are given in Table I. It is difficult to construct a dimensionless temperature profile in this experiment, since the temperature difference was small, and there were so many factors to influence such

a small temperature difference. For example, the free stream velocity, the wavy surface, evaporation rate, radiation and conduction all contributed to this transfer mechanism. For better results, further study is recommended.

5.4 Humidity Profiles and Evaporation Rates

The specific humidity at the water surface can be determined under the assumption that it is equal to the saturated humidity q_s at T_s, where T_s is the water surface temperature. With the value q_s at $z = 0$, the measured humidity profiles at the different fetches are shown in Figures 16, 17, and 18. In the cold water case, the gradient of the humidity profile, which showed the amount of mass transfer rate, increased slowly with x when x was small, but the gradient started to increase faster when x was large, indicating the effect of wind waves. In the warm-water case, the tendency was similar, except at $x = 610$ cm. At that particular point, the humidity difference between different height seemed linearly increasing with height.

Several vertical distributions of humidity at different heights are shown in semi-logarithmic form in Figures 24 and 25. Most of the data points form a straight line on this type of plot, indicating that a logarithmic profile seems to be a useful approximation for many of the humidity profiles. The application of the logarithmic profiles will be discussed in Chapter VI.

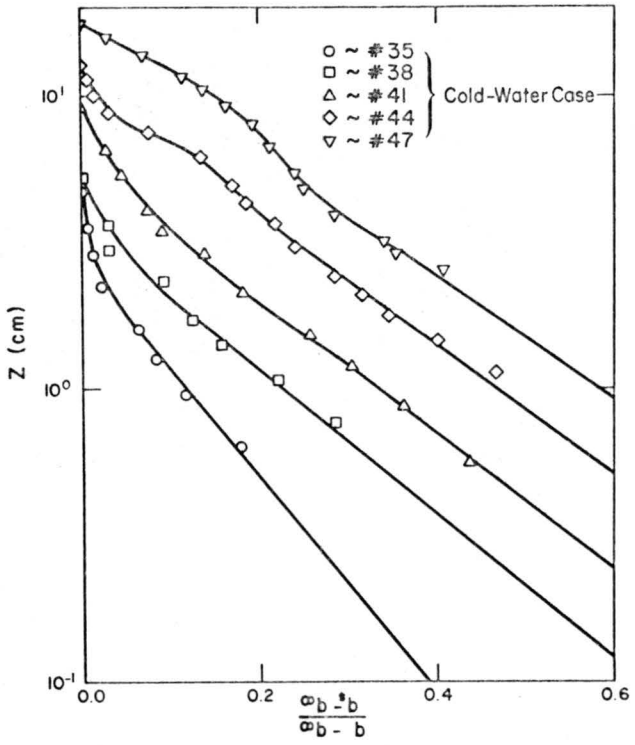

Fig. 24. Vertical specific humidity distribution for cold and warm water cases.

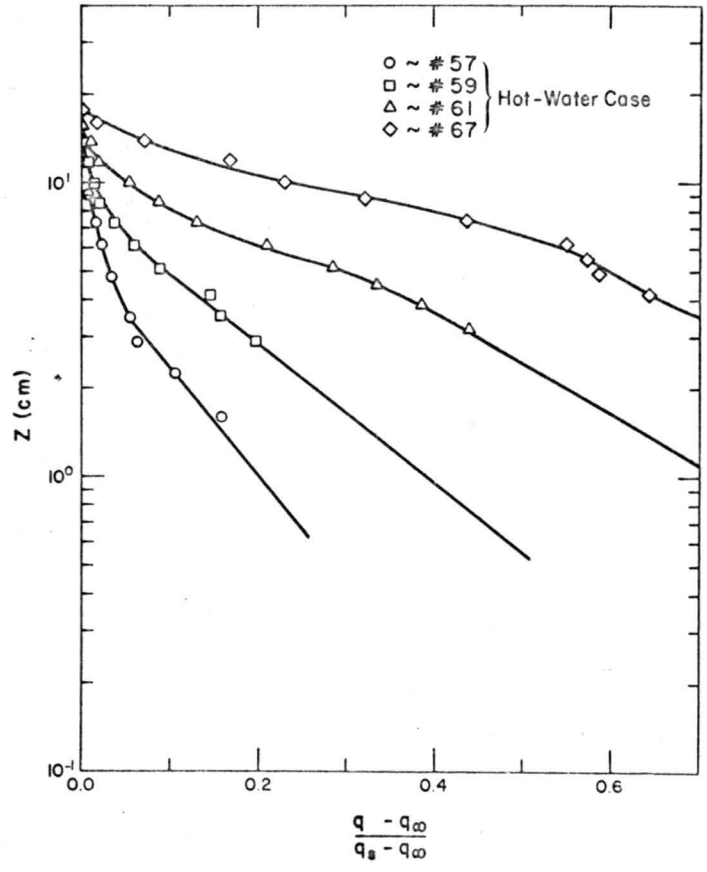

Fig. 25. Vertical specific humidity distribution for cold and warm water cases.

The evaporation rate, E, in $gm/cm^2/sec$ can be evaluated from the experimental data for $q(z)$ and $u(z)$ by considering a mass balance on a control volume in the air (Figure 2). By considering the mass flux in terms of such a volume and neglecting v_s at the surface (see Chapter II),

$$E = \rho \frac{d}{dx} \int_0^\infty u(z) \, [q(z) - q_\infty] \, dz \, . \qquad (5\text{-}4)$$

To find the experimental values of the evaporation rate from Equation (5-4), the values of $u(q - q_\infty)$ were plotted against z on linear paper. An optical planimeter (Milano Co., Type 236) was used to obtain the value of the integral. When z was small, it was not possible to obtain experimentally the data for q and u, so they were extrapolated according to logarithmic law to give q and u at small z. Some typical curves of this linear plot are shown in Figure 26. The values of E calculated by this method are given in Table III. The values of E decreased along the downstream direction until x is approximately 3 m, then the values of E increased. This indicates that the waves seemed to increase the evaporation rate in this experiment once their amplitude exceeded $\sigma = 0.1$ cm.

The thickness of the concentration boundary layer, δ_e^*, was defined as the value of z, where the local specific humidity difference was equal to $0.01 \times (q_s - q_\infty)$.

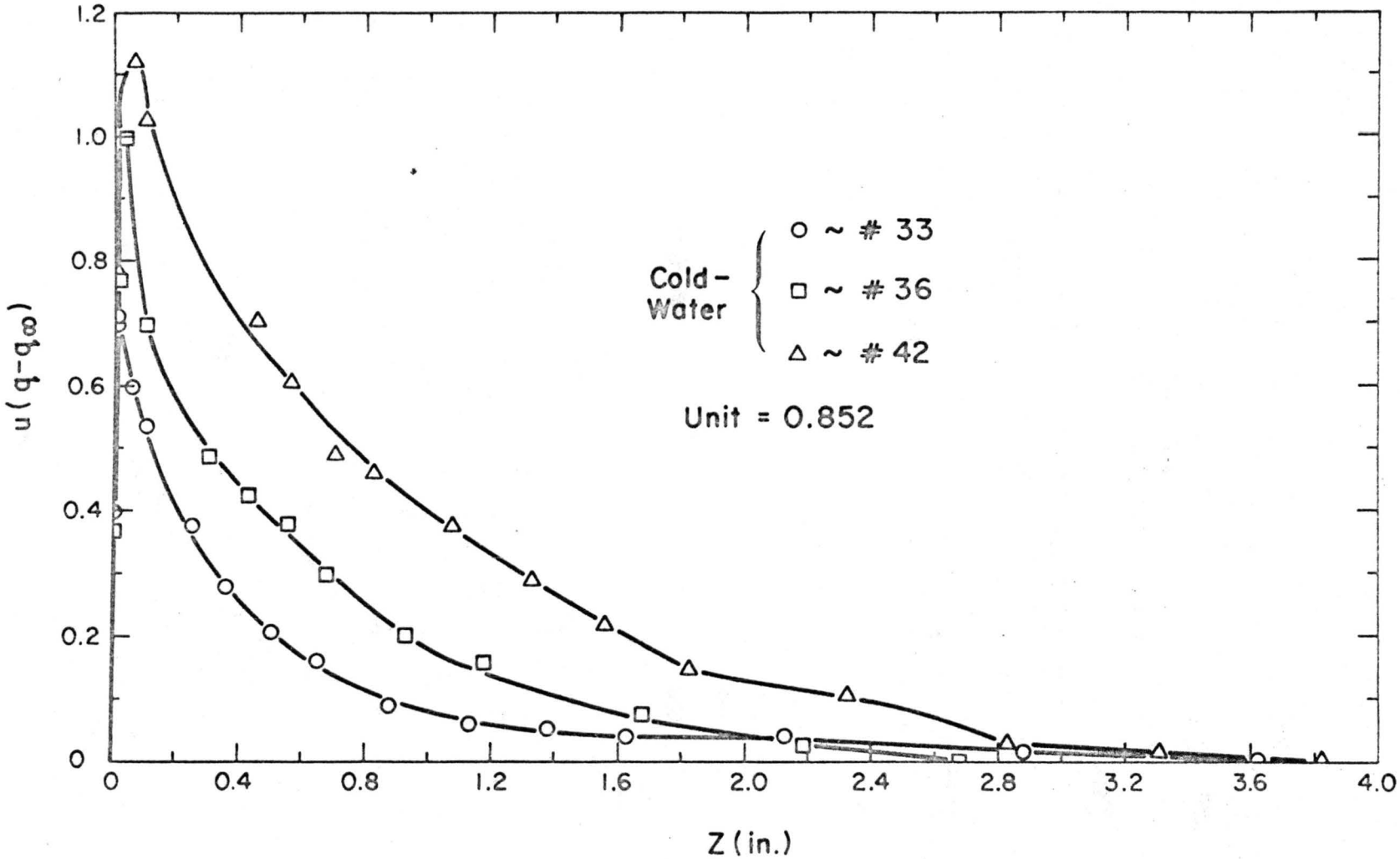

Fig. 26. Mass flux against the variation of Z.

The boundary layers of vapor concentration are shown in Figures 16, 17 and 18. The effect of thermal stability in raising the internal boundary layer was predicted by Elliott (1968). The tendency of his results are consistent with the experimental data of the present study. The strong effect of surface temperature on evaporation can be seen in Figure 18 at the upstream position or transition zone, while the values of δ_e^* showed a sharp increase due to the increasing of positive temperature difference between air and water. For the fully developed turbulent flow, the boundary layer thickness of mass transfer eventually became the same for both cold- and warm-water cases. The values of δ_e^*, which are obtained from experimental data, are given in Table II.

Another concentration thickness, ℓe, has been defined by Kays (1966) as:

$$\ell e = \frac{1}{u_\infty (q_s - q_\infty)} \int_0^\infty u(q - q_\infty)\, dz \quad . \tag{5-5}$$

The concentration thickness of the boundary layer in mass transfer problems is analogous to the momentum thickness of the flow field. The values of ℓe are connected with the flow of mass through an area normal to the surface. The values of ℓe are listed in Table II. In solving the boundary layer equation of mass flow, ℓe should be an important characteristic length.

Table I. Boundary conditions of flow systems.

Run No.	x (cm)	u_∞ (m/sec)	σ (cm)	f_m (Hz)	T_w (°C)	T_s (°C)	T_∞ (°C)	$q_s \times 10^3$ ($\frac{\text{gm of water}}{\text{gm of dry air}}$)	$q_\infty \times 10^3$ ($\frac{\text{gm of water}}{\text{gm of dry air}}$)
34	56	5.64	--	--	13	11.9	25.6	8.8	4.28
37	112	5.67	--	--	12	10.7	25.0	8.1	4.14
40	214	5.95	--	--	12	10.7	22.6	8.0	2.98
43	460	6.40	--	--	12	10.7	20.8	8.1	3.7
46	778	6.95	--	--	12	10.7	20.2	8.1	3.31
35	56	6.89	--	--	13	11.9	24.2	8.8	3.72
38	112	7.24	0.0245	10.5	12	10.7	25.0	8.2	3.72
41	214	7.61	0.0701	7.02	12	10.7	22.6	8.2	3.36
44	460	8.54	0.165	4.25	12	10.7	20.8	8.1	3.52
47	778	9.25	0.323	3.2	12	10.7	20.2	8.0	3.14
48	610	7.98	0.253	3.9	15.4	14.5	27	10.35	3.76
49	610	8.78	0.309	3.3	11.2	9.7	20.8	7.6	4.24
51	610	9.88	0.37	3.0	11.0	9.6	21.6	7.5	3.86
52	610	12.1	0.449	2.8	12.2	10.9	21	8.2	3.59
53	610	13.3	0.523	2.5	11.7	10.4	21	7.95	4.42
57	116	6.70	0.0248	10.5	30	29	22.6	27.5	7.05
59	214	6.83	0.0659	7.3	34	33.2	27	33.2	6.74
61	460	7.90	0.101	4.65	30	29	22	24.1	5.03
67	610	8.05	0.227	3.6	33.8	32.1	26.8	30	5.25
56	116	6.69	0.0173	11	26.6	25.6	21.6	20.9	6.44
58	214	6.86	0.0559	7.4	30.5	29.3	24	28.2	6.92
60	460	7.87	0.0897	4.6	25.9	25.2	23	19.1	4.6
64	610	8.04	0.0237	3.7	27.1	26.4	25.4	22	5.17

Table II. Characteristic parameters of flow system.

Run* No.	x (cm)	u_* ($\frac{cm}{sec}$)	$z_o x10^4$ (cm)	$-q_* x10^4$ ($\frac{gm\ of\ water}{gm\ of\ air}$)	$z_{om} x10^3$ (cm)	ℓ_e (cm)	δ^*_e (cm)	$E x10^5$ ($\frac{gm}{cm^2-sec}$)
34	56	17	2.54	6.38	2.54	0.283	3.5	1.3
37	112	21	5.85	6.8	12.7	0.52	4.31	1.05
40	214	26.3	17.7	8.2		0.522	5.1	0.737
43	460	30.2	30.2	9.32	81.2	1.403	10.2	0.845
46	778	34	45.7	9.97	127	1.96	12.7	0.865
35	56	25.5	2.44	5.83	0.36	0.284	2.88	1.79
38	112	29.5	6.22	7.51	7.86	0.488	4.82	1.43
41	214	36.3	25.0	8.66	18.8	0.781	7.64	1.36
44	460	46.0	82.0	9.30	57	1.35	11.4	1.16
47	778	52.0	175	9.84	132	2.33	16.2	1.36
48	610	42	115	12.0	76.3	2.1	14.6	18.3
49	610	51.9	150	5.85	122	2.96	15.2	14.5
51	610	57.2	228	6.80	183	3.12	16.5	18.6
52	610	79	381	10.9	330	3.43	17.4	31.7
53	610	90	485	9.48	510	3.53	17.8	27.4
57	116	27.4	5.08	26.4	0.813	0.531	7.36	6.24
59	214	33.1	25.5	50.8	54	1.11	9.8	9.35
61	460	37.7	61	65	234	2.15	13.7	7.0
67	610	42.6	192	105	1430	4.11	15.6	13.4
56	116	23.5	1.78	23	6.35	0.484	6.5	4.02
58	214	31.4	15.5	44.8	44.5	1.16	8.39	7.88
60	460	37.6	45.3	50.5	144	1.93	12.4	4.77
64	610	41.6	152	66	965	3.56	15.7	7.85

*Run no. 34-46 and 35-47 are cold water cases.
Run no. 48-53 are cold water cases at fixed position.
Run no. 57-67 and 56-64 are warm water cases.

Chapter VI

DISCUSSION OF RESULTS

The experimental results of this study have been presented in Chapter V. To check the data of this study, both the momentum and mass transfer phenomena will be compared with experimental or analytical results of earlier authors. To better understand the transport mechanism, the physical background of different parameters was considered and is discussed to some extent in the light of the experimental results. An empirical relationship between momentum and mass transfer has been worked out using the experimental data. Finally, a direct and practical method to evaluate the evaporation rate is proposed.

6.1 Nature of the Water Surface

The temperature difference between water and air has some effect on structure of the surface waves (Fleagle, 1956). One way to estimate the thermal effect on wave structure is to evaluate the net amplification rate of waves resulting from the temperature difference. A theoretical approach which includes physical parameters that vary with temperature has been suggested by Miles (1962) and Benjamin (1959). Miles showed that (see also Hidy and Plate, 1968) the net amplification rate for small waves is given by:

$$m = m_a + m_w \qquad (6\text{-}1)$$

where m_a is the growth factor predicted by Miles' mathematical model, and m_w is the damping factor:

$$m_w = - 2k^2\nu_w - (2k^3\nu_w c)^{1/2} \quad e^{-2kd} \qquad (6\text{-}2)$$

where c is the phase speed of wave, ν_w is the kinematic viscosity of water, k is wave number, and d is water depth.

The growth factor has the form:

$$m_a \simeq 1/2 \frac{\rho_a}{\rho_w} u'_s \left[\frac{0.322}{w^2} \left(\frac{u_*^2}{k\nu_a}\right)\left(\frac{c}{u_*}\right) + \frac{0.343}{w} \left(\frac{u_*}{k\nu_a}\right)^{1/3}\right], \qquad (6\text{-}3)$$

where w is a complex stability function which is given in terms of the variable

$$Z = c/u'_s\delta^* \qquad (6\text{-}4)$$

where u'_s is the slope of air velocity profile at the water surface.

Some calculations of $m(k)$ have been shown in Table II of Hidy and Plate (1968). They assumed that $\tau_s = 1$ dyne/cm^2 and $\Delta T = \pm 10°C$, and they used Miles' estimated value of w adjusted for the change in the physical properties with temperature. They found an approximately 10% change in net amplification rate for this range of temperature difference. Experimental data of this study (Figures 9, 10 and 11) show that the values of f_m decrease and the values of σ increase as the temperature difference, $T_s - T_\infty$, changes from positive to negative. By using

Figure 10 to account for the temperature effect in the change of f_m and σ, one obtains for a temperature difference of $\Delta T = + 12°C$ to $\Delta T = - 6°C$ and the same free stream velocity, that the standard deviation increased about 25%. Since the standard deviation also indicates the wave height, the increased standard deviation shows the difference in amplification rate for such a temperature difference. It was found from the experimental data and the thermal conditions of this study, that the net amplification rate, which was calculated from Equations (6-2) and (6-3), showed a 30% increase from $\Delta T = + 12°C$ to $\Delta T = - 6°C$. The decrease of the damping factor (Eq. (6-2)) was largely due to the temperature difference. However, the increase of growth factor (Eq. (6-3)) due to the temperature difference was small. Thus, while the Benjamin-Miles theory also shows that m increases with increase of water temperature, it does not predict the large increases observed in the experimental results.

Roll (as quoted by Fleagle, 1956) devised a statistical method to study the temperature effect on wave generation. He found that for the same winds, the mean wave height increased 22% as the air and sea temperature difference increased from 0° to 6.7°C. His results were based on measurements taken by North Atlantic weather ships. Fleagle (1956) later used the mean tabulated data of wind speed, wave height and air temperatures, based on measurements by

Atlantic and Pacific weather ships, to plot a relationship between air-sea temperature difference and wave height. His results showed that higher waves are generated on warm water (relative to air temperature) than on cold water. The difference amounted to an increase in wave height of roughly ten percent per degree centigrade. Rolls' results agree with the experimental data of this study. Yet Fleagles' results showed a stronger effect on temperature difference. This may have been partially due to the deficiency in measuring sea surface temperature, and the way he selected the field data and excluded the cases of a randomly agitated sea.

6.2 Air Flow

In the warm-water case, an unstable stratification developed in the flow system, which may have had some effect on the air flow near the water. A criterion for the magnitude of this effect is based on the flux form of the Richardson number, which is defined by:

$$R_f = - gH/C_p T_o \tau \left(\frac{\partial \bar{u}}{\partial z}\right) , \qquad (6\text{-}5)$$

where H is the heat flux at the surface and T_o is the mean absolute temperature. The values of H are contributed by:

$$H = H\ell + Hc \qquad (6\text{-}6)$$

where $H\ell$ = latent heat due to evaporation ($\equiv \rho_w EL/C_p$),

Hc = sensible heat due to temperature gradient $(= C_p (\frac{\partial T}{\partial z})_s)$. The sensible heat was contributed by air and water. Here, only sensible heat of air was considered and denoted by Hc.

The ratio between Hc and Hℓ is the Bowen ratio (B = Hc/Hℓ). In this experiment, the values of B were equal to (+) 0.2 ~ 0.3 for the cold-water case and equal to (-) 0.003 - 0.004 for the warm-water case. This indicated that the sensible heat of air was an important source for evaporation of the cold-water case, while the sensible heat of water was an important source for evaporation of the warm-water case. For the first approximation in the warm-water case, which had the greater heat flux at the surface than the cool surface, the following assumptions were made:

$$\tau = \rho K_m \frac{\partial \bar{u}}{\partial z} = \rho \frac{K_m}{k} u_* \quad , \tag{6-7a}$$

$$H = H\ell \equiv \rho_w EL/c_p \quad , \tag{6-7b}$$

and

$$R_f = \frac{K_h}{K_m} Ri \simeq Ri \quad , \tag{6-7c}$$

where Ri is the Richardson number in gradient form. The difference between Ri and R_f depends on the value of K_h/K_m. Here, K_h/K_m is assumed equal to unity. The values of Ri can be calculated by:

$$R_f \simeq Ri = gx\Delta xE/T_s \left(\frac{u_*}{k}\right)^2 \quad . \tag{6-8}$$

In the experiments of this study, Ri is the order of 10^{-3}. For small Ri, the flow system can be considered as near-adiabatic, which leads to the following equation to describe the velocity distribution (Roll, 1965):

$$\frac{\partial \bar{u}}{\partial z} = \frac{u_*}{K_z} \frac{1}{1 - \alpha Ri} , \qquad (6\text{-}9)$$

where α is a constant and approximately equal to 10. On the basis of Equation (6-9), the velocity profile in the warm-water case would involve 2% error by neglecting the thermal effect of the Richardson criterion. Therefore, the effect of the unstable density stratification on momentum exchange was considered negligible. The values and relationships between u_* and z_o in warm-water case, such as expressed in Equations (5-1) and (5-2), were similar for the same free stream conditions in the cold-water case. Therefore, it was assumed that temperature difference between the air and the water did not modify the momentum transfer in this experiment.

The correlation between z_o and $u_*\sigma/\nu$ for both cold- and warm-water cases can also be used to check the thermal effect on momentum transfer. As shown in Figure 23, the correlation held reasonably well for both cases, but there was a small difference which may not be accounted for by applying the Richardson criterion. Since virtually no information is available on the combined effects of waves and temperature difference on shearing flow of air overhead,

this question should be investigated further in later studies.

6.3 Humidity and Evaporation Rates

6.3.1 Universal Concentration

The "logarithmic law" for mean humidity profiles in turbulent boundary layers over a flat or a wavy surface has been derived in the previous section and is given by Equation (2-9). The curves of dimensionless humidity profiles placed in the form of $(q - q_s)/q_*$ with dimensionless height (z/z_{om}) are shown in Figures 27 and 28. Most of the experimental data are well correlated along the line which is given by Equation (2-9), except at large values of z/z_{om}. Large values of z/z_{om} for each run indicate large distances from the mean water surface, where the logarithmic law did not hold, as is also the case for the velocity profiles. The results of this study suggested that the law of wall for the humidity distribution was a satisfactory approximation near the water surface for both the cold-water case (inversion condition) and warm-water case (lapse conditions).

Using Equation (2-9), the values of q_* were evaluated from the humidity profiles by the relationship:

$$\frac{q_3 - q_s}{q_4 - q_s} = q_* \ln z_3/z_4 \ , \qquad (6\text{-}10)$$

where q_3 and q_4 designated the specific humidity at z_3

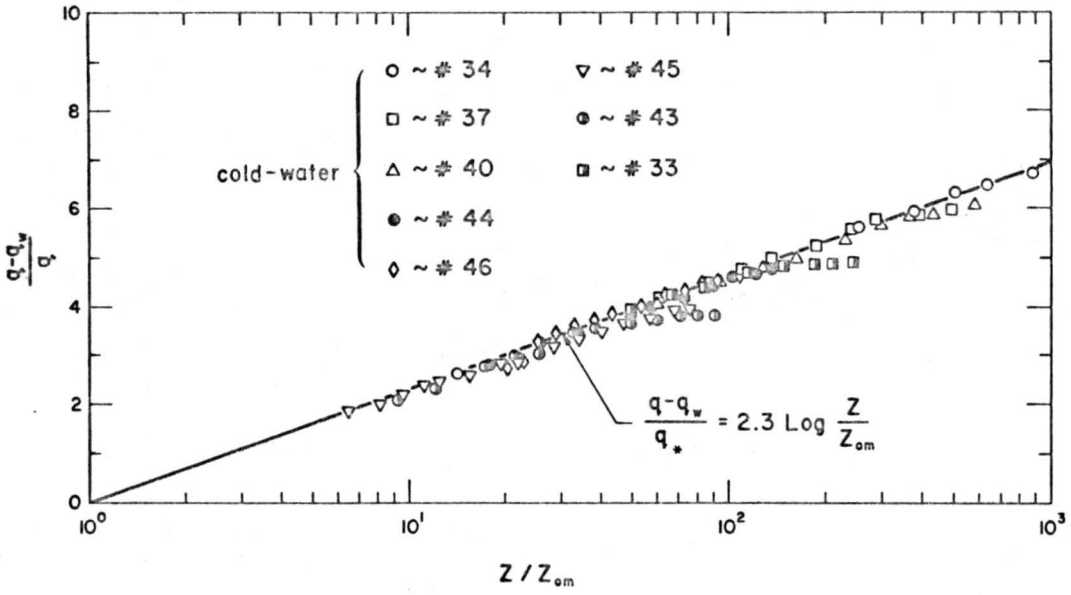

Fig. 27. Dimensionless specific-humidity distribution over small water waves.

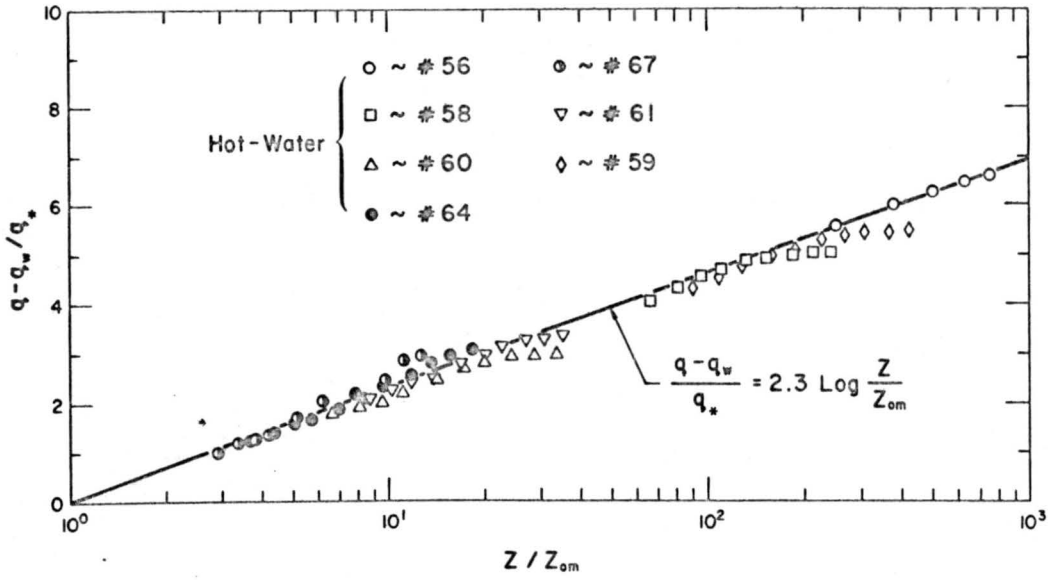

Fig. 28. Dimensionless specific-humidity distribution over small water waves.

and z_4 and lay in the curve of the logarithmic part. After determining the values of q_*, z_{om} was evaluated from Equation (2-9). The numerical values of q_* and z_{om} for this study are given in Table II.

The trends of q_* were similar to that of u_*. The variation of q_* with fetch is shown in Figures 21 and 22. The values of q_* appeared to be mainly affected by the temperature difference between air and water. The effect of air velocity on q_* was smaller than the effect of temperature difference. To compare the properties of q_* with u_*, the effect of temperature difference between air and water on q_* was similar to the effect of free stream velocity on u_*.

The length scale, z_{om}, is analogous to z_o, and is introduced as a characteristic length for the (logarithmic) humidity profiles. Estimation of the values of z_{om} from the momentum field is a useful and practical way for predicting the universal profile of humidity. A reasonable correlation was found for the set of experiments. The dimensionless roughness lengths (z_o/σ) are shown in Figure 29 as a function of the Peclet number $Pe = u_* z_{om}/D$, which is based on the length z_{om}. The standard deviation of z_o/σ from a straight line was $\pm$ 15%, which is considered to be a satisfactory fit for both the cold- and warm-water cases studied. From this correlation, the values of evaporation can be estimated from knowledge of the

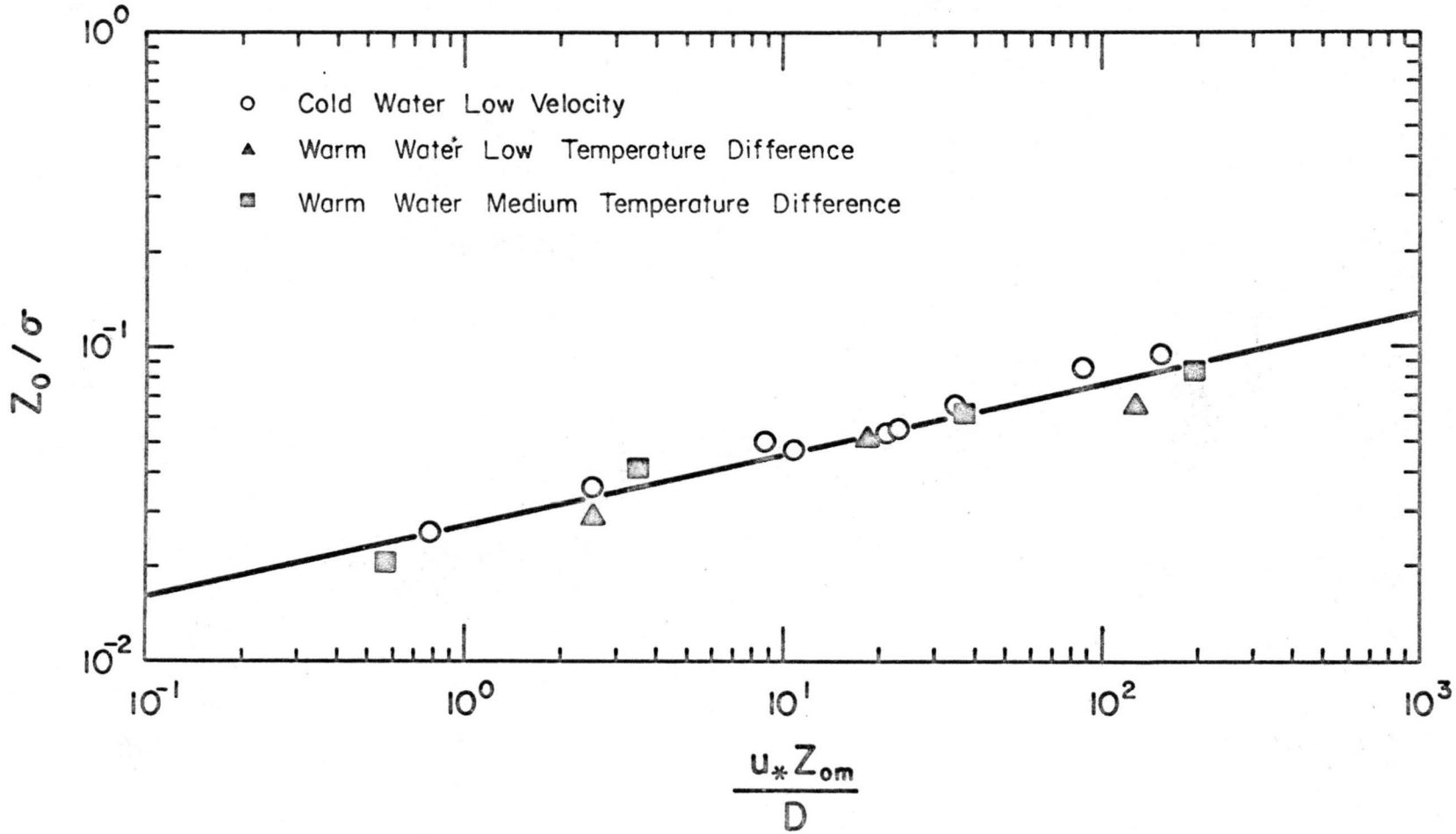

Fig. 29. Correlation between Peclet number $u_* z_{om}/D$ and dimensionless roughness length.

velocity field only, provided the thermal conditions at the water surface and free stream are given, or measured.

6.3.2 Methods of Obtaining the Evaporation Rate

In Chapter II, several semi-empirical methods for estimating the evaporation rate were outlined. In this section, these results are compared for consistency with those of previous investigators and with each other. For the latter comparison, the data of E calculated by the mass balance method, as shown in Table II, were taken as the standard. The other approximate methods were each shown to be useful for estimating E over a certain range of boundary layer development.

From the measured humidity distribution, the profile coefficient, Γ_D, can be calculated by means of Equation (2-22). One set of the results at a fixed position, x = 6.10 m, is shown in Figure 30, together with Okuda and Hayami's results taken in a wind-water tunnel under identical conditions. When the wind speed, u_∞, was less than 10 m/sec, the values Γ_D were nearly independent of u_∞. Okuda and Hayami observed that above u_∞ = 10 m/sec, the surface became sufficiently agitated to produce spray from breaking waves. This caused a marked increase in evaporation rate. The data taken in this study showed a similar sharp increase in Γ_D at about u_∞ = 10 m/sec, which evidently was related to spray formation. Droplets of spray

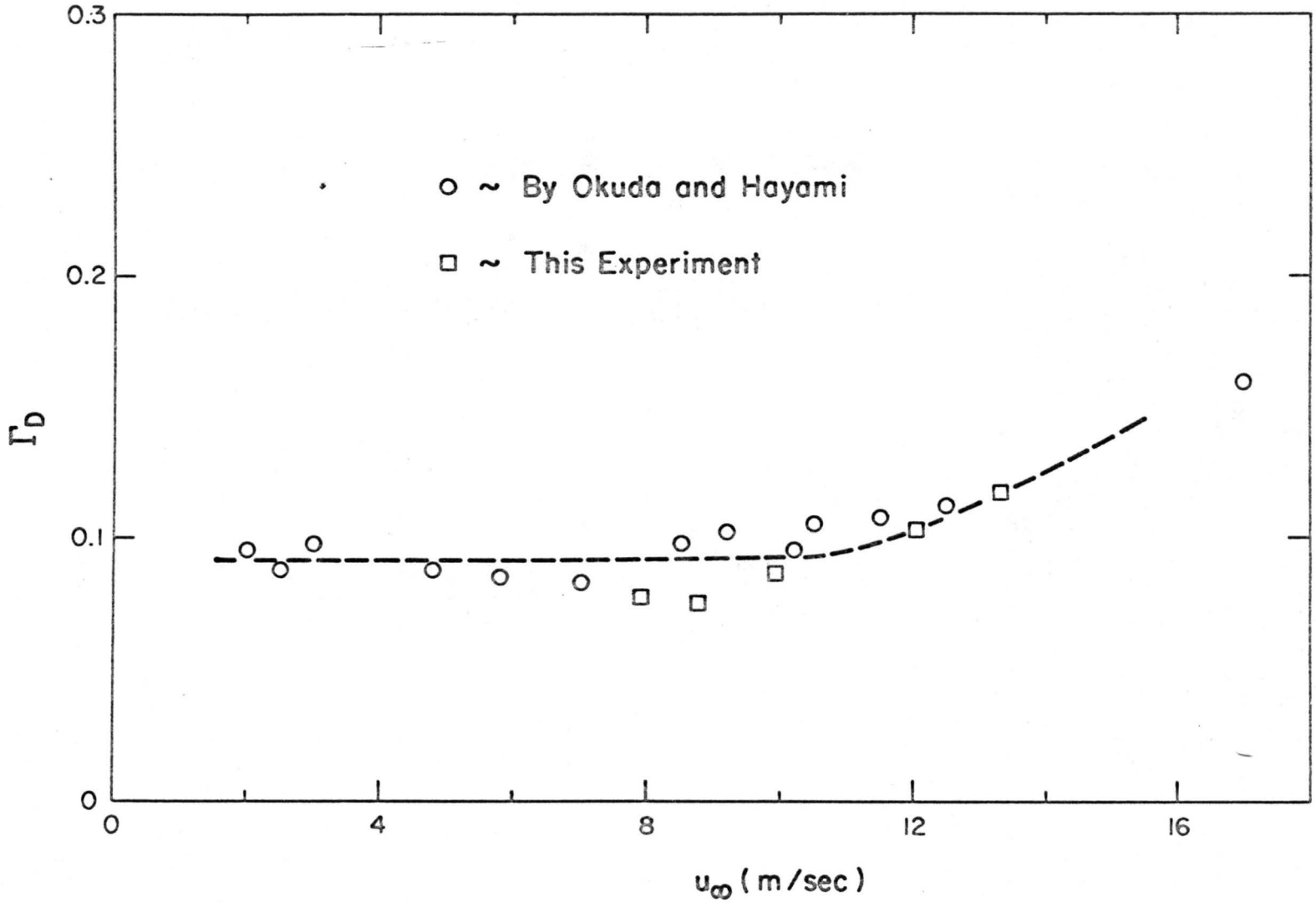

Fig. 30. Variation of evaporation coefficients against U_∞ .

were actually observed above the wavy surface around or above this wind speed.

From experimental knowledge of the profile parameters of the fields of velocity, temperature, and vapor concentration, the evaporation rate can be calculated by the approximate methods outlined in Chapter II as:

$$E_1 = - \rho k \, u_* q_* \qquad (2\text{-}9b)$$

$$E_2 = \rho k \, u_* (q_s - q_\infty) / \ell n \, [(D + k u_* \delta_e^*)/D] \qquad (2\text{-}6)$$

and

$$E_3 = \rho \frac{d}{dx} \int_o^{\delta_e^*} u(q - q_\infty) \, dz, \qquad (2\text{-}2)$$

where the values of E_1, E_2, and E_3 refer to the profile method, integral method, and experimental data, respectively. The values of E's are listed in Table III and plotted against the x-coordinate in Figures 31 and 32. E_3 is the measured evaporation rate which is taken as the standard for comparison. In the cold-water case, and for $x > 3$ meters, the difference between E_2 and E_3 was small, so that Equation (2-6) gave a satisfactory simplified method to evaluate the evaporation rate in a well-developed turbulent boundary layer. However, the difference between E_1 and E_3 was large and systematic over $x > 3$ meters, so the constant of Equation (2-9b) had to be adjusted from Karman's constant of 0.4. As pointed out earlier, the Karman constant, K, was used only for a first approximation. A

Table III. Evaporation rates by different methods.

Run No.	x (cm)	$E_1 \times 10^5$ **	$E_2 \times 10^5$ **	$E_3 \times 10^5$ **	$E_1^* \times 10^5$ **	$E_4 \times 10^5$ **
34	56	0.438	0.605	1.30	--	1.55
37	112	0.56	0.631	1.05	--	1.23
40	214	0.871	0.97	0.745	0.706	0.885
43	460	1.14	0.935	0.91	0.911	1.04
46	778	1.37	1.0	0.995	1.09	1.27
35	56	0.601	0.995	1.79	--	1.82
38	112	0.859	1.06	1.43	--	1.48
41	214	1.27	1.14	1.36	1.02	1.51
44	460	1.56	1.26	1.16	1.25	1.35
47	778	1.70	1.41	1.36	1.36	1.76
48	610	2.04	1.68	1.83	1.63	--
49	610	1.33	1.03	1.25	1.06	--
51	610	1.57	1.19	1.56	1.26	--
52	610	3.48	1.97	3.17	2.79	--
53	610	3.45	1.68	2.74	2.77	--
57	116	3.03	3.63	6.24	--	7.21
59	214	6.36	5.39	9.35	--	9.54
61	460	8.21	4.5	7.0	6.58	5.75
67	610	14.2	6.75	13.4	11.40	17.10
56	116	2.15	2.43	4.02	--	4.2
58	214	5.61	4.26	7.88	--	8.07
60	460	6.45	4.52	4.77	5.15	4.96
64	610	9.27	5.49	7.85	7.42	9.75

** $\left(\frac{\text{gm of water}}{\text{cm}^2\text{-sec}}\right)$

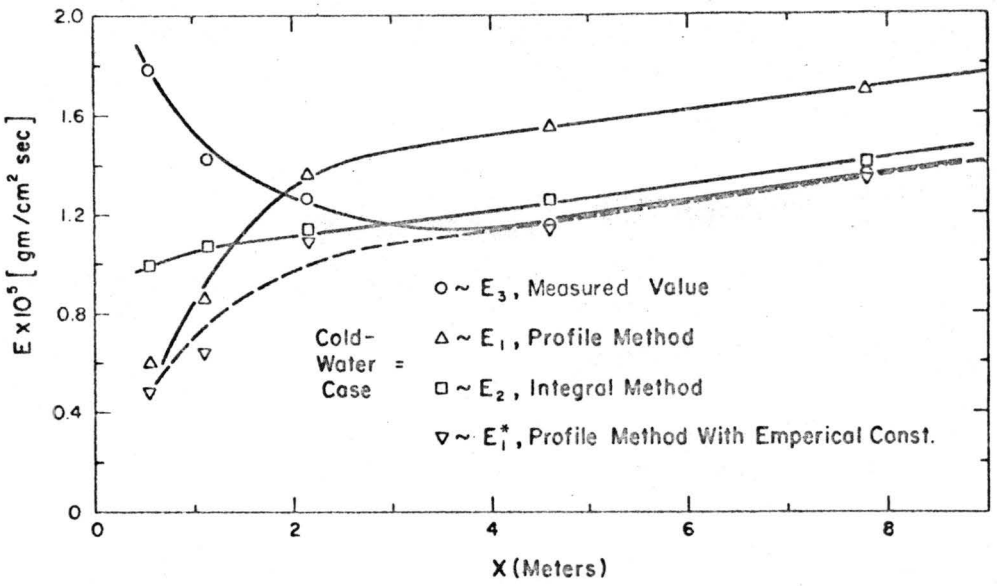

Fig. 31. Evaporation rates against fetch.

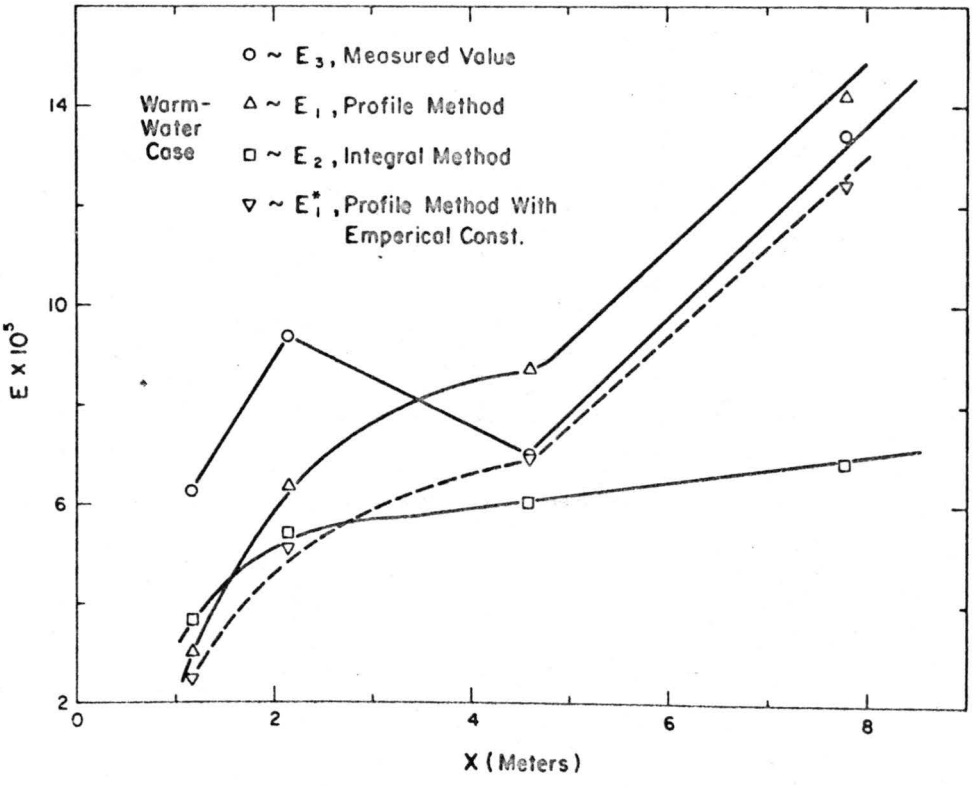

Fig. 32. Evaporation rates against fetch.

result of this experiment showed that the constant in Equation (2-9b) should be 0.32 instead of 0.4. In other words,

$$E_1^* = - 0.32\rho\ u_* q_* \ , \qquad (6\text{-}11)$$

corresponding best to the experimental data for cold water in this study. In the warm-water case, the values of E_2 calculated in Equation (2-6), did not agree with experimental data. This was due mainly to the fact that Equation (2-6) did not include the effect of temperature difference on surface conditions. However, the values of E_1^* estimated in Equation (6-11), still agreed satisfactorily with the experimental data.

The constant 0.32 in Equation (6-11) has another physical significance. In deriving Equation (2-9b), the evaporation rate should be:

$$E = - \rho k \left(\frac{K_e}{K_m}\right) u_* q_* \ . \qquad (6\text{-}12)$$

For the first approximation, K_e was assumed to be equal to K_m, so Equation (6-12) became equal to Equation (2-9b), consequently the factor 0.32 is actually equal to $\frac{K_e}{K_m}\ k$, or with $k = 0.4$, it follows that:

$$\frac{K_e}{K_m} = 1.25 \ . \qquad (6\text{-}13)$$

This relationship is similar to that obtained from Rider's observation (1954):

$$\frac{K_e}{K_m} = 1.12 \pm 0.04 \quad . \tag{6-14}$$

The 10% difference between laboratory study and field observation is an allowable margin for satisfactory results.

The logarithmic profiles of humidity and velocity can be related at the same z by the following relations:

$$k \frac{u}{u_*} = \frac{q - q_s}{q_*} + \ell n \frac{z_{om}}{z_o} \quad . \tag{6-15}$$

Equation (6-15) has been verified by the experimental data of this study. By differentiation of (6-15) and assumed that z_o and z_{om} were independent of y, one obtains:

$$\frac{\rho}{E} \frac{dq}{dy} = \frac{1}{\tau_w} \frac{du}{dy} \quad . \tag{6-16}$$

If the local mass flux is equal to the evaporation rate and if Equation (6-11) is used, one obtains the turbulent Schmidt number as:

$$Sc,_t = 0.8 \quad . \tag{6-17}$$

This value has been suggested by many earlier workers (Spalding, 1964), and it is confirmed by the experimental data of this study.

6.4 Roughness Effect on Evaporation Rates

The water surface condition is an important factor in the mass transfer from the free surface. As waves grow by

wind action from ripples to well developed gravity waves, the effect on evaporation and momentum transfer may be considered in terms of an increasingly rough surface. When the waves develop there are two effects that modify the evaporation process: one kinematic and the other dynamic in character. As waves grow, the equivalent surface area increases for a normal fetch, measured horizontally along the mean water depth. This produces an apparent increase in evaporation with wave growth by a kinematic effect of increasing the apparent surface area. In the second case, a dynamic effect can occur when separation of air flow takes place over the waves. The latter influence has been discussed to some extent by Levich (1965) and Easterbrook (1968). It is not intuitively obvious how separation would influence evaporation. For example, one could argue that separation would give rise to lower local air speeds near the surface in the trough of the water waves and reduce evaporation. On the other hand, if the evaporation rate depends on turbulent diffusion away from the surface as well as on the molecular diffusion layer near the surface, one might suspect that increased turbulence by separation might contribute to an increase in evaporation rate. The latter tendency of turbulent transport may be observed in the results for the evaporation rate shown in Figures 31 and 32. The values of E_3 tended to decrease with x initially as a mass transfer boundary

layer developed. There was an exception to this at x = 214 m in the warm-water case. This position was located close to the largest heater in the channel. This localized heat source increases the evaporation rate by an amount which exceeds the decrease due to the developing concentration boundary layer. After $\sigma > 0.15$ cm, the values of E_3 tend to increase somewhat as waves grow. Since it is known that separation occurs at least intermittently over waves in this range, where $c \approx u_*$ (Chang, 1968), one can interpret the increase in E_3 with flow over waves partly as a kinematic modification, and partly as a dynamical influence of separation.

An increase of surface area due to the waves action has been estimated by assuming sine waves with wave height, a (where $a = 2\sigma$) of water waves. The local increase of surface area was up to 16% due to sine water waves in this experiment with the assumption $a/L = 0.1$, where L is wave length and a is wave height. This amount of correction was not enough to account for the total increase of evaporation by the wavy surface. The total increase of evaporation was 40% in the cold-water case and up to 100% in the warm-water case. Thus, the dynamic effect on evaporation rate evidently is more important than the kinematic effect.

An influence of separation on evaporation has been suggested by Easterbrook (1968) based on a laboratory

study. Using a large wave tank-wind tunnel to measure the effect of wave conditions, he indicated that for certain combinations of wind speed and well-developed waves the evaporation rate was minimal as the wave parameter, i.e., the ratio of wave height, H , to wave period, P , increased. The appearance of a minimum in the evaporation rate effect was explained by Easterbrook based on the phenomenon of separation. The separation of air flow from the lee side of the wave forms a vortex flow near the water surface. The vortices resist the transfer of heat and mass and become an effective barrier to the vertical transport of water vapor. The stability of these vortices will determine the evaporation rate. The evaporation rate will increase in unstable cases. These unstable cases are caused by the strong wind over wavy surface or positive temperature difference between air and water. The evaporation rate will decrease in stable cases. These stable cases exist in some ranges of mechanically generated waves and wind (see Figure 33).

Easterbrook's results are compared with the results of this study in Figure 33. Due to the different wave conditions, the wave paramter (H/P ft-sec^{-1}) of this study lies between 0.02 and 0.08 ft-sec^{-1}, so the data points of this study do not fall into the shadowed area where the evaporation rate decreases with increasing wave motion. Figure 33, taken from Easterbrook's report shows an increase of the

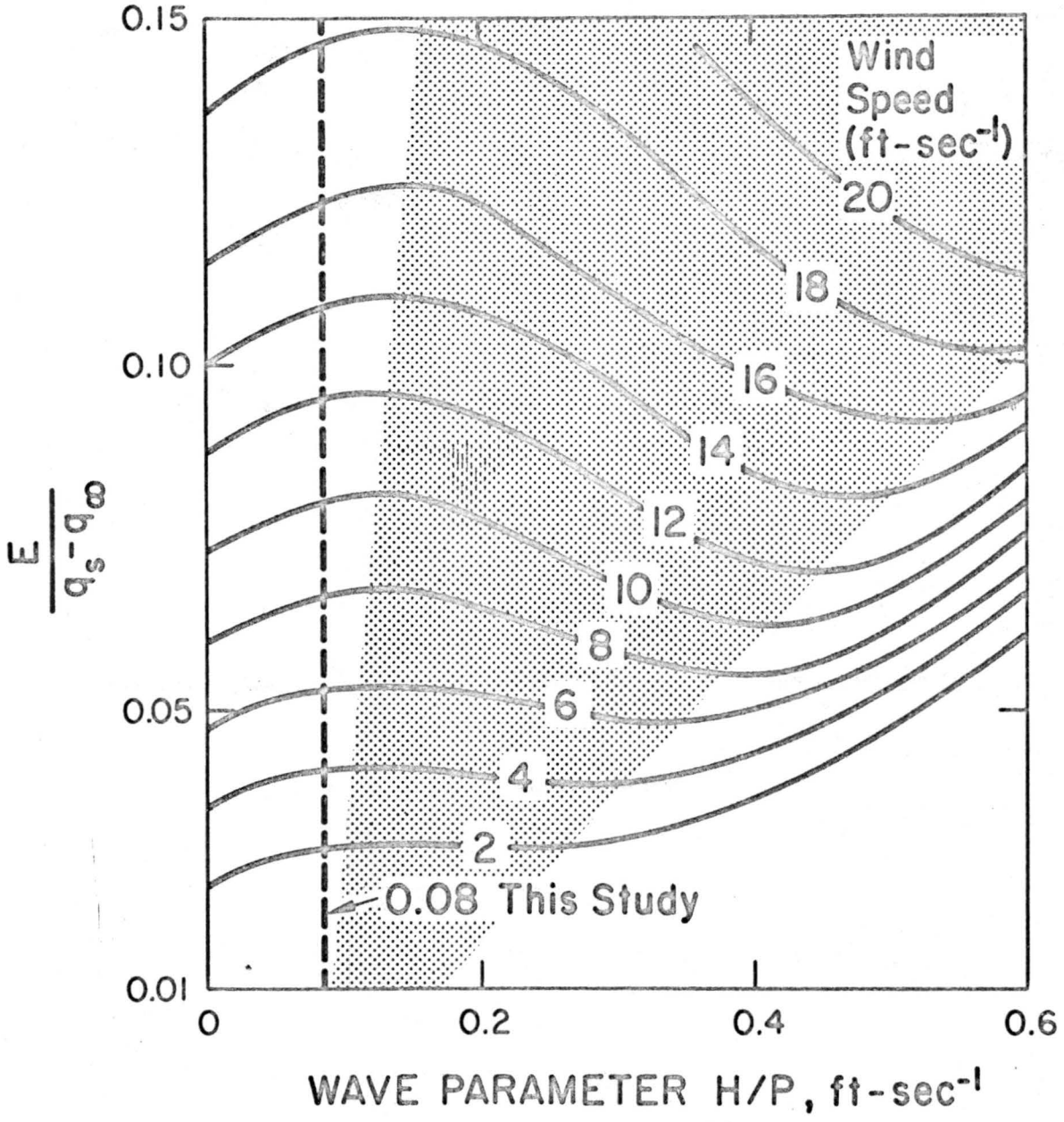

Fig. 33. Evaporation coefficient against wave parameter. (from Easterbrook, 1968).

evaporation rate with increasing wave parameter up to 0.08 ft-sec^{-1}. The figure also indicates that the higher the free stream velocity, the larger the expected evaporation rate. This is qualitatively consistent with the results of the present study.

6.5 Evaporation Rates Expressed by Dimensionless Groups

In the wind-water channel, where a steady wind blew over a smooth aluminum plate onto the water surface, the air motion itself induced the waves. The waves started as tiny ripples growing with increasing fetch to well-developed gravity waves. This process caused a change from an aerodynamically smooth surface to a rough surface (Kunishi, 1963; Plate and Hidy, 1967). According to the different boundary conditions in a wind-water channel the mass transfer problem was divided into different problems. First, the turbulent air with low vapor concentration flowed over the aluminum plate (Roughness 1) onto the water surface (Roughness 2) with stepwise changes in vapor concentration at the water surface. When the fetch was small, or for cases close to the leading edge ($x = 0$), the water surface was also an aerodynamically smooth surface for the mass transfer problem. Then, the turbulent air passed over the ripple-waves onto the well-developed gravity waves. In the mass transfer problem, this was the turbulent flow over the rough surface with high vapor concentration at the surface.

The experimental correlation in terms of dimensionless groups in this study can be expected to follow different laws for different boundary conditions. In Figure 34 a plot of Sherwood number vs. Schmidt number and drag coefficient vs. Reynolds number is given. The Schmidt number of this study is 0.71, which is calculated from the ratio ν/D. In the range $Re < 7 \times 10^5$, the correlation for laminar flow over the flat plate (Equation (2-10)) fit the experimental data for cold- and warm-water cases except for an exponent of 0.6 for the power law of Reynolds number. In the range, $7 \times 10^5 < Re < 5 \times 10^6$, the correlation of turbulent flow (Equation (2-12)) fits the experimental data of the cold-water case, but not for the warm-water case and the case where the spray of water dominates the evaporation process. The spray of water caused by strong wind was also clearly shown in Figure 34 at $Re > 5 \times 10^6$ where the departure from Equation (2-12) existed. The failure of Equation (2-12) to correlate the data for the warm-water case, suggested that the temperature difference between air and water had a significant effect on the transport mechanism, possibly through volumetric evaporation or by changing the structure of surface wave, or by modifying the flow system near the water surface.

Smolsky and Sergeyev (1962) introduced the Gukhmann number, Gu, (see Chapter II) into the correlation of dimensionless groups. Their correlation line is also plotted in

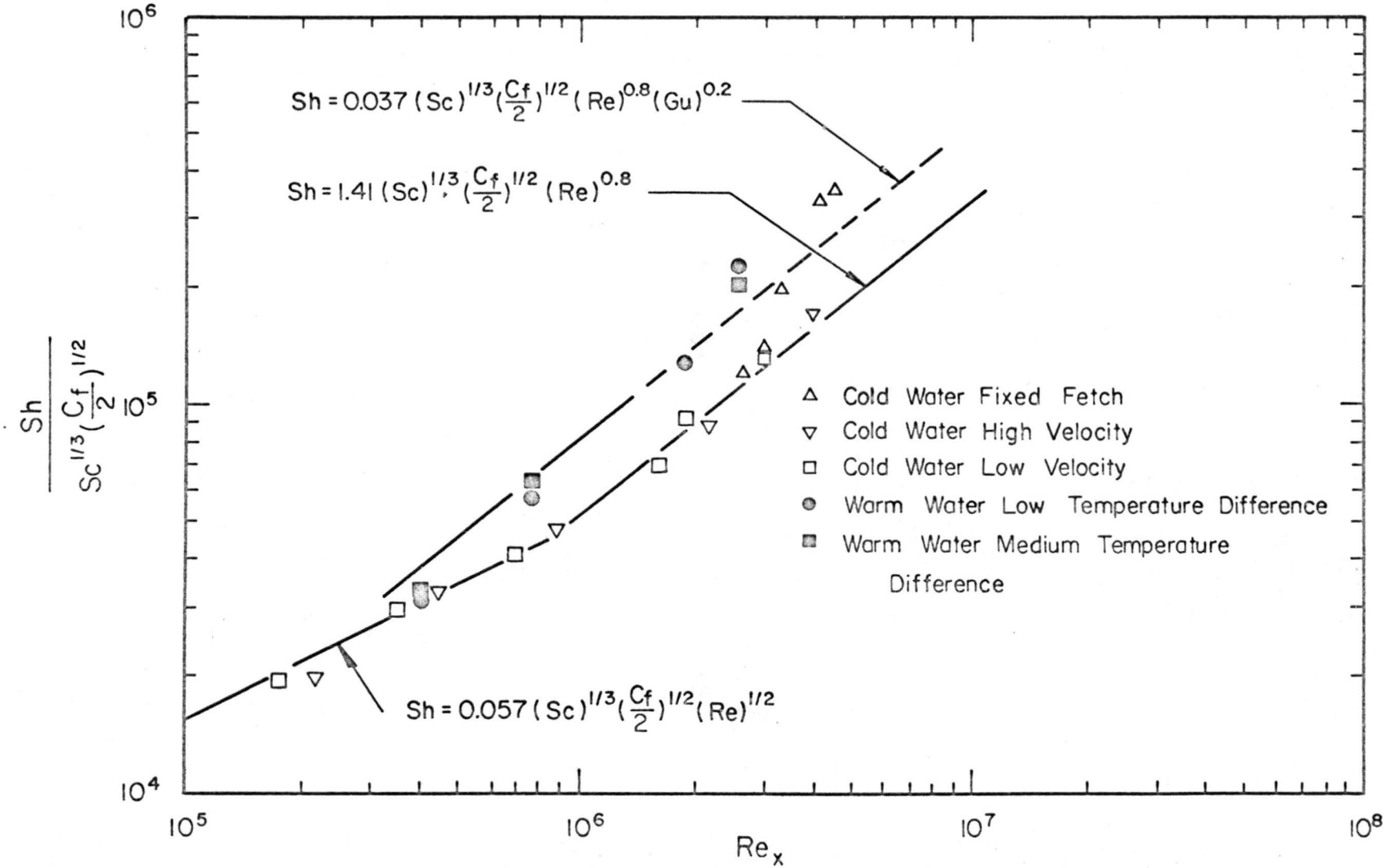

Fig. 34. Correlation in dimensionless groups analogous to the heat transfer problem.

Figure 34 (dashed line) to compare with this study. Most of the data points of this experiment are lower than the dashed line, except some points of the warm-water case. Therefore, Smolsky and Sergeyev's correlation does not apply to correlate the data of this study. Instead, it is more likely that the temperature effect is associated with the observed change in wave structure.

The Levich theoretical model for turbulent flow over a rough surface has been tried to correlate the cold- and warm-water cases. The results were not completely satisfactory (Figure 35). The scattering of data above one line for both cases was slightly improved, compared with Figure 34, over the range, $7 \times 10^5 < Re < 5 \times 10^6$; but the power of Reynolds number is 0.85 instead of 0.5, which was predicted by Levich. The Levich model, of course, is derived for a solid rough boundary which should be different from the dynamically deformable and moving boundary. The wind-waves in the channel were moving and growing along with increasing fetch. The temperature difference was observed to have some effects on wave structure, as indicated in Figure 11. For such a complex mechanism, it is very difficult to derive the roughness effect in dimensionless form based on a simple theoretical argument. However, an attempt has been made to combine the Levich theoretical model and experimental results by modifying Levich's idea to account for a moving boundary. Instead of using Equation (2-15)

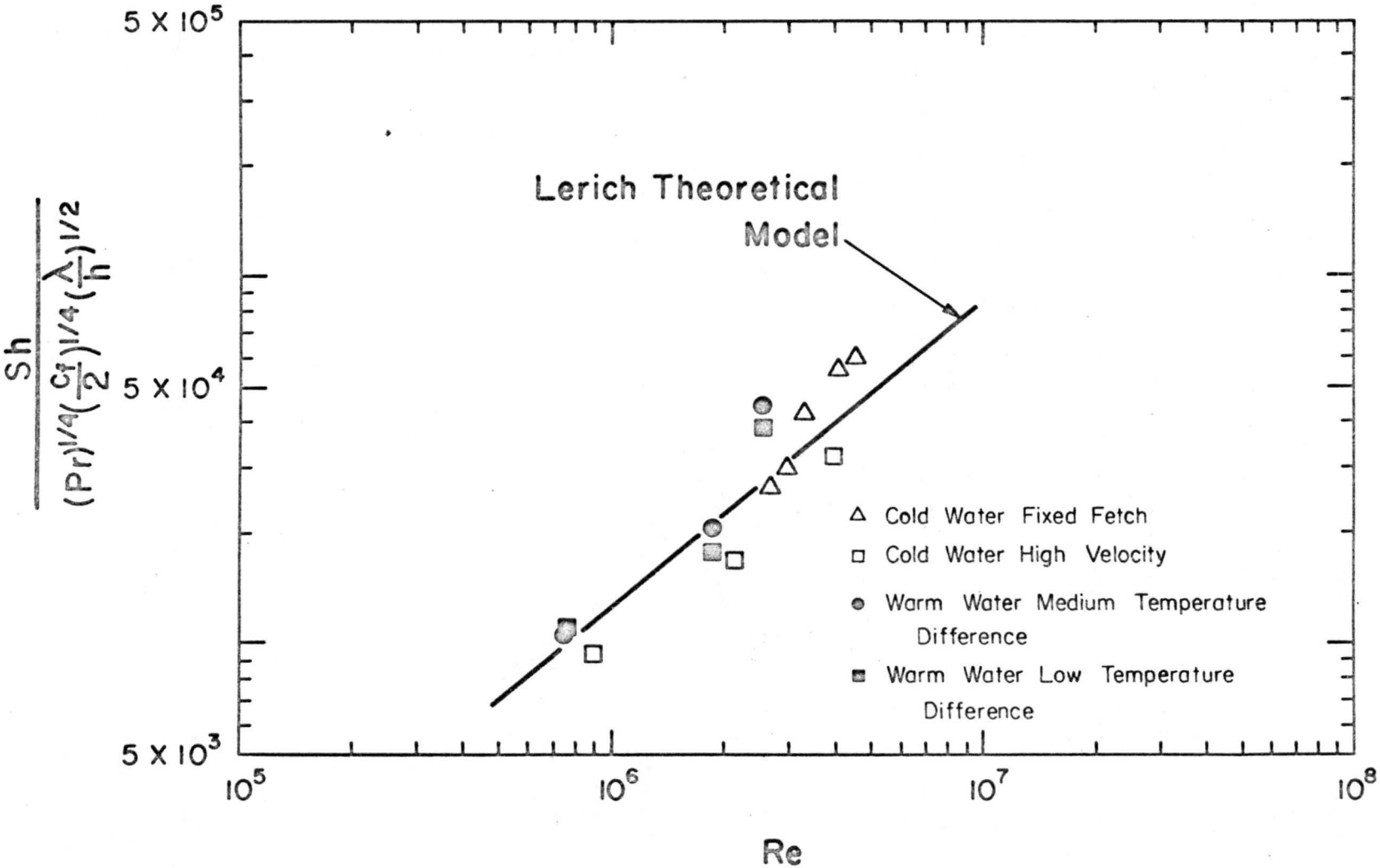

Fig. 35. Compared with Levich theoretical model.

for the diffusion sublayer, a modified diffusion sublayer, δ_m, was proposed by the following equation:

$$\delta_m = \left(\frac{\nu h}{u_*}\right)^{1/2} g\left(\frac{\lambda}{h} , \frac{c}{u_*}\right) \qquad (6\text{-}18)$$

where λ/h is the roughness coefficient, c the phase speed of wave and c/u_* the parameter which should account for the moving boundary and the air flow at the lee side of the waves. The function of $g\left(\frac{\lambda}{h} , \frac{c}{u_*}\right)$ was assumed based on the experimental data of this study, which was:

$$g\left(\frac{\lambda}{h} , \frac{c}{u_*}\right) = \left(\frac{\lambda}{h}\right)^{-1/4} \left(1 - \frac{c}{u_*}\right)^{-1/4} . \qquad (6\text{-}19)$$

There was a critical condition at $c = u_*$, analogous to the critical layer of wave generation. This may be the zone where the air flow forms a dead air pocket which inhibits the convective transport penetration of water vapor further into the boundary layer. Using Equation (6-19), the final form of dimensionless number which was used is:

$$Sh \sim \left(\frac{C_f}{2}\right)^{1/4} (Sc)^{1/4} (Re)^{1/2} \left(\frac{\lambda}{h}\right)^{1/4} \left[\left(1 - \frac{c}{u_*}\right)^{-1}\right]^{1/4} \qquad (6\text{-}20a)$$

or

$$Sh \sim \left(\frac{C_f}{2}\right)^{1/4} (Sc)^{1/4} (Re)^{1/2} (Rgn)^{1/4} , \qquad (6\text{-}20b)$$

where Rgn = modified roughness coefficient $\left(= \frac{\lambda}{h} \frac{u_*}{u_* - c}\right)$. The results are shown in Figure 36. This correlation

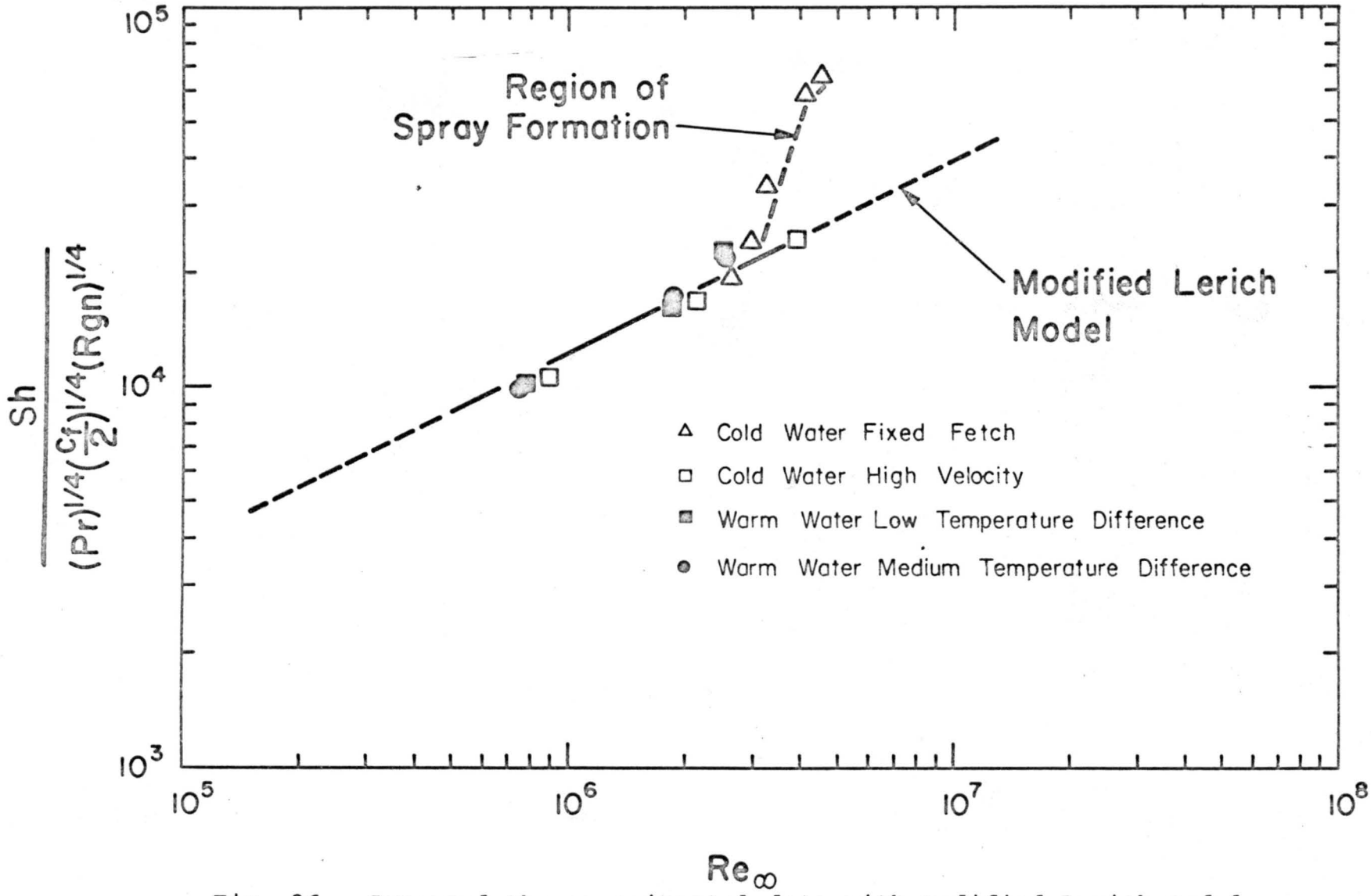

Fig. 36. Compared the experimental data with modified Levich model.

reduced the error to within $\pm$ 6% over the range $7 \times 10^5 < Re < 5 \times 10^6$. The error was defined as the percentage deviated from the solid line in Figure 36. Compared with previous results (with an error of $\pm$ 20%), this is a satisfactory correlation over the range below $Re = 5 \times 10^6$ and when the spray of water droplets is apparently insignificant. Three triangle data points in the upper portion of Figure 36 shows the region of spray formation which corresponds to the case of $u_\infty > 11$ m/sec. This information of spray agrees with the results of previous workers, such as Okuda and Hayami (1959).

The values of z_{om} were tabulated in Table II which shows that the values of z_{om} increased with wave conditions and temperature difference. The properties of z_{om} were similar to Rgn modified roughness coefficient. So the relationship of z_{om} and Rgn is shown in Figure 37. The straight line was found in Figure 37 to correlate z_{om} and Rgn. Thus, the values of z_{om} are an important characteristic length, which accounted for the effect of temperature difference and of wave condition as Rgn did. For a given velocity profile and surface geometry of water surface, the values of z_{om} could be found from Figure 37 within $\pm$ 20%. Then the values of q_* could be evaluated from Equation (2-9) and the evaporation rate estimated from the profile method as discussed in section 6.3.2.

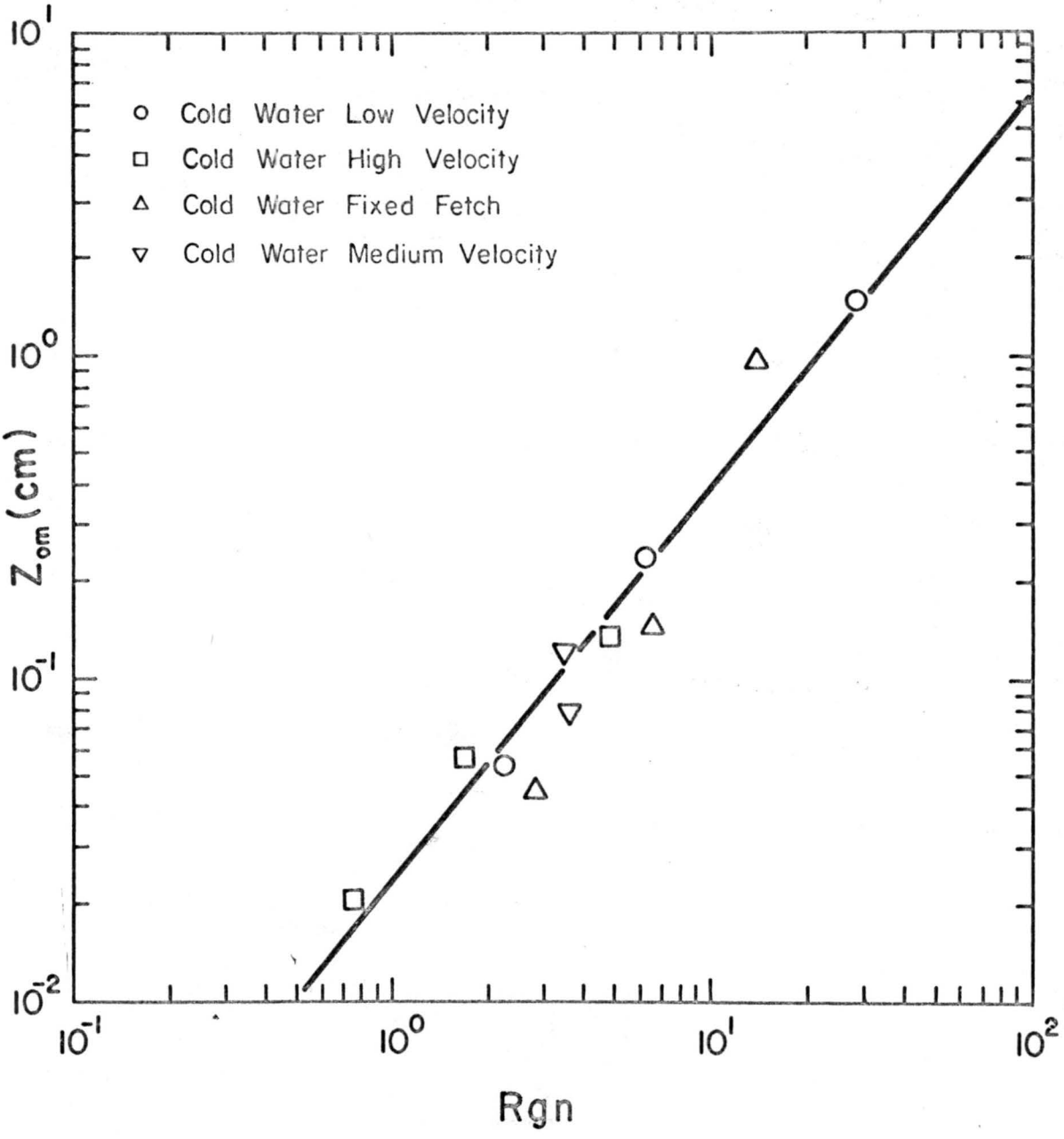

Fig. 37. Variation in z_{om} with modified roughness coefficient.

6.6 Stepwise Change and Evaporation

The problem of stepwise change in wall vapor concentration due to the evaporation in the turbulent flow has been discussed in Chapter II. Here, the experimental results of this study are compared with Spalding's (1963) numerical integration in Figure 38, and the author's theoretical approach in the next paragraph. For $x^+ < 2 \times 10^4$, the experimental data for both cold- and warm-water cases were consistent with Spalding's solution, except that the data line of this study was shifted to the right. The shift of the line was due to (1) the stepwise change of wall roughness, caused by the change of the flow system over the smooth flat plate (Roughness 1) onto an agitated water surface (Roughness 2); and (2) a smaller Schmidt number (Sc = 0.71) used in this experiment, while Spalding's solution was based on the assumption that Sc = 1. For $x^+ = 2.7 \times 10^4$, the data did not agree with numerical results. This simply indicated that Spalding's solution, which was obtained under the assumption that the wall was smooth and flat, was not valid for this study at the downstream position. The breakdown point of this experiment was located at $x^+ \geq 2.7 \times 10^4$, which is identical to the $Re = 7 \times 10^5$ of Figure 20. Further downstream, the evaporation rate was affected both by the wave conditions and positive temperature difference between air and water.

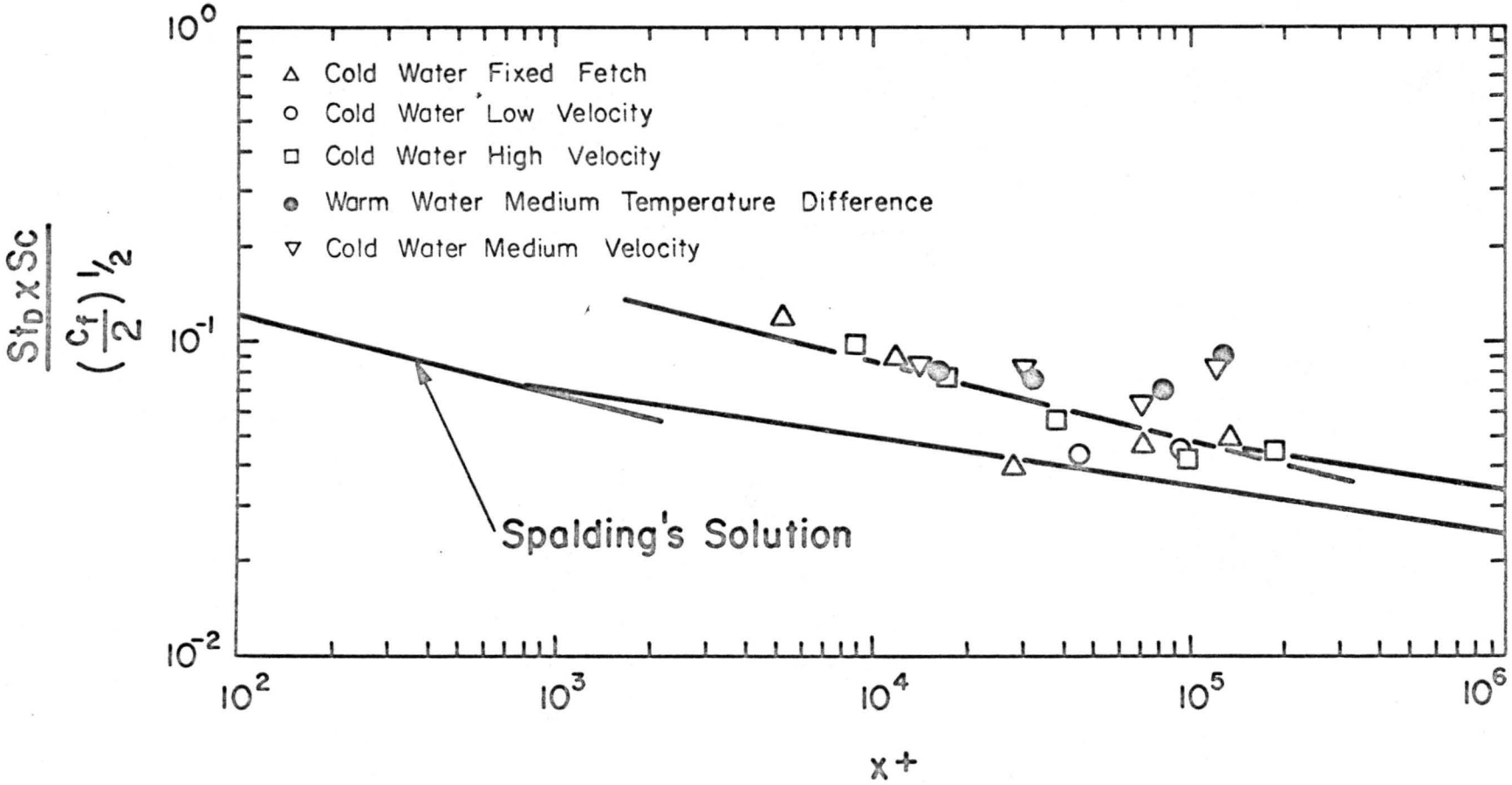

Fig. 38. Compared the experimental data with Spalding's numerical solution.

The thermal effect on evaporation near the leading edge (or in transitional region) is also included in the author's theoretical model. On deriving Equation (3-6), all factors are considered. Thus, the thermal effect appeared in the values of B(mass transfer parameter) and δ_e^* (boundary layer thickness of vapor concentration).

The numerical values of evaporation rates, which were calculated directly from Equation (3-6) are denoted by E_4 in Table III. Logarithmic profiles of velocity and humidity distribution were assumed during the calculating process. The values of E_4 decreased initially with x and increased at the downstream position, which agreed with experimental results. When x was small, the error of E_4 was within $\pm$ 10%, but when x increased, the error of E_4 was increased to $\pm$ 20%. The error of this method is associated with uncertainties in the quantities q_*, z_{om}, z_o, and u_*, which were determined from the experimental profiles. Each of these characteristic values can generate $\pm$ 2 ~ 5% error. Thus, the total error of 20% is also satisfactory for a check of consistency between this type of theory and the experiment in integral method.

Equation (3-6) appeared to be a good approximation for evaluating the evaporation rates during the transitional process provided log profiles in humidity are observed. For the fully developed turbulent flow, Equation (2-9), the profile method was the more accurate method with less error induced by the experimental results of this study.

Table IV. Numerical values of dimensionless groups.

Run No.	$Sh \times 10^{-3}$	$(\frac{C_f}{2})^{\frac{1}{2}}$	$Re_\infty \times 10^{-5}$	Rgn	λ/h
34	0.528	0.0301	1.73	--	--
37	0.975	0.0370	3.47	--	--
40	1.23	0.0442	6.96	--	--
43	2.83	0.0471	16.1	--	--
46	5.73	0.0489	29.5	--	--
35	0.648	0.0370	2.11	--	--
38	1.17	0.0407	4.43	--	--
41	1.97	0.0477	8.97	0.75	1.13
44	3.81	0.054	21.5	1.66	1.31
47	7.14	0.0502	39.3	4.86	1.20
48	5.68	0.0526	26.6	3.61	1.01
49	7.5	0.0591	29.3	3.5	1.21
51	10.2	0.058	32.9	3.3	1.17
52	13.7	0.0653	40.3	0.965	1.11
53	15.5	0.0677	44.3	1.00	1.19
57	1.15	0.0408	3.99	--	--
59	2.45	0.0484	7.50	2.3	1.27
61	5.46	0.0477	18.6	6.25	1.80
67	10.7	0.0529	25.2	28.9	1.32
56	1.04	0.0351	3.98	--	--
58	2.56	0.0457	7.53	2.83	1.40
60	4.91	0.0477	18.6	6.7	1.88
64	9.20	0.0517	25.2	13.5	1.27

Chapter VII

CONCLUSIONS

Work toward the goals of this investigation, which were stated in Chapter I, has led to some concluding remarks. On the basis of experimental results, some general and practical methods of predicting the evaporation rates from wind generated waves are established. Some phenomena of transfer mechanism and temperature effects have been observed. Specifically, the results of this study were:

(1) For conditions where turbulent air flows over water with small waves, far downstream from any zone of transition between flow over a smooth and aerodynamically rough surface, the local evaporation rate could be described satisfactorily by the following simple formula:

$$E^*_I = - 0.32\rho\, U^*\, q^* \qquad (6\text{-}11)$$

where U^* and q^* are analogous functions of mean velocity and humidity profiles, derived from the "law of the wall."

(2) For a stepwise change in vapor concentration at a wall, a direct mass balance method considering the vertical velocity at interface and possible thermal effects was derived (Equation (3-6)). Compared with experimental results, Equation (3-6) offered a satisfactory result in the zone of a transitional convective boundary layer while

the other methods (for example, Equation (2-6) (integral method) and (2-9) (profile method)) were unsatisfactory. The dimensionless correlation shown by the solid line of Figure 34 at the range $Re < 7 \times 10^5$ was also a good approximate method in transitional region.

(3) In contrast to the recent work of Smosky and Sergeyev (1962), the results of this study indicate that the difference between the wet bulb and the dry bulb temperature in the free gas stream does not influence the evaporation rate. However, the nature of the wavy surface has to be accounted for. A method representing an extension of Levich's theory appears to offer a satisfactory correlation with experimental results, as indicated in Figure 36.

(4) The surface waves influence the evaporation rates in two ways, first by increasing the apparent surface area, and second, dynamically, by modifying the air flow close to the water surface in contrast to flow over a smooth surface.

(5) The air flow over free water surface generates the waves and increases the evaporation rate. In strong wind, where $u_\infty > 11$ m/sec, the spray of water from a wavy surface increases the evaporation rate rapidly. The amount by which the evaporation is increased has not been expressed either analytically or experimentally.

(6) The temperature difference between air and water had a large effect on evaporation from a wavy surface. From direct measurements of wave height, or by means of

an indirect argument based on the large increase of evaporation rates of the warm-water case (see also Figure 34), it was shown that when the temperature of water was higher than that of the air (lapse conditions), the wave height was greater than during inversion conditions at the same free stream velocity.

(7) There was some indication that the temperature of the water surface also affected the velocity field near the surface. This difference has not been explained because Richardson's criterion indicates that the effect of stratification on the velocity field of the air should be negligible under the experimental conditions.

There are two important studies which should be done. One is the thermal effect in lapse conditions on wave structure and air stratification (or unstable stratification). Due to the heating capacity of CSU's wind-water channel, the lapse conditions were not too well controlled throughout this study. With better temperature control, the problem of heat transfer from wind generated waves by forced convection can be more effectively studied.

Secondly, it is necessary that the phenomenon of separation at the lee side of wave be further investigated. The concept of separation has been adopted in many places as a basis of physical explanation. Yet, there was no direct measurement to show the existence of separation. The separation creates a vortex near the peak and trough,

and the vortices build a barrier to vertical transport of water vapor. If a humidity probe could be used which is mounted on a wave follower that always stays at a fixed distance from the water surface then a constant value of humidity would indicate the existence of separation.

REFERENCES

REFERENCES

1. Benjamin, T.B., J. of Fluid Mech., 6, 161 (1959).

2. Bird, R.B., W.E. Stewart and E.N. Lightfoot, Transport Phenomena, John Wiley and Sons, Inc., 7th edition, 1966.

3. Blackman & Tukey, The Measurement of Power Spectra, Dover, 1958.

4. Brutsaert, W., Equations for Vapor Flux as a Fully Turbulent Diffusion Process under Diabatic Conditions, Bull. Intern. Assoc. Sci. Hydrol., 10, 11-12, 1965.

5. Cermak, J.E., and P. N. Lin, Vapor Transfer by Forced Convection from a Smooth Plane Boundary, CER No. 55, JECI Report No. 9, 1956.

6. Chang, P. C., Laboratory Measurements of Air Flow over Wind Waves Following the Moving Water Surface, Ph.D. Dissertation, Dept. of Civil Eng., Colorado State Univ., 1968.

7. Chilton, T.A. and P.A. Colburn, Ind. Eng. Chem. 26, p. 98, 1183-7, 1934.

8. Deacon, E.L., and E. K. Webb, Small-scale Interaction, In "The Sea" (M.N. Hill, ed.) Vol. I, pp. 43-87, Wiley (Interscience), New York, 1962.

9. Donovan, L.F., O.T. Hanna and S. Yerazunis, Similar solutions of turbulent boundary layer heat and mass transfer problems. The Engineering Science, Vol. 22, pp. 595-610, 1967.

10. Easterbrook, C.C., A Study of the Effects of Waves on Evaporation from Free Water Surface, CAL. Report No. RM-2151-P-1, 1968.

11. Eckert, E.G. and R.M. Drake Jr., Heat and Mass Transfer, McGraw-Hill, New York, 1959.

12. Elliott, William P., The Growth of the Atmosphere Internal Boundary Layer, Transaction, American Geophysical Union, Vol. 39, No. 6, 1958.

13. Fleagle, R.G., Note on the Effect of Air-Sea Temperature Difference on Wave Generation, Transaction, American Geophysical Union, Vol. 37, No. 3, 1956.

14. Gupta, A.K., and E.L. Mollo-Christensen, An Experimental Investigation of Air Flow over a Wavy Surface. M.I.T. Aeroelatic and Structure Lab, 1966.

15. Hess, G., G. Hidy and E. Plate, "The Structure of Turbulence in Air Flowing over Small Water Waves," Submitted to J. Fluid Mechanics.

16. Hasse, L., On the Cooling of the Sea Surface by Evaporation and Heat Exchange, Tellux XV, 4, pp. 363-366, 1963.

17. Harriot, P., A Review of Mass Transfer to Interfaces, The Canadian Journal of Chemical Eng., April 1962.

18. Hicks, B.L., Ocean Wave Spectra, Englewood Cliffs, N.J., Prentice-Hall, Inc., 1963.

19. Hidy, G.M. and E. Plate, On the Frequency Spectrum of Wind Generated Waves., Phys. Fluids, 8, 1387, 1965.

20. Hidy, G.M. and E. Plate, Wind Action on Water Standing in a Laboratory Channel, J. of Fluid Mech., Vol. 26, pp. 651-687, 1966.

21. Hidy, G.M. and E. Plate, Turbulent Transport Across a Gas-Agitated Liquid Boundary, presented at the A.I.Ch.E., National Meeting, Los Angeles, Calif., December, 1968.

22. Kays, W.M., Convective Heat and Mass Transfer, McGraw-Hill, Inc., N.Y., 1966.

23. Kinsman, B., Wind Waves, Englewood Cliffs, N.J., Prentice-Hall, 1965.

24. Kunishi, H., An Experimental Study of the Generation and Growth of Wind Waves, Disaster Prevention Res. Inst. Bull. 61, Kyoto University, Kyoto, Japan, 1963.

25. Kolar, V., Heat Transfer in Turbulent Flow of Fluids through Smooth and Rough Tubes, Int. J. Heat and Mass Transfer, 8, 639, 1965.

26. Karaki, S., and E. Y. Hsu, An Experimental Investigation of the Structure of a Turbulent Wind over Water Waves, Dept. of Civil Eng., Tech. Rept. 88, Stanford Univ., Calif. 1968.

27. Kestin, J. and P. D. Richardson, Heat Transfer across Turbulent Incompressible Boundary Layers, Int. J. Heat and Mass Transfer 6, 147-189, 1963.

28. Kestin, J., Effect of Free Stream Turbulence on Heat Transfer Rates, in Adv. in Heat Transfer, 3, ed. by T. Irvine, Jr. and J. Hartnett, Academic Press, N.Y. 1, 1966.

29. Lumley, J.L. and H.A. Panofsky, The Structure of Atmospheric Turbulence, Interscience Publisher, John Wiley and Sons, N.Y., 1964.

30. LaMer, V.K., and V.J. Schaefer, Evaporation of Water, Its Retardation by Monolayers, Science, 148, 36, 1965.

31. Levich, V.G., Physicochemical Hydrodynamics, Englewood Cliffs, N.J., Prentice-Hall, Inc., 1962.

32. Lighthill, M.J., Contributions to the Theory of Heat Transfer Through a Laminar Boundary Layer, Proc. Roy. Soc. A, Vol. 202, p. 359, 1950.

33. LyKov, A.V. and Y.A. Milhailov, Theory of Heat and Mass Transfer, Daniel Davey and Co., Inc. 1965.

34. Marlatt, W.E. and R.L. Grossman, An Investigation of Water Surface Temperature by an Airborne Infrared Radiometer, Dept. of Atmos. Sci., Paper No. 119, 1968.

35. Maha, B.K., and L.W. Shemitt, Effect of Surface Roughness on Mass Transfer, Chem. Eng. Sci., Vol. 23, pp. 183-185, 1968.

36. Miles, J.W., On the Generation of Surface Waves by Shear Flow, Part 4, J. of Fluid Mech., 13, p. 433, 1962.

37. Montgomery, R.B., Observations of Vertical Humidity Distribution above the Ocean Surface and Their Relation to Evaporation, Papers Phys. Oceanog. Meteorl. 7, No. 4, 1940.

38. Okuda, S. and S. Hayami, Experiments on Evaporation from Wavy Water, Records Oceanog. Works Japan (NS) 5, 6-13, 1959.

39. Owen, P.R. and W.R. Thompson, Heat Transfer across Rough Surface, J. of Fluid Mech., 15, 321-334, 1963.

40. Penman, H.L., Evaporation: An Introductory Survey, Netherlands J. of Agr. Sci., 4, 9-27, 1956.

41. Phillips, O.M., Dynamics of the Upper Ocean, Cambridge Univ. Press, 1966.

42. Plate, E.J., Diffusion from a Ground Level Line Source into the Disturbed Boundary Layer far Downstream from a Fence, Int. J. Heat and Mass Transfer, Vol. 10, pp. 181-194, 1967.

43. Plate, E.J., P.C. Chang and G.M. Hidy, Experiments on the Generation of Small Water Waves by Wind, to be published in J. of Fluid Mech.

44. Plate, E.J., and G.M. Hidy, Laboratory Study of Air Flowing over a Smooth Surface onto Small Water Waves, J. of Geophysical Research, Vol. 72, No. 18, 1967.

45. Poreh, M., and J.E. Cermak, Study of Diffusion from a Line Source in a Turbulent Boundary Layer, Int. J. of Heat and Mass Transfer 7, 1083-1095, 1964.

46. Reynolds, W.G., W.M. Kays and S.J. Kline, Heat Transfer in the Turbulent Incompressible Boundary Layer, II - The Step-Temperature Distribution, N.A.S.A. Memo, 12-2-58W, 1958.

47. Rider, N.E., J.R. Philip, and E.F. Bradley, Horizontal Transport of Heat and Moisture - a Micrometeorological Study, Quart. J. Royal Meteo. Soc. Vol. 89, No. 382.

48. Roll, H.U., Physics of the Main Atmosphere, Ch. 4 and 5, Academic Press Inc., N.W., 1965.

49. Schlichting, H., Boundary Layer Theory, 4th Ed., McGraw-Hill Publ. Co., Inc., p. 497, 1962.

50. Shemdin, O.H. and E.Y. Hsu, The Dynamics of Wind in the Vicinity of Progressive Water Waves, Stanford Univ., Dept. of Civil Eng., Tech. Rept., No. 66, 1966.

51. Shemdin, O.H., Experimental and Analytical Investigation of the Air Velocity Profile above Progressive Waves. Stanford Univ., Dept. of Civil Eng., Tech. Rept., No. 82, 1967.

52. Sheppard, P.A., Transfer across the Earth's Surface and through the Air Above, Quart. J. Royal Meteo. Soc. 84, 205-224, 1958.

53. Sherwood, T.K., Mass, Heat and Momentum Transfer between Phases, Chem. Eng. Progress Symposium Series, 55, 25, 1959.

54. Smith, J.W. and N. Epstein, Effect of Wall Roughness on Convective Heat Transfer in Commercial Pipes, A.I.Ch.E. J. 3, 242, 1957.

55. Smolsky, B.M. and G.T. Sergeyev, Heat and Mass Transfer with Liquid Evaporation, Int. J. Heat and Mass Transfer, 5, pp. 1011-1021, 1962.

56. Spalding, D.B., Heat Transfer to a Turbulent Stream from a Surface with a Step-wise Discontinuity in Wall Temperature, Int. Developments in Heat Transfer, 439, 1963.

57. Spalding, D.B., Contribution to the Theory of Heat Transfer across a Turbulent Boundary Layer, Int. J. Heat and Mass Transfer, Vol. 7, pp. 743-761, 1964.

58. Spence, D.A., Velocity and Enthalphy Distributions in the Compressible Turbulent Boundary Layer on a Flat Plate, J. Fluid Mech. 8, 368-387, 1960.

59. Stewart, R.W., The Wave Drag of Wind over Water, J. Fluid Mech., 10, pp. 189-194, 1961.

60. Zagustin, K., E.Y. Hsu, R.L. Street, and B. Perry, "Flow over a Moving Boundary in Relation to Wind-Generated Waves," Stanford Univ., Dept. of Civil Eng., Tech. Rept. No. 60, 1966.

Typist: Arlene M. Nelson
491-8539